

AALBORG UNIVERSITY
SCHOOL OF ENGINEERING AND SCIENCE
ENERGY DEPARTMENT



AALBORG UNIVERSITY
STUDENT REPORT

Implementation of Exhaust Gas Recirculation for Double Stage Waste Heat Recovery System on Large Container Ship

MASTER THESIS

MATTHIEU MARISSAL - MORTEN ANDREASEN

03/06/2014

Supported by:



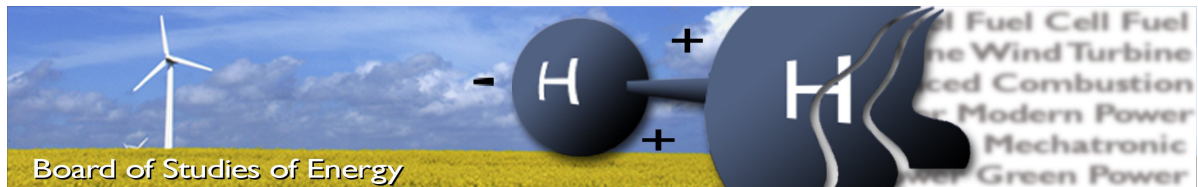
We would like to say a big thank you to our respective families who helped and supported us all along our university years. This journey would not have been the same without them, and we are very thankful for always having them on our side.

The authors would like to thank our three supervisors, Kim Sørensen and Thomas Condra Associate professors , and Vincenzo Liso Postdoc at Aalborg University for their help. Managing to have all three in the same room at the same time was often challenging, curves were always too small, the amount of explanations was never enough, it took 4 month to understand how tables should look, and the sums always reached 99.9%; but they were always available to help, encourage and to provide us advice every hour of the day, and for that we are extremely grateful.

We would also like to thank MAN Diesel & Turbo for its collaboration and especially Bent Ørndrup Nielsen, Senior Researcher, and Kari Anne Tveitaskog, Marine Engineer, who had the kindness and generosity to help us all along this semester when we had inquiries, and whose help and prompt responses were superb and above and beyond the call of duty.

"La vérité de demain se nourrit de l'erreur d'hier"
"The truth of tomorrow thrives on yesterday's mistake"
- Antoine de Saint-Exupéry

"Ak, af all Fjender er maaskee Vanen den lumskeste"
"Alas, of all enemies, the habit may be most devious"
- Søren Kierkegaard



Title: Implementation of Exhaust Gas Recirculation
for Double Stage Waste Heat Recovery System on Large Container Ship

Semester theme: Master Thesis

Semester: 4th M.Sc.

Project period: 03.02.14 to 03.06.14

ECTS: 30

Supervisors: Kim Sørensen, Thomas Condra, Vincenzo Liso

Project group: TEPE4-1000

Synopsis:

WHRS combined with EGR is a potential way to improve efficiency while reducing emissions. This project investigates the feasibility of combining the two systems. EGR dilutes the fuel, lowering the combustion temperature and therefore the formation of NO_x . Tier III limitation can then be reached.

A WHRS is set up to utilize available heat sources to reach the highest possible combination of pressure and temperature. The system design is optimized and found capable of producing from 400 to 1900 kW, with a weighed average power of 958 kW. The consumption profile is found to significantly impact the weighed average power, where the Tier II/Tier III operation distribution have a much smaller influence. Furthermore, it is found that the low pressure should be kept near minimum, while the optimum high pressure increases from 7 to 12 bar with the load.

By increasing the efficiency of the overall system, the CO_2 emissions can be reduced and therefore the EEDI can be improved by 3.5%. The addition of a third cycle, used only in Tier III is investigated. While increasing the total heat exchanger areas by approximately 40%, the cycle is found to increase the power production in Tier III operation by almost 50%.

Matthieu Aurelien Marissal

Morten Lind Andreasen

Copies: 6
Pages, total: 142
Appendices: A-F
Supplements: CD

By signing this document, each member of the group confirms that all group members have participated in the project work, and thereby all members are collectively liable for the contents of the report. Furthermore, all group members confirm that the report does not include plagiarism.

Executive Summary

The IMO has introduced the Tier III regulation when a ship is operating inside ECAs. This enforces extremely strict NO_x emission limits. To reach this level, an Exhaust Gas Recirculation (EGR) system can be implemented on the ship. However, this could be detrimental to the Waste Heat Recovery System (WHRS). Having both an EGR and a WHRS compatible and operational on a ship would allow energy savings while reducing emissions, and complying with international regulations. The purpose of this project is to study this compatibility.

An EGR system sends part of the exhaust gas back to the engine combustion chamber. This lowers the temperature of combustion, which reduces the amount of NO_x formed by up to 70%, which allows a ship to meet the strict Tier III emission regulations.

A double stage WHRS recovers energy from the exhaust gas in the stack by evaporating water in the stack heat exchangers. The steam is then sent through a turbine to generate electricity. In this project two cycles are used: high and low pressure. When EGR is employed, the amount of energy in the exhaust gas in the stack is reduced, bringing the viability of the WHRS into question.

An EGR/WHRS system was modelled including heat recovery from the EGR. Operation pressures were optimized for all loads and used to optimize the component sizes. Reasonable physical constraints were also applied to reach a feasible configuration.

Excellent compatibility is found between the WHRS and EGR. With only minor modifications to the overall system, the estimated power savings barely change from Tier II to Tier III operation for a given compatible system. The expected power generation was estimated to be between 400 and 1900 kW for both Tier II and Tier III. Optimum pressures are found to be within a reasonable range. The efficiency improvement has also a positive impact on the EEDI index by reducing CO₂ emissions of a large container vessel of about 5 000 ton/year for the case study operation profile. To keep focus on the overall system, individual components were not modelled extensively. Some of the system data, such as the outlet engine properties, are provided by MAN.

Since emissions limit are mandatory, a combined system should become more attractive if the ECAs are expanded. If Tier III operation was to become sufficiently dominant, a third cycle could be installed, increasing the expected savings by an additional 38% and covering up for larger installation costs.

Abstract

A Waste Heat Recovery System allows large vessels to save energy and reduce CO₂ emissions. However, the IMO is putting strict regulation in place regarding NO_x and SO_x emissions inside ECAs. A way to reach these emissions is to implement an Exhaust Gas Recirculation system. Whether these two systems can work together has been investigated.

Fuel composition is evaluated from the lower heating value using the statistical method. A mixture, with similar LHV and atomic composition, of three known lighter fuels, was used to simulate combustion with the Glassman mechanism. The excess air ratio has been taken as given by MAN with no cross-over considered.

EGR is applied, re-introducing a part of the exhaust gas back into the combustion chamber. This reduces the concentration of O₂ and decreases the adiabatic flame temperature. The production of NO_x is highly dependent on the temperature of the combustion. Lowering this temperature lowers the formation of NO_x. By applying EGR, the Tier III limitation can be reached.

The WHRS converts part of the thermal energy in the exhaust gas to electricity through one or more Rankine cycles. Water is evaporated and superheated, and is then sent through a condensation turbine. Higher temperatures and higher pressures at the turbine inlet is found to increase the system efficiency. This is in accordance with previous investigations. A WHRS with 2 cycles is set up to utilize available heat sources to reach the highest possible combination of pressure and temperature.

The system design is optimized using a genetic solver, with an embedded Hessian-based solver to optimize operation. The system is found capable of producing from 400 to 1900 kW, with a weighed average power relative to the consumption profile of 958 kW. The consumption profile is found to significantly influence the weighed average power, where the Tier II/Tier III operation distribution have a much smaller influence. It is furthermore found that the optimum low pressure is generally between 3.5 and 4 bars, while the optimal high pressure goes as high as 12.4 bar.

By increasing the efficiency of the overall system, the CO₂ emissions can be reduced and therefore the EEDI can be improved. Taking an average heat recovery value, the CO₂ emissions can be reduced by around 5 000 tons/year, corresponding to a 3.5% reduction in EEDI.

The addition of a third cycle, used only in Tier III is investigated. While increasing the total heat exchanger areas by approximately 40%, the cycle is found to increase the power production in Tier III operation up to almost 3000kW, corresponding to an increase of up to 50%.

Nomenclature

Symbol	Description	Unit
A	Area	m^2
c	Heat capacity	$\frac{J}{K}$
C_F	CO ₂ emission ratio	$\frac{kg}{kg}$
C_T	Turbine constant	m^2
h	Enthalpy	$\frac{J}{kg}$
k	Kinetic constant	—
K	Equilibrium constant	—
m	Mass	kg
M	Molar weight	$\frac{kg}{kmol}$
n	Mole, Number of drum recirculation	<i>mole</i> , -
p	Pressure	Pa
P	Power	W
Q	Heat	W
s	Entropy	$\frac{J}{kg \cdot K}$
T	Temperature	$K, ^\circ C$
v	Specific Volume	$\frac{m^3}{kg}$
V	Velocity	$\frac{m}{s}$
w	Mass fraction	—
x	Quality	$\frac{kg}{kg}$
Y	Mole fraction	-
z	Altitude	m

η	Efficiency	-
γ	Mass fraction	-
λ	Excess air ratio	-
ϕ	Equivalence ratio	-
ψ	Specific exergy	$\frac{kJ}{kg}$
Ψ	Air Nitrogen content, Exergy	$-, kJ$

Prescript

Δ	Difference
----------	------------

Subscript

AE	Auxiliary Engine
------	------------------

Continued on next page

Continued from previous page

Symbol	Description
<i>b</i>	Burned
<i>eg</i>	Exhaust gas
<i>egr</i>	Exhaust gas recirculated
<i>eq</i>	Equilibrium
<i>evap</i>	Evaporation
<i>f</i>	Fuel
<i>fg</i>	Formation
<i>i</i>	Intake
<i>in</i>	Inlet
<i>lm</i>	Logarithmic mean
<i>max</i>	Maximum
<i>mid</i>	Middle
<i>mix</i>	Mixture
<i>out</i>	Outlet
<i>p</i>	Constant pressure
<i>s</i>	Isentropic
<i>sat</i>	Saturated
<i>scav</i>	Scavenge air
<i>st</i>	Steam turbine
<i>stoic</i>	Stoichiometric
<i>SH</i>	Superheating
<i>T_{II}</i>	Tier II
<i>T_{III}</i>	Tier III
<i>tc</i>	Turbocharger
<i>tot</i>	Total
<i>turb</i>	Turbine
<i>u</i>	Unburned
<i>v</i>	Constant volume
0	Dead state

Superscript

.	Flow	$\frac{1}{s}$
+	Forward	—
—	Reverse	—
'	Including pressure loss	—

Abbreviations

A/F	Air to Fuel ratio
ECA(s)	Emission Control Area(s)

Continued on next page

Continued from previous page

Symbol	Description
EEDI	Energy Efficiency Design Index
EG	Exhaust Gas
EGR	Exhaust Gas Recirculation
FEU	Forty-foot Equivalent Unit
GHG	Greenhouse Gas
HFO	Heavy Fuel Oil
HP	High Pressure
ICE	Internal Combustion Engine
IFO	Intermediate Fuel Oil
IMO	International Maritime Organization
LHV	Lower Heating Value
LMTD	Logarithmic Mean Temperature Difference
LNG	Liquefied Natural Gas
LP	Low Pressure
LR	Load Repartition
MARPOL	Marine Pollution
MCR	Maximum Continuous Revolution
MEPC	Marine Environment Protection Committee
NTU	Number of Transfer Units
PT	Power Turbine
PV	Pressure Volume
RPM	Round Per Minute
SCR	Selective Catalytic Reduction
SEEMP	Ship Energy Efficiency Management Plan
SFOC	Specified Fuel Oil Consumption
SMCR	Specified Maximum Continuous Rating
SPP	Steam Power Production
TC	Turbocharger
TEU	Twenty-foot Equivalent Unit
WHR(S)	Waste Heat Recovery (System)
WTS	Water Treatment System
WTU	Water Treatment Unit
@	At

Preface

This thesis is written by a group of 4th semester M.Sc students at the School of Engineering and Science at Aalborg Univerisity, following a Thermal Energy and Process Engineering major.

Reading Instructions

Throughout the report there will be references to sources used, which can be found in the Bibliography. The used method for referring to sources is the Harvard Method, where the source will be written as [Author, Year]. If the reference is included in a sentence before the dot, the reference covers the sentence. If the reference is after a dot, it covers the section or paragraph. If there are more than one source with the same name and year, the source gets a letter after the year. A reference leads to the bibliography where the sources is given by the author, year, title, edition, publisher, hyperlink etc. depending on the source.

Figures, tables and equations are numbered so that it indicates which chapter they belong to. Appendixes are indicated with a letter. This means that the first figure in Chapter 3 is numbered 3.1 and the next figure is numbered 3.2. Appendix B is numbered B.1 and the next figure numbered B.2. The explanatory text will be attached to the given figure or table in a caption.

A CD is attached to the report, which contains all data given, data sheets, program files, the report in PDF and PDF copies of all web-sources. The CD appendix refers to the CD sources.

Publication of the entire report or parts of this thesis is allowed only with references and in agreement with all authors.

Contents

Executive Summary	vii
Abstract	ix
Chapter 1 Project Proposition	1
Chapter 2 Introduction	3
2.1 Background	3
2.2 Case Study and Specifications	9
2.3 Ship and EGR Operation Profiles	11
Chapter 3 Problem Statement	15
I Exhaust Gas and Recirculation	17
Chapter 4 HFO Combustion for Tier II Application	19
4.1 Fuel Composition	19
4.2 Stoichiometric Conditions out ECAs and Air to Fuel Ratio	20
4.3 Fuel Model	20
4.4 Combustion Conditions	21
4.5 Impact of Excess Air Ratio on the Combustion	22
4.6 Exhaust Gas Composition without Dissociation	24
4.7 Tier II Outlines	26
Chapter 5 HFO Combustion and EGR for Tier III Application	27
5.1 Exhaust Gas Composition Including EGR	27
5.2 Excess Air Ratio for Tier III Conditions	30
5.3 Influence of EGR on Adiabatic Flame Temperature	30
5.4 Influence of EGR on Dissociation	31
5.5 Exhaust Gas Composition and Properties	32
5.6 Tier III Outlines	34
Chapter 6 NO_x Emission Control	35
6.1 NO _x Denomination and Formation	35
6.2 NO Formation Kinetic	35
6.3 NO ₂ Formation	40
6.4 Estimation of NO _x Emissions	41
6.5 Discussion	43

6.6	Conclusion	44
II Waste Heat Recovery Models		45
Chapter 7 Base System		47
7.1	Waste Heat Recovery System: General	47
7.2	Stack Heat Transfer	49
Chapter 8 System Design		53
8.1	Exergy	53
8.2	Utilizing Heat Sources	57
8.3	Proposed System	59
Chapter 9 WHRS Models		61
9.1	Turbine	61
9.2	Pump	62
9.3	Heat Exchangers	63
9.4	Power Turbine	69
9.5	Design Model	70
9.6	Performance Model	71
9.7	Electric Production	73
III Optimization, Results and Further Investigation		77
Chapter 10 Optimization		79
10.1	Design Approach	79
10.2	Design Parameter Optimization	80
10.3	Partload Operation Optimization	82
Chapter 11 Results Analysis and Discussion		85
11.1	Operation Profile Sensitivity Analysis	85
11.2	Tier II / Tier III Operation Repartition Sensitivity Analysis	86
Chapter 12 CO₂ Reduction and EEDI		91
12.1	CO ₂ Emission Reduction	91
12.2	EEDI	91
12.3	Influence of Heat Recovery on EEDI	92
Chapter 13 Tier III Exclusive Cycle		93
13.1	Remaining EGR Power	93
13.2	Revised System	93
13.3	Results	94
13.4	Conclusion	96
Chapter 14 Conclusion		97
Chapter 15 Recommendations for Future Work		99

References	101
Appendix A CD Content	105
Appendix B IMO Emissions Regulations	107
B.1 Nitrogen Oxides - Regulation 13	107
B.2 Sulfur Oxides - Regulation 14	108
Appendix C SO_x and Scrubbing	109
C.1 Sulfur Oxidation in the Exhaust Gas	109
C.2 System Outline	110
Appendix D Sulfuric Acid	113
D.1 Sulfur Concern	113
D.2 Interest of Sulfur Control	113
D.3 Dew point Evaluation	114
D.4 Security Margin and Energy Losses	115
D.5 Conclusion	116
Appendix E Heat transfer formulas	117
E.1 Log mean temperature difference (LMTD)	117
E.2 Number of transfer units (NTU)-method	117
Appendix F Thermodynamic Charts	119

List of Figures

2.1	Development of the global merchant fleet over the years [KG].	4
2.2	Fuel cost evolution over the last 14 years [Finace&Economics, 2014].	5
2.3	EEDI limits as function of deadweight and time[IMO, 2011].	6
2.4	MARPOL convention NO _x and SO _x limits.	7
2.5	Emission Control Areas [Wärtsilä, 2012].	7
2.6	WHRS Sankey example [Wärtsilä, 2011].	8
2.7	Triple-E class ship.	9
2.8	EGR system diagram with two turbochargers [Turbo, 2013].	10
2.9	Integrated EGR [Turbo, 2013].	11
2.10	Time of operation repartition over the load [Tveitaskog, 2013].	12
2.11	SFOC as function of the load and fuel penalty by switching to Tier III operation [Tveitaskog, 2013].	13
4.1	Example of measured pressure and temperature as function of the crank angle.	22
4.2	Adiabatic flame temperature as function of the equivalence ratio including dissociation.	23
4.3	Mole fractions of CO _x , NO _x and SO _x per Argon as function of the equivalence ratio ϕ	24
4.4	Exhaust gas mass flow as function of the load.	25
5.1	System sketch.	28
5.2	EG mass flows as function of the load for Tier III.	31
5.3	Influence of EGR on the adiabatic flame temperature.	32
5.4	Influence of EGR on SO _x mole fractions per Argon.	32
5.5	Recirculation percentage as function of the load.	33
6.1	NO formation rate for various intake temperature and excess air ratio.	38
6.2	NO formation rate for various adiabatic flame temperatures and excess air ratio.	39
6.3	NO mole fraction as function of the EGR(%).	40
6.4	Mole fractions of NO ₂ and NO at various EGR(%).	41
6.5	Tier II NO _x emissions.	42
6.6	Tier III NO _x emissions.	43
7.1	Schematic of a double stage WHRS [Diesel&Turbo, 2013a].	48
7.2	T-s diagram of a double stage WHRS [M&M, 2013].	48
7.3	T-Q diagram example. The HP cycle was shown in Figure 7.2 [M&M, 2013].	49
7.4	The stack heat transfer in the process diagrams.	50
8.1	Development of specific exergy of water for varying temperature.	54

8.2	Influence of pressure on exergy for constant temperature.	55
8.3	Maximum theoretical efficiency at 10 bar pressure.	56
8.4	Maximum theoretical efficiency.	56
8.5	Diagram of available heat sources in Tier II and Tier III conditions.	57
8.6	Scavenge air utility at high load.	58
8.7	Adapting the system design to EGR availability.	59
8.8	Schematic of the proposed WHRS system.	60
9.1	Focus on the turbine in the T-s diagram.	62
9.2	Sketch of the drum and evaporator system.	63
9.3	Basic condensation diagram.	64
9.4	Subscript illustration.	67
9.5	Temperatures and mass flows of the heat sources in Tier II.	67
9.6	Temperatures and mass flows of the heat sources in Tier III.	68
9.7	Focus on power turbine.	69
9.8	Flowchart of the Design Model.	71
9.9	Flowchart of the Performance Model.	72
9.10	The stack block in Tier II and Tier III conditions.	73
9.11	Electric production (LP: 4.5 bar, HP: 8.5 bar).	74
9.12	Power turbine electric production ratio.	75
10.1	Illustration of the optimization process.	79
10.2	Evolution of the function value in the genetic optimization	81
10.3	Example of fmincon convergence, the numbers represents the order in which the points are reached.	83
10.4	Optimised performance for design pressures of 12.14 and 4.41 bar.	83
11.1	Tested operation profiles.	85
11.2	Energy and Exergy efficiencies as function of the load.	88
11.3	Second law efficiencies for the heat transfers in the stack and EGR. Note the scale of the y-axis.	89
12.1	Calculated EEDI for case study.	92
13.1	Schematic of the proposed WHRS system.	94
13.2	System performance of the retro-fit third cycle.	95
B.1	NO _x Regulations [IMO, 2013a].	107
B.2	SO _x Regulations [IMO, 2013b].	108
C.1	Scrubbing system diagram [Turbo, 2013].	110
D.1	Optimization of the exhaust outlet temperature.	114
D.2	Available energy in the stack in Tier II and Tier III conditions.	116
F.1	T-s diagrams of the designed system.	119
F.2	p-h diagrams of the designed system.	119
F.3	T-s diagrams of the designed system.	120
F.4	p-h diagrams of the designed system.	120

List of Tables

2.1	Operation profile in Tier III. [Turbo, 2013]	12
4.1	Fuel Composition.	20
4.2	Modeled fuel composition.	21
4.3	Exhaust gas composition computed with Cantera.	25
5.1	Burned fuel composition without EGR. No dissociation.	29
5.2	Unburned mixture composition.	30
5.3	Exhaust gas recirculation properties in Tier III per kg.	33
5.4	Exhaust gas composition computed with Cantera.	34
9.1	Heat exchangers sizing.	69
11.1	Optimum design settings for the operation profiles shown in Figure 11.1.	86
11.2	Optimum design settings for ratios of Tier II to Tier III operation.	86
13.1	Performance of the system including a third cycle in the EGR string. All values use the MAN operation profile.	95
13.2	Changes in total estimated heat exchanger area.	96

Project Proposition 1

Container ships are the most commonly used mean of intercontinental cargo freight. Due to the vast size of these ships the amount of energy required for transport is similarly large. The interest in larger container ships results in a reduction of transport costs. Recently, rising oil costs and increased focus on CO₂, NO_x and SO_x emissions have made even small savings in energy a great deal for shipping companies.

The propeller shaft work is often provided by a two-stroke engine consuming HFO (Heavy Fuel Oil). The efficiency of this kind of engine is generally around 50% meaning that around half of the energy is rejected. So an on-board WHRS (Waste Heat Recovery System) has become attractive. However the IMO (International Maritime Organization) has been putting in place strict regulation regarding the emissions, the most restrictive being the NO_x emissions in the ECAs (Emission Control Areas). Since Tier III regulation will be implemented in ECAs and needs to be addressed by means of NO_x reducing techniques such as an EGR (Exhaust Gas Recirculation), this implementation can compromise the application of the WHRS. If the two systems do not work together, a shipowners might be reluctant to invest in both.

CO₂ emissions are also a great deal of concern. The IMO has put in place an index called EEDI (Energy Efficiency Design Index) that represents the amount of CO₂ emitted per mile and per amount of good transported. It is mandatory for a ship owner to respect this index. By increasing the energy efficiency of the ship, and therefore decreasing its CO₂ impact, a WHRS has the capability to improve the EEDI index.

The purpose of this project is to set up a model of EGR combined with a WHRS. The feasibility of combining an EGR and WHR systems should be determined by evaluating the possible energy savings disregarding economic investments. NO_x and CO₂ emissions should also be calculated to demonstrate the positive effect on the ship environmental impact.

Introduction 2

This chapter will introduce ship transportation. The main concerns and challenges will be described to get a better understanding of the utility of Waste Heat Recovery (WHR) and Exhaust Gas Recirculation (EGR) with regard to emissions and efficiency. Relevant emission limits and regulations such as EEDI and Tier III will be introduced. The study case and the WHRS/ EGR system considered are described. The associated operation profiles for Tier II and Tier III are shown.

2.1 Background

2.1.1 Challenges of Ship Transportation

International economic and trade development, especially with emergent countries, have grown for the last 30 years. Increasing international trade leads to a larger demand for transportation, most of which is met by shipping. Over 95% of intercontinental freight volume is carried by ship [KG]. In order to reduce operational costs per capacity, larger and larger container ships are built.

Ship transportation traffic has increased significantly for the last decades, corresponding to the demand and will likely continue to grow since the demand for transport capacities has increased by about 7% every year for the last 20 years. Figure 2.1 shows the evolution of global merchant fleet in terms of capacities.

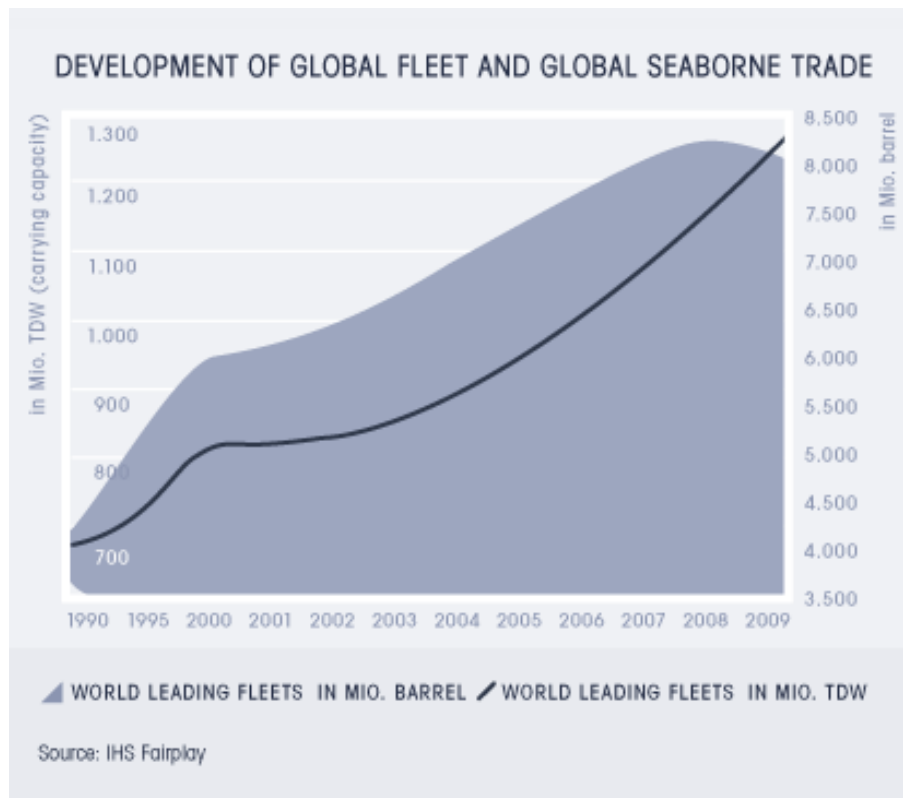


Figure 2.1: Development of the global merchant fleet over the years [KG].

Three main issues have pushed owners and designers to improve the ship performance(s):

- Transport costs: Even if a larger ship will consume more energy, increasing the capacity will reduce the specific costs (\$/mile/ton) .
- Fuel cost increase: The increase of fuel price and the large consumption of large container ships have made it important to optimize energy savings (i.e. minimizing the fuel consumption).
- Environmental impacts: The large consumption of those ships implies large emissions of CO_x, SO_x and NO_x. International conventions and regulations make it mandatory for ships to reach certain levels of emission before they are allowed to travel. Some countries have limited the access to their national seas to ships complying with the strictest regulations (Tier III).

2.1.2 Fuel Prices

Large container ships operate primarily using HFO (Heavy Fuel Oil). Moreover different qualities of HFO are used, low and high sulfur content, depending on the amount of sulfur that the ship is allowed to emit, which will increase the cost per barrel.

The prices of fuel have more than doubled for the last 10 years as it can be seen on Figure 2.2.

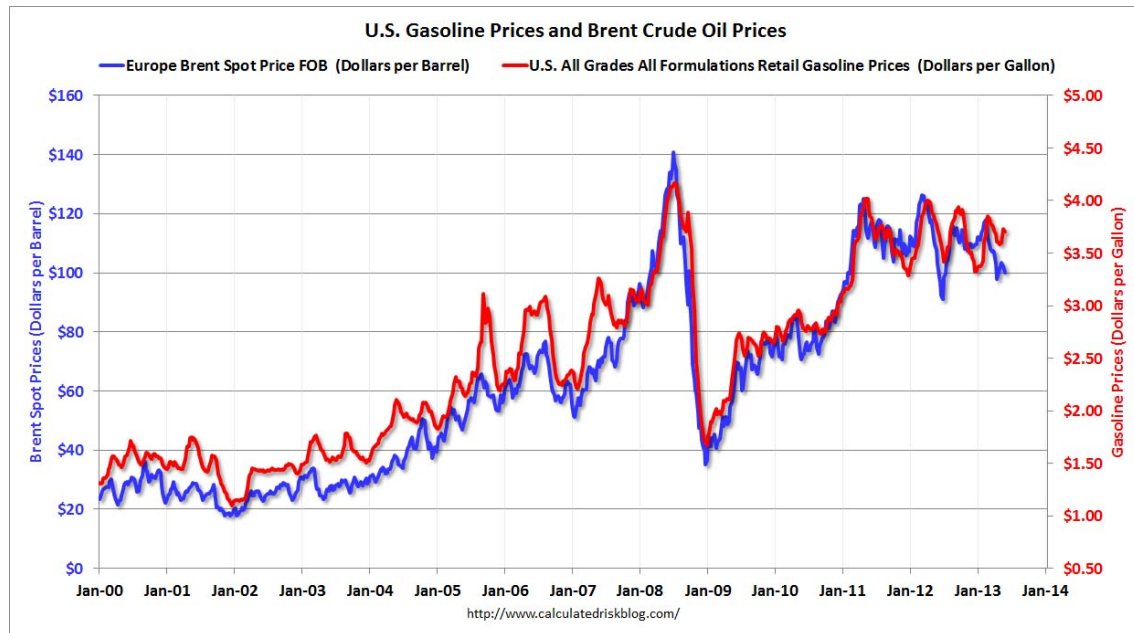


Figure 2.2: Fuel cost evolution over the last 14 years [Finace&Economics, 2014].

A large container ship such as the Triple E Mærsk Line class consumes around a hundred tons of fuel a day [Diesel&Turbo, 2012]. Hence, saving even a few percent has a huge economic and environmental impact.

2.1.3 Environmental Concerns

Container shipping is one of the most efficient mean of transportation regarding the amount of CO₂ emitted per capacity. However, due to the size of the container ships and their consumption, significant amount of harmful gases are emitted.

- CO_x concerns: CO₂ is the primary GHG (Green House Gas) emitted through human activities. The combustion of fossil fuel is the second largest source of CO₂ emissions [EPA, 2014].
- NO_x concerns: Nitrogen oxides will react with water molecules in the atmosphere and, by oxidizing, will produce acid rain. These acid rain will impact the surrounding fauna and flora.
- SO_x concerns: Sulfur oxides will also react with water and produce acid rain. However a too large amount in the fuel will also imply material problems for the ship owners. It will leads to formation of soot in the chimney, and will form sulfuric acid in the stack if allowed to condense. It will be mostly controlled by the use of fuel with low sulfur content and by on-board scrubbing systems.

2.1.4 International Regulations

In order to reduce harmful gases emission, the international community has adopted mandatory measures via the MARPOL convention presented by the Marine Environment Protection Committee (MEPC) of the IMO. It is the first mandatory harmful gas reduction

regime for an international industry sector ever adopted. It has been made mandatory to reach the EEDI, for new ships, and the Ship Energy Efficiency Management Plan (SEEMP) for all ships [IMO, 2011].

The IMO describes the EEDI as *a non-prescriptive, performance-based mechanism that leaves the choice of technologies to use in a specific ship design to the industry. As long as the required energy-efficiency level is attained, ship designers and builders would be free to use the most cost-efficient solutions for the ship to comply with the regulations* [IMO, 2011]. The various limits can be seen on Figure 2.3.

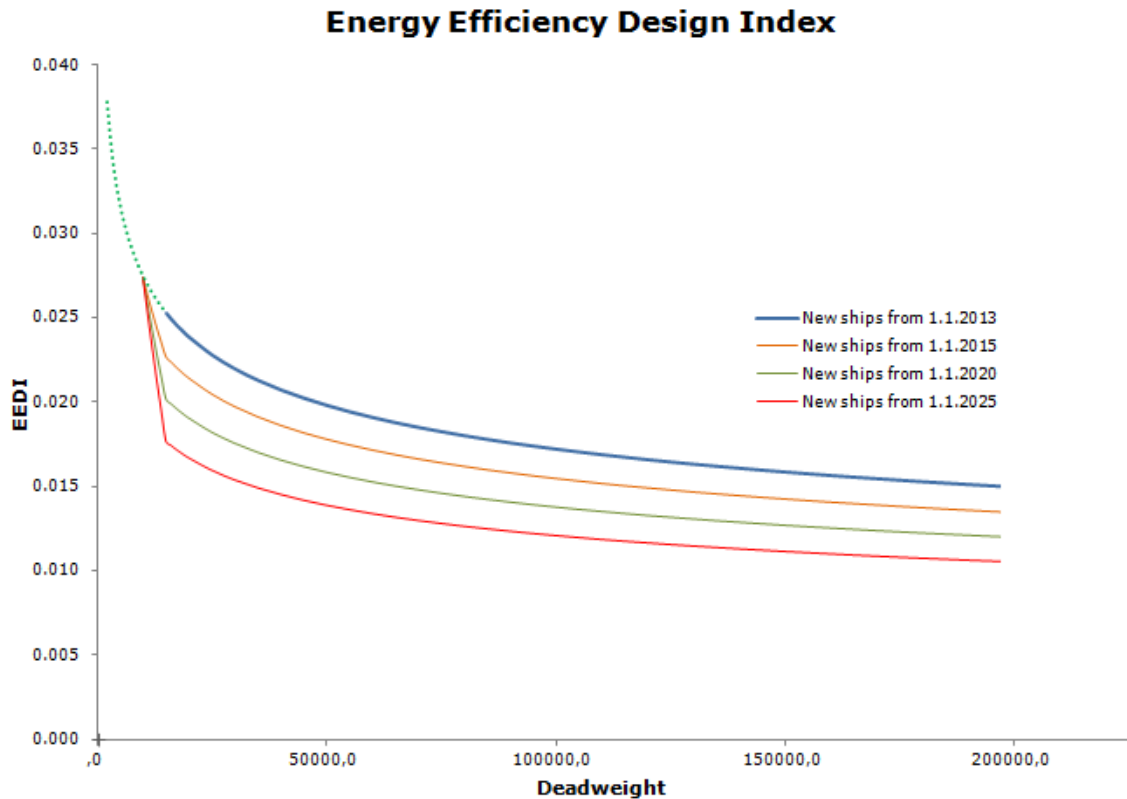


Figure 2.3: EEDI limits as function of deadweight and time[IMO, 2011].

The EEDI per deadweight will decrease every 5 years to become stricter and stricter, and it will be mandatory to be in compliance with it. The fact that no particular technology is imposed by the IMO allows for companies to innovate.

Regulation 13 and 14 of the MARPOL convention regulating the NO_x and SO_x emissions are shown in Figure 2.4a and 2.4b. They will depend on the engine rated speed and the ship construction date. The most restrictive emission level is called Tier III and applies while operating in ECAs. The different emission limits are stated below, and a more detailed analysis can be found in Appendix B.

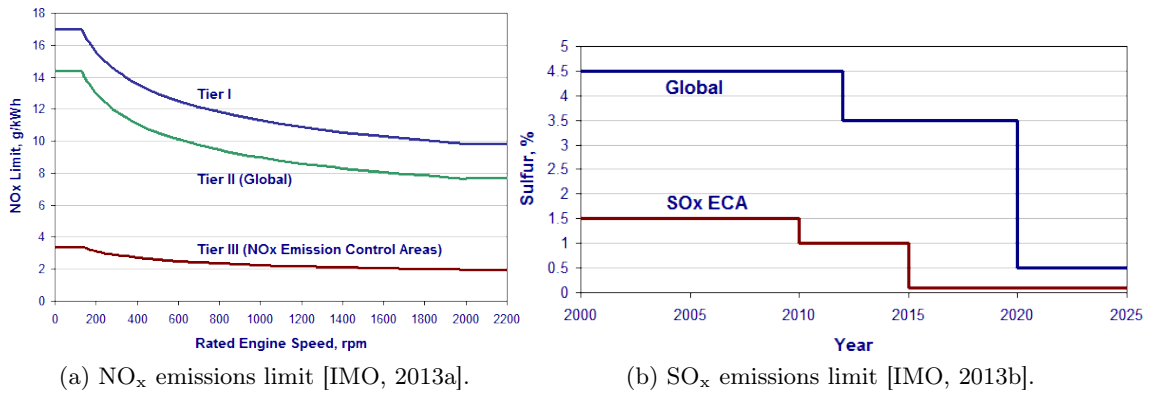


Figure 2.4: MARPOL convention NO_x and SO_x limits.

- NO_x: After the 1st of January 2016 for an engine rated speed lower than 130 rpm the total weighted cycle emission limit in Tier III should not exceed 3.4 g/kWh [IMO, 2013a].
- SO_x: After the 1st of January 2015 fuel sulfur concentration should not exceed 0.1% mass inside ECAs [IMO, 2013b].

The ECAs are currently located around the coasts of the USA, the North sea and the Baltic Sea. However they will likely be extended soon to the Mediterranean sea, the coasts of Japan, Norway, Australia, Canada and Mexico. Figure 2.5 represents the current ECAs and the one to come [Wärtsilä, 2012].

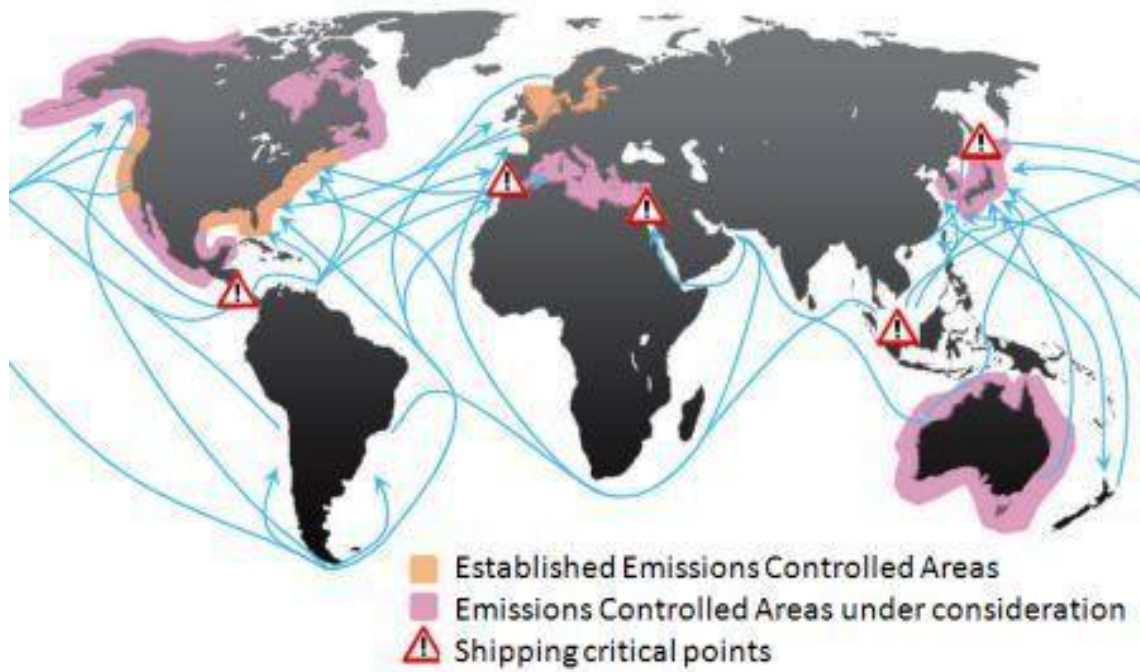


Figure 2.5: Emission Control Areas [Wärtsilä, 2012].

2.1.5 Emission Reduction Systems

To comply with the IMO regulations, different systems can be implemented such as Waste Heat Recovery (WHRS) for CO₂, Selective Catalytic Reduction (SCR) and Exhaust Gas Recirculation (EGR) for NO_x and SO_x.

Waste Heat Recovery

With an engine efficiency around 50%, a large amount of heat is lost during the journey. A WHRS allows to recover a part of this energy to produce electricity, which would otherwise have come from auxiliary engines. Even if it will imply a slight increase in the SFOC (Specific Fuel Oil Consumption), the electricity produced will lower the global amount of CO₂ emitted by the ship. A WHRS will have a great influence on emissions and a positive economic impact by increasing the overall efficiency. Figure 2.6 shows an example of a Sankey diagram for a ship with and without a WHRS.

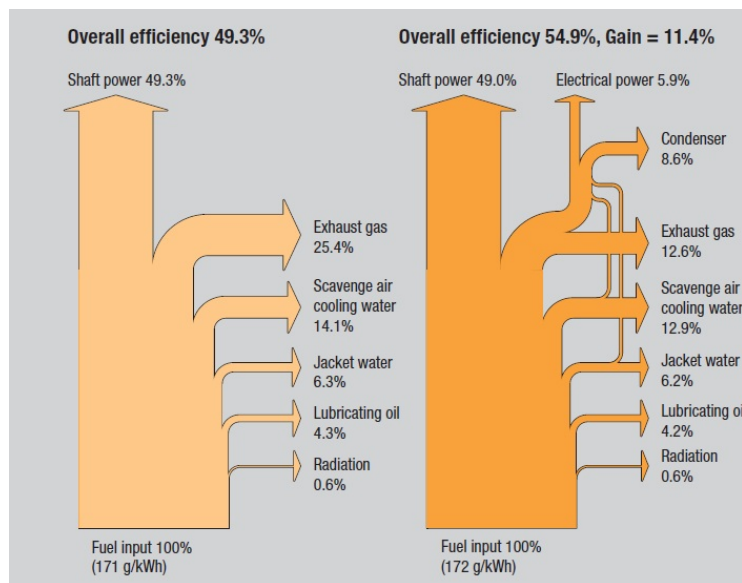


Figure 2.6: WHRS Sankey example [Wärtsilä, 2011].

Selective Catalytic Reduction

Selective Catalytic Reduction is a technology used since the late seventies and more particularly on marine application since 1989. The main principle is to convert NO_x into N₂ and water via a catalytic process. It is implemented on large on-shore power plants, but is still not convenient for marine applications due to its size and temperature requirements. [Diesel&Turbo, 2013a]

Exhaust Gas Recirculation

Since the seventies Exhaust Gas Recirculation has been tested on small 4-stroke diesel engines and has been found to be a very efficient measure to reduce NO_x emissions. It recirculates a part of the exhaust gas through the combustion chamber, and by doing so, reducing the adiabatic flame temperature. This temperature reduction reduces the formation of NO_x molecules by lowering the level of dissociation. [Diesel&Turbo, 2013a]

2.2 Case Study and Specifications

Now that the different challenges of ship transportation have been introduced, a category of ship and more particularly a specific engine are elected for the study. The various characteristics of this ship and the engine have to be presented as well as the WHR and EGR systems put in place.

2.2.1 Ship and Engine Data

This analysis will apply for large container ships (i.e TEU > 8000). Figure 2.7 shows an example of such a ship, the Mærsk Triple E class ship. This class of ship is designed by A.P Møller-Mærsk. It is the largest class of container ship currently in operation.



Figure 2.7: Triple-E class ship.

As an example, the Mary Mærsk is one of the Triple-E class ship and has the following characteristics:

- Completion year: 2013.
- Deadweight: 165 000 tons.
- Overall length: 400 m.
- Capacity: 18 270 TEU.
- Power output: Two engines of 30 MW at 73 rpm each.

The engine used in this report is a MAN 9S90ME-C9.2 designed by MAN Diesel & Turbo. It is a Tier II compliant engine with the following characteristics [Diesel&Turbo, 2013a]:

- Engine type: 9S80ME-C9.2.
- SMCR: 36490 kW at 72.5 rpm.
- Nominal engine speed: 84 rpm.
- Mean effective pressure: 20 bar.
- IMO NO_x emission limit: Tier II.
- WHR with exhaust gas power turbine: Yes.

2.2.2 Fuel for Tier II and Tier III

The fuel used for large container ships are Heavy Fuel Oil (HFO) or Residual Fuel Oil (RFO). It represents what is left after crude oil has been cracked to produce lighter

hydrocarbon chains. The composition of such fuels are not exactly defined and differs from source to source. MAN usually tries to reach IFO180 or IFO380 by adjusting the viscosity blending residual fuels with lighter ones [Tveitaskog, 2013].

To reach the Tier III requirements, the fuel used inside ECAs can be taken with low sulfur content. Another way to reach the Tier III would be to use the same fuel as in Tier II and to treat the sulfur present in the exhaust gas with a scrubbing process.

2.2.3 Waste Heat Recovery System

The Waste Heat Recovery System considered in this report is designed by MAN Diesel & Turbo. It has already been studied and modeled in a previous project made by the authors [M&M, 2013]. It is a double stage (low and high) pressure cycles system combined with a power turbine at the outlet of the engine on board of the Mærsk Triple-E ships. More details about the system can be found in [Diesel&Turbo, 2013a].

2.2.4 Exhaust Gas Recirculation System

For EGR, two main systems are used: By-pass matching and TC cut-out matching. In this report, the last solution is investigated and can be seen on Figure 2.8.

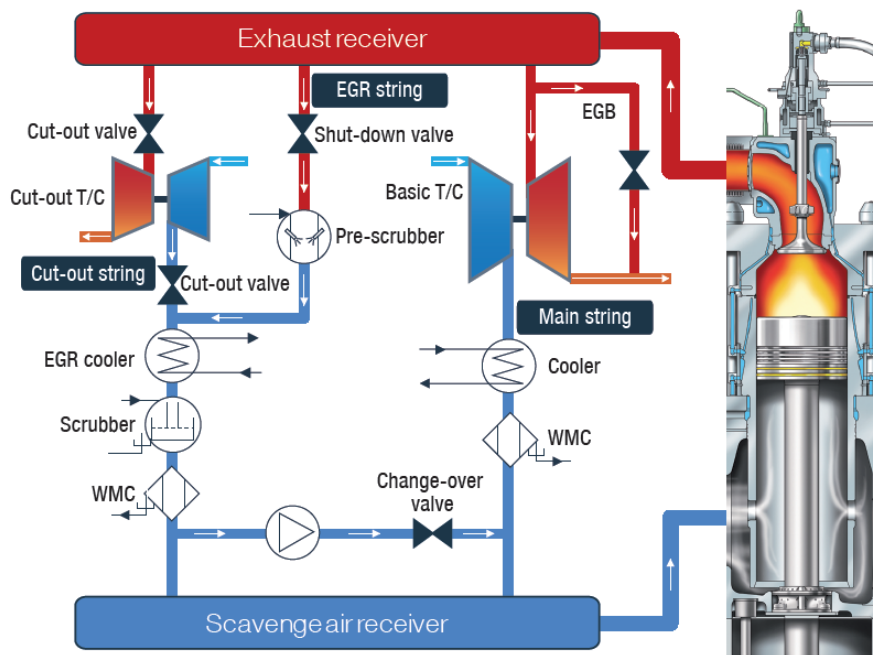


Figure 2.8: EGR system diagram with two turbochargers [Turbo, 2013].

This system allows operation in Tier II and a Tier III mode. In the first case (out of ECAs), both the main string and the cut-out string are in operation. However the EGR string is kept closed. About 40% of the scavenge air is passed through the cut-out string. In the second case (inside ECAs) the EGR string is opened with a mass flow regulated as function of the amount required to reach the NO_x emission limit [Diesel&Turbo, 2013a].

The integrated system is shown on Figure 2.9.

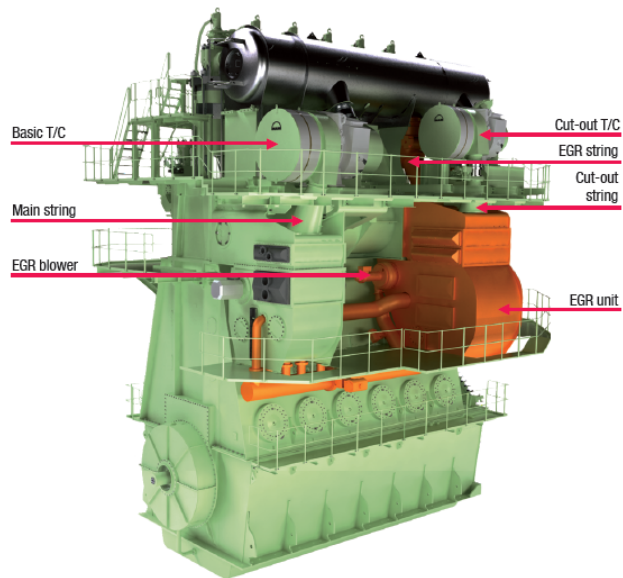


Figure 2.9: Integrated EGR [Turbo, 2013].

2.3 Ship and EGR Operation Profiles

Various ambient conditions can be considered to model the performances of the systems. Indeed, a ship operating in arctic conditions will not have the same operational characteristics as a ship operating in tropical seas. However, for simplification, a typical condition of 25°C of ambient temperature and cooling water temperature can be used for this report. In this section, a classic operation profile is described as well as the SFOC per load.

2.3.1 Ship Operation Profile

During its operation the ship may face bad weather and/or significant head winds. This will increase the resistance of the surrounding environment and force the ship to increase the propulsion power to maintain constant speed. Therefore, when determining the necessary engine power it is common practice to add an extra power capacity of about 15%, and set the design load at 85% of MCR (Maximum Continuous Revolution) [Diesel&Turbo, 2013a]. Thus, full-load will not be the best operational choice.

Figure 2.10 shows a typical operational profile. It is assumed that the number of hours at sea represents 75.3% of the year [Tveitaskog, 2013].

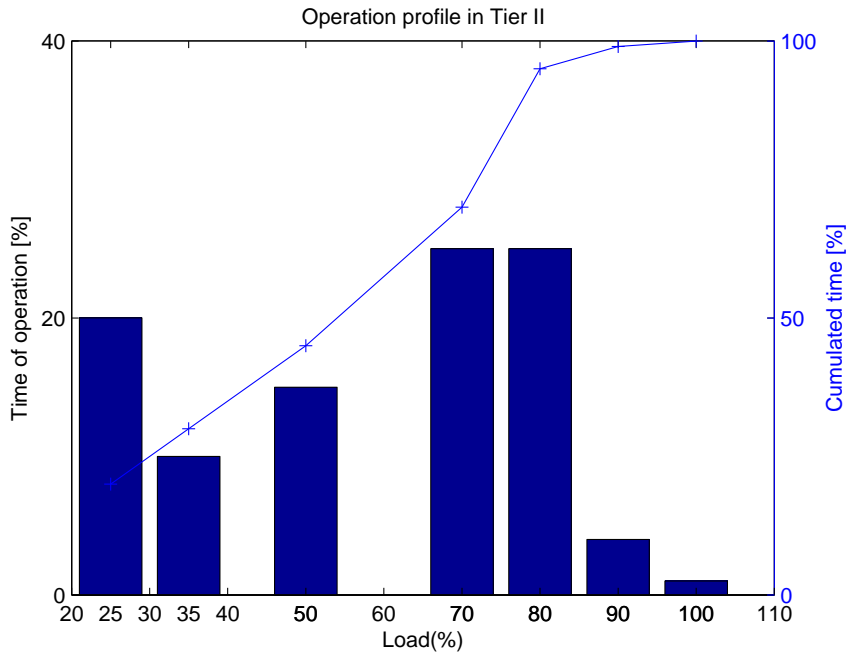


Figure 2.10: Time of operation repartition over the load [Tveitaskog, 2013].

Figure 2.10 shows that approximately half of the operation occurs between 70% and 80% load. The ship operates at 90 and 100% less than 5% of the time. The load has therefore to be considered for analysis.

It is considered that the ship will run for a total of 2000 hours per year in Tier III conditions. The load repartition over this period of time is shown in Table 2.1 [Tveitaskog, 2013].

Load	Repartition	Number of hours
25 %	15%	300
50%	15%	300
75%	50%	1000
100%	20%	400
Total	100%	2000

Table 2.1: Operation profile in Tier III. [Turbo, 2013]

2.3.2 Consumption profile

It has been shown in Section 2.3.1 that the ship is mainly operated between 70 and 80% load. Thus manufacturers are designing the engine to have an optimal consumption over this operation part. Reducing the design operation load more and more is a relatively new concept. In the past engines were designed for 85-90 % MCR. Figure 2.11 shows the SFOC (Specific Fuel Oil Consumption) in g/kWh for 25°C ambient temperature with the 9S90ME-C9.2 engine [Diesel&Turbo, 2013a]. The implementation of a cut-out system will reduce the consumption at low load by lowering the heat losses and improving the

compression of the scavenge air. Cut-out will not be used for load higher than 50%. Once the Tier II cut-out is not used anymore the fuel consumption penalty is less significant. Overall, the penalty is in a range of 2 g/kWh to 7 g/kWh at 50% load.

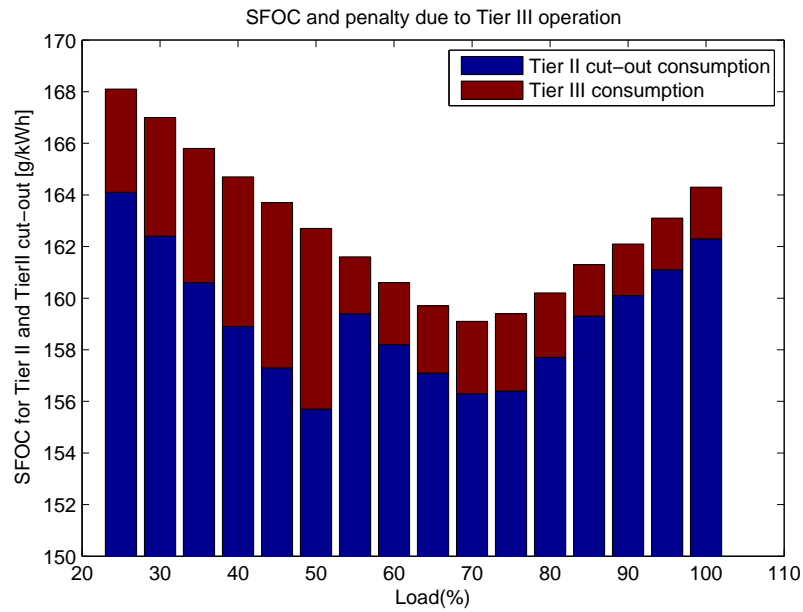


Figure 2.11: SFOC as function of the load and fuel penalty by switching to Tier III operation [Tveitaskog, 2013].

Problem Statement 3

The project investigates the influence of EGR on the feasibility of WHRS. The changing properties of the exhaust gas is modelled and used in the design of the exhaust gas WHRS. The focus of the project will be to study the feasibility and maximizing the power regeneration, while meeting Tier III requirements in ECAs.

Goals

- Estimate influence of EGR on exhaust gas properties.
- Check the compliance with Tier II and Tier III emissions.
- Optimize WHRS design for operational profile and on/off EGR operation.
- Optimize the power savings.
- Determine CO₂ savings and EEDI improvement with WHRS.
- Determine feasibility of WHRS under constraints of EGR.
- Evaluate the impact of different operation profiles on the feasibility.

Project Strategy

- Model a fuel equivalent to the HFO.
- Model the engine combustion and exhaust gas content using Cantera.
- Determine the degree of EGR required to reach Tier III for operational loads.
- Set up WHRS design model in MATLAB with and without EGR.
- Set up WHRS performance model in MATLAB with and without EGR.
- Optimizing the system and comparing with MAN data using MATLAB.
- Apply various operational profiles and draw conclusions.

Limitations

- HFO will be modelled as a combination of various fuels to meet its properties.
- Crossover of air in the combustion chamber is not taken into account.
- Combustion will be modelled at equilibrium.
- EGR amount as well as few other parameters values over the load are given by MAN.
- The steam turbine will be separated into a low and a high pressure turbine.
- Heat exchanger properties are considered as constant and given.
- The EEDI will be calculated for standard ship equipped with the power of the main engine.
- No financial perspectives will be taken into account.

Part I

Exhaust Gas and Recirculation

HFO Combustion for Tier II

Application 4

The following chapter will identify the chemical composition of HFO used in Tier II. A way to model the HFO is explained. The influence of the equivalence ratio on the adiabatic flame temperature on harmful gases mole fraction is shown. The exhaust gas composition is also detailed.

4.1 Fuel Composition

This section is based on a previous project issued by the authors [M&M, 2013]. The fuel consumed by large container ships for combustion is called Heavy Fuel Oil (HFO). According to the norm ISO 8217, HFO is: *A residual oil from distillation and/or the cracking system of natural gas processing and serves as fuel for marine diesel engines.* The HFO category includes both finished products and the primary refinery streams from which they are blended. It is highly viscous and may contain some unwanted residuals.

HFO composition is complex to determine. However, according to the statistical method [Condra, 2013], the mass fraction of chemical constituents can be calculated as follow:

$$(4.1) \quad \gamma_C = 0.64241 + 0.00505 \cdot LHV$$

$$(4.2) \quad \gamma_H = -0.22426 + 0.00826 \cdot LHV$$

$$(4.3) \quad \gamma_O = 0.27603 - 0.00628 \cdot LHV$$

$$(4.4) \quad \gamma_S = 0.30582 - 0.00702 \cdot LHV$$

Nitrogen, due to the low concentration in the fuel ($< 0.34\%$) is neglected. Considering a LHV of $42 \frac{\text{MJ}}{\text{kg}}$ [J.Moldanova, 2009], the mass fraction values of the components can be found in Table 4.1. In this study, the fuel composition will be simplified to a carbon chain of the form $C_xH_yO_zS_w$ with x, y, z and w as the number of atoms of Carbon, Hydrogen, Oxygen and Sulfur respectively. Since the fuel is used inside and outside ECAs, the Sulfur content will be sufficiently low to satisfy the Tier III regulation. For each element X, the mole fraction can be found as shown in Equation 4.5.

$$(4.5) \quad Y_X = \frac{n_X}{n_{tot}}$$

Solving a system with Equation 4.5 for each component, a relation between the coefficients x, y, z and w can be found. Quantities are summarized in Table 4.1.

Element	Mass Fraction (%)	Number of atoms per Carbon (-)
Carbon	84.57	1
Hydrogen	10.89	1.54
Oxygen	2.27	0.02
Sulfur	2.27	0.01

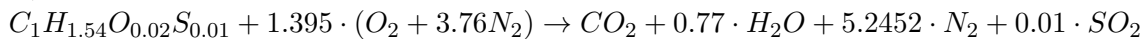
Table 4.1: Fuel Composition.

Setting a value $x = 1$ for the number of carbon moles, the composition of the fuel can be simplified as $C_1H_{1.54}O_{0.02}S_{0.01}$. The corresponding molecular weight of fuel will be 14.18 kg/kmol. This is representative of the fuel used outside of ECAs.

4.2 Stoichiometric Conditions out ECAs and Air to Fuel Ratio

The fuel will be mixed with air and then burned. The main stoichiometric chemical equation is shown in Equation 4.6 [Turns, 2000].

(4.6)



The air to fuel ratio represents the mass of air compared to the mass of fuel used during the combustion. It is defined as shown in Equation 4.7.

$$(4.7) \quad (A/F)_{stoic} = \left(\frac{m_{air}}{m_{fuel}} \right)_{stoic}$$

$$(4.8) \quad (A/F)_{stoic} = 13.51$$

However it is very common to use more air than the stoichiometric conditions in order to reduce the adiabatic flame temperature. The notion of excess air ratio is defined by Equations 4.9. Equation 4.10 shows the equivalence ratio [Turns, 2000].

$$(4.9) \quad \lambda = \frac{(A/F)_{actual}}{(A/F)_{stoic}}$$

$$(4.10) \quad \phi = \frac{1}{\lambda}$$

4.3 Fuel Model

To obtain accurate properties of the exhaust gas, the combustion and its characteristics are modelled. Different software more or less complex and accurate are available on the market to do such a model, however most of them are not freely available. The software Cantera is freely available online, and can be used to model combustion. It was successfully linked with MATLAB and REFPROP to simplify further use of the exhaust gas composition. Mechanisms can be found online and converted into a Cantera user format to model the different reactions and properties.

The mechanism used to model the fuel combustion is of great importance since it has to include Sulfur radicals and appropriate fuels. Mechanisms for long carbon chains include a very long list of different possible reactions, which can make simulation extremely slow. Moreover, most of the long carbon chains mechanisms do not include sulfur. Since SO_x are of interest, those mechanisms are not suited to this study.

A mechanism including various smaller fuels and Sulfur has been found online called the Glassman mechanism [GALCIT, 1997] [Glassman, 1996]. However this mechanism does not include long carbon chains. The information about the fuel to model are: The LHV, the Carbon to Hydrogen ratio and the Carbon to Oxygen ratio. They are all described in Section 4.1. In order to model the fuel, three different fuels with shorter carbon chains are going to be used. It will be assumed that the fuel can be approximated as a mixture of Methanol, Acetylene and Propane. A system of three equations with three unknowns (being the fraction of each fuel in the global mixture) can be set up to reach the good LHV, C/H ratio and C/O ratio. An extra amount of Sulfur can be added to the mixture to reach the appropriate amount of each element in the fuel evaluated in Section 4.1.

The composition of the modeled fuel is shown in Table 4.2.

Molecule	LHV [MJ/kg]	C/H ratio	C/O ratio	Mole Fraction
Methanol	19.92	1/4	1/1	0.2078
Acetylene	48.28	1/1	-	0.7489
Propane	46.34	3/8	-	0.0433
Average/Total	42.0	1/1.54	1/0.02	1

Table 4.2: Modeled fuel composition.

The resulting specific heat at constant pressure is 1.68 kJ/kg·K which is consistent data on fuel properties for heavy diesel in gaseous phase (1.7 kJ/kg·K) [Heywood, 1988].

4.4 Combustion Conditions

The conditions for combustion will change as a function of the load. MAN provides the mean effective pressure for most of its engines. However this pressure is not representative of the conditions when the combustion occurs since the piston will compress the fuel-air mixture to a very high pressure. Data have been gathered for a smaller engine at different loads. Figure 4.1 shows the temperatures and pressures for varying the crank angle of a smaller engine. It is assumed that the pressures are similar to the case study engine. The data provided are for an excess air ratio of 3.2.

Data from the same engine are also gathered at different load. The impact on the temperature is not extremely significant but the pressures changes drastically from 25% load to 100% (lower load implying lower pressure). From Figure 4.1 it is assumed that the equilibrium can be modeled further in this section with a pressure of 140 bar and 800 K. These values will be considered as the conditions just before ignition. However since the data from Figure 4.1 are for a smaller engine, it is possible that they can differ from real values of the case study engine.

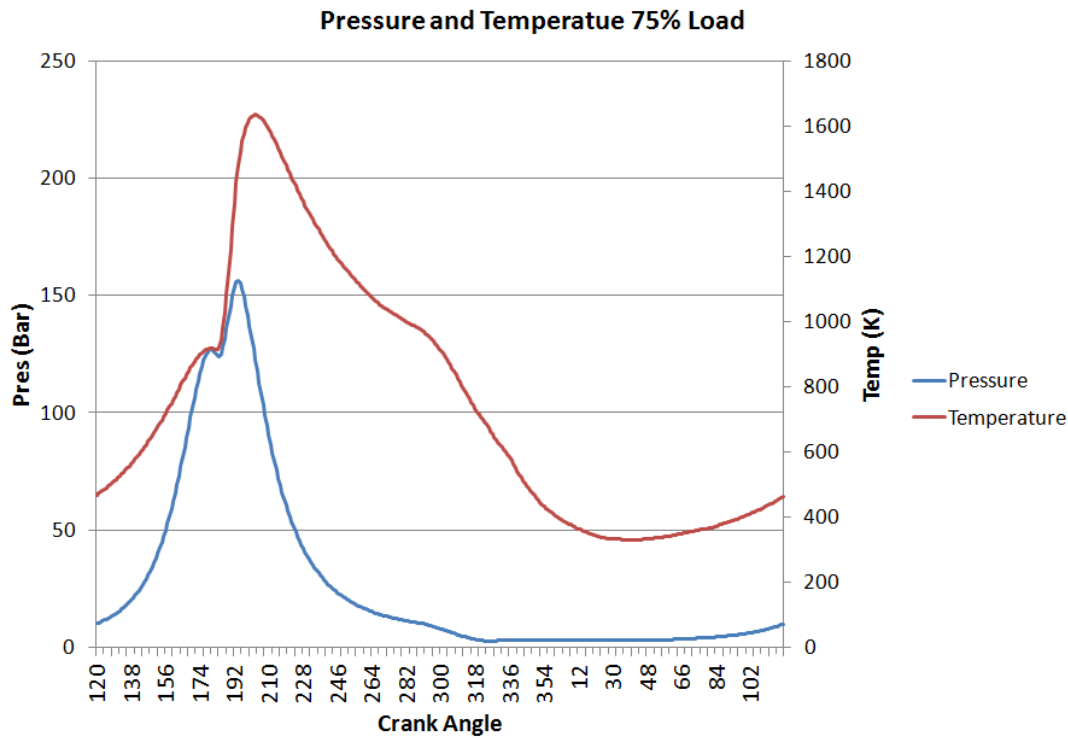


Figure 4.1: Example of measured pressure and temperature as function of the crank angle.

4.5 Impact of Excess Air Ratio on the Combustion

The excess air ratio will have an impact on various aspects of the combustion. This section will introduce them. All figures are made with Cantera Software linked to MATLAB using the Glassman mechanism [Glassman, 1996].

4.5.1 Dissociation

Dissociation is the result of molecules breaking due to high kinetic energy. Due to this energy, the molecules will vibrate and, in certain conditions, dissociate. Therefore for high temperature conditions, such as during the combustion, the products will not only include ideal molecules but also radicals. For example, dissociation is the reason for the appearance of CO molecules (the CO_2 will for example dissociate into CO and O_2). It will be shown in this section that the equivalence ratio ϕ will have an impact on the adiabatic flame temperature and therefore on the combustion products.

4.5.2 Adiabatic Flame Temperature

Figure 4.2 shows the adiabatic flame temperature of the mixture as a function of various ϕ values for an initial equilibrium temperature of 800 K and a constant pressure of 140 bar. While these conditions cannot be used for the real combustion, they can show the influence of the amount of air in the mixture.

The adiabatic flame temperature will rise drastically until it reaches its maximum value after stoichiometric conditions. The temperature then decreases in fuel-rich conditions. Therefore, the lower the equivalence ratio is (i.e. the more air is present in the combustion

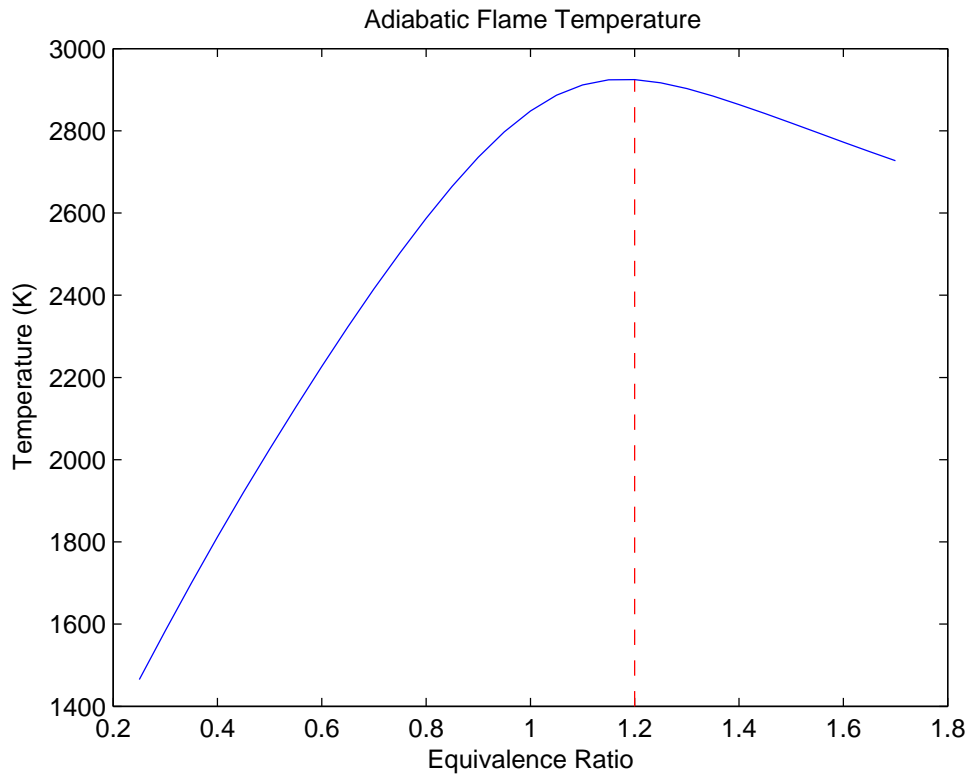


Figure 4.2: Adiabatic flame temperature as function of the equivalence ratio including dissociation.

chamber), the lower the temperature. Thus, lower flame temperature is of interest since the surrounding material may not be capable of containing the extremely high temperature.

4.5.3 Influence on Emissions

Figure 4.3 shows the molar concentration of the harmful gases under the same combustion conditions as in Section 4.5.2. The molar concentrations are shown per concentration of Argon, to account for dilution. The Argon will not react with any of the other component during the combustion and therefore its amount will not change. This is useful in demonstration for the impact of the excess air ratio on the formation of molecules, without having to account for the additional quantity of air present in the reaction. The calculation procedure is shown in Equation 4.11.

$$(4.11) \quad \frac{n_X}{n_{tot}} \cdot \frac{n_{tot}}{n_{Ar}} = \frac{n_X}{n_{Ar}}$$

As it can be seen on Figure 4.3, the main noticeable variation concerns the CO mole fraction. It increases quickly with the equivalence ratio. The CO₂ seems to increase until the stoichiometric condition. Lean conditions seem more suitable to reach low CO_x fractions.

NO_x fractions will increase until an equivalence ratio of 0.8 and then decrease again. Lean conditions again achieve low NO mole fractions due to lower temperature.

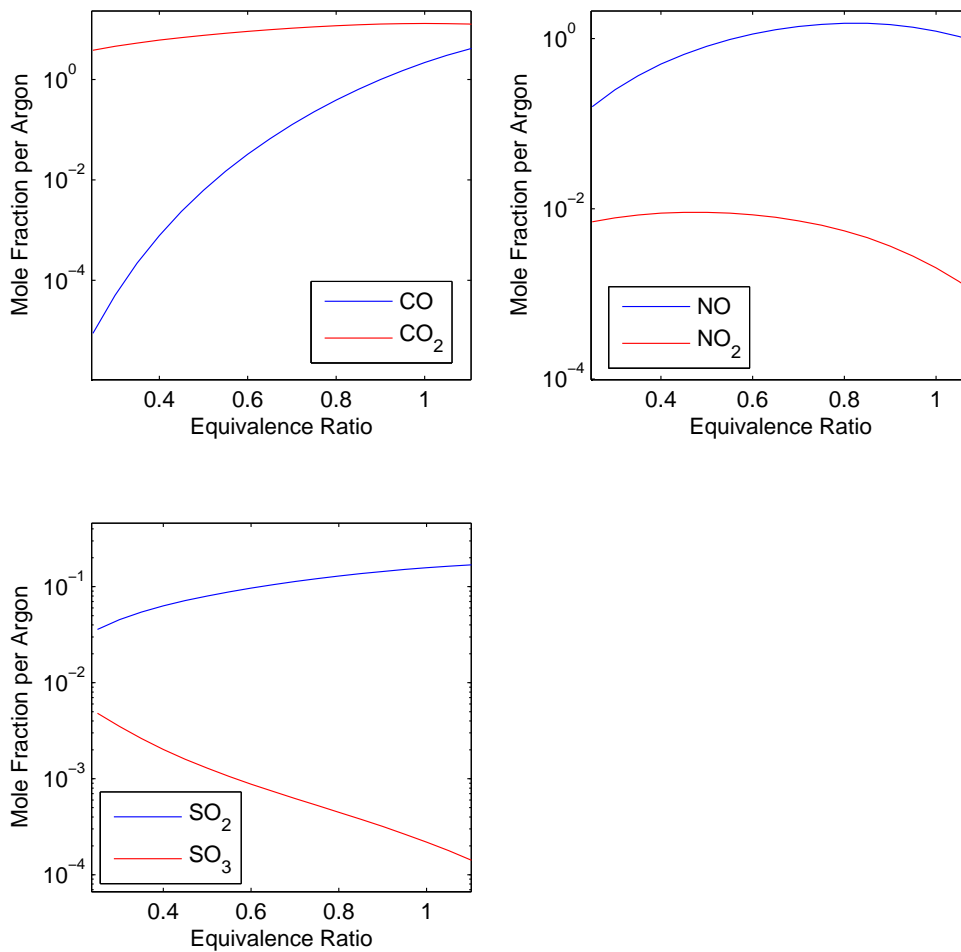


Figure 4.3: Mole fractions of CO_x, NO_x and SO_x per Argon as function of the equivalence ratio ϕ .

The SO_x follows a different pattern in that the SO₃ mole concentration decreases when the mixture get richer. However the SO_x emissions are mainly controlled by the sulfur content of the fuel or by a system of scrubbing and not by trying to play on the combustion parameters.

4.6 Exhaust Gas Composition without Dissociation

MAN provided data for the amount of exhaust gas as function of the load of the engine. Figure 4.4 shows the amount of exhaust gas given by MAN compared with various amounts calculated by the model for different excess air ratio assuming conservation of mass.

From Figure 4.4 it seems that the excess air ratio is not constant over the range of operating loads. The value varies between an excess air ratio of 3.5 to 4. The real excess air ratio might be lower than this value. Indeed when the exhaust is pushed out of the

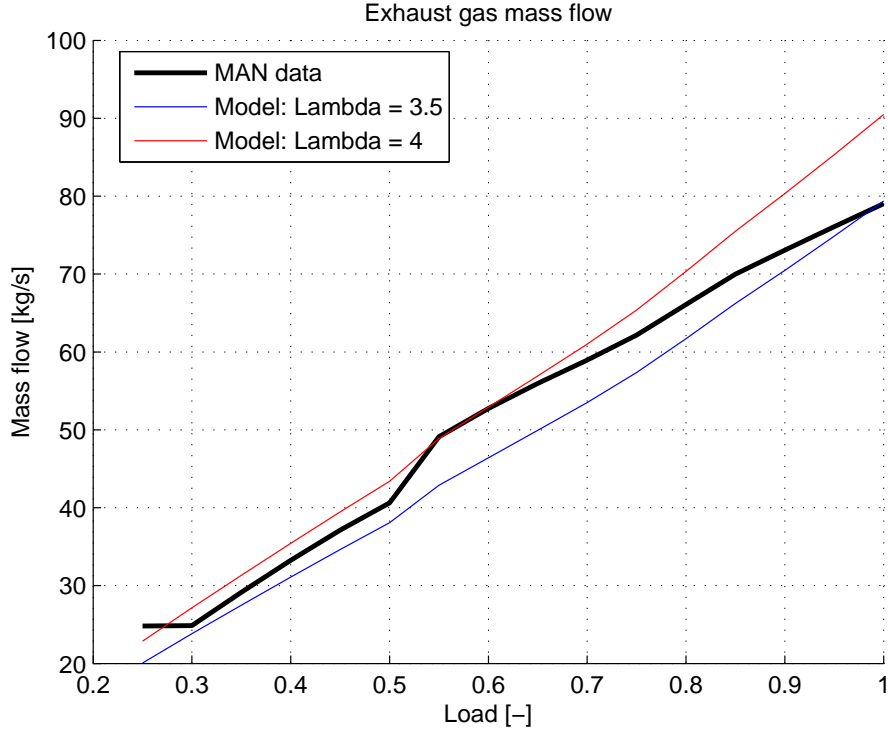


Figure 4.4: Exhaust gas mass flow as function of the load.

cylinder by the fresh air, a part of the fresh air is directly evacuated from the combustion chamber and will not take part in the combustion. For the model it will be assumed that only 90% of the air entering in the combustion chamber will actually participate in the combustion itself.

Table 4.3 shows the exhaust gas composition computed with Cantera. This composition is evaluated for the previously stated HFO with a medium excess air ratio value of 1/3.75 and assuming 90% of the air participating in the combustion. It does not include exhaust gas recirculation or dissociation. The composition will be used to determine the thermodynamic properties of the exhaust gas in Tier II applications, for waste heat recovery with the REFPROP software.

Molecule	Mass Fraction
Ar	0.0097
CO ₂	0.0403
N ₂	0.7700
O ₂	0.1500
H ₂ O	0.0298
SO ₂	0.0002
Total	1.0000

Table 4.3: Exhaust gas composition computed with Cantera.

4.7 Tier II Outlines

In this chapter it has been shown that the HFO used in Tier II condition can be written as $C_1H_{1.54}O_{0.02}S_{0.01}$. The sulfur mass fraction respects the MARPOL convention for Tier II application. The equivalence ratio has an influence on the adiabatic flame temperature. Indeed the leaner the mixture is, the lower the adiabatic flame temperature will be. The equivalence ratio also influences the molar fraction of the harmful gases, with lower value achieved in leaner conditions for CO_x and NO_x . Due to the varying excess air ratio, a mean value of 3.75 has been taken for evaluating thermal properties. The mass fractions for the main components of the exhaust gas is found by computing the combustion with Cantera. The thermodynamic properties are then computed with REFPROP software and will be used for further calculations.

HFO Combustion and EGR

for Tier III Application

5

The following chapter will explain the purpose and concept of exhaust gas recirculation. The composition of the mixture of exhaust gas, fresh air and fuel is described. The influence of recirculation on the combustion and on the exhaust gas properties is studied. The final composition for the recirculation case study is shown as well as the properties.

5.1 Exhaust Gas Composition Including EGR

This model is based on a method described in [Heywood, 1988] for hydrocarbon combustion. A re-arrangement has been made to fit to the alcohol-hydrocarbon combustion initially neglecting dissociation. Every molar composition will be expressed per mole of O₂ reactant.

5.1.1 Fuel Composition in ECAs

When operating in the ECAs, it is assumed that the fuel will have a sulfur content low enough to respect the Tier III regulation (see Appendix B). To simplify, it will be noted as CH_xO_yS_z with x, y and z being the ratio to Carbon for Hydrogen, Oxygen and Sulfur respectively.

5.1.2 EGR Definition

Exhaust gas recirculation recycles a part of the exhaust gas, bringing it back to the combustion chamber. By doing so, the fresh mixture (new fuel and fresh air) will be diluted and NO_x emissions can be controlled.

In this report the percentage of EGR will be defined as the percent of the total intake mixture which is recycled as shown in Equation 5.1.

$$(5.1) \quad EGR(\%) = \left(\frac{\dot{m}_{EGR}}{\dot{m}_i} \right) \cdot 100$$

The definition shown in Equation 5.1 is related on the total mass input for the combustion. However, MAN uses a different definition, which is related to the mass flow for the waste heat recovery. MAN's definition is shown in Figure 5.2.

$$(5.2) \quad EGR^*(\%) = \left(\frac{\dot{m}_{EGR}}{\dot{m}_{egr} + \dot{m}_{air}} \right) \cdot 100$$

The link between the two definitions is shown in Equation 5.3.

$$(5.3) \quad EGR(\%) = \left(\frac{m_{air} \cdot EGR^*}{(1 - EGR^*) + m_{stack}} \right) \cdot 100$$

Figure 5.1 shows the main principle of exhaust gas recirculation. A more detailed figure including all the components can be found in Section 2.2.4 Figure 2.8.

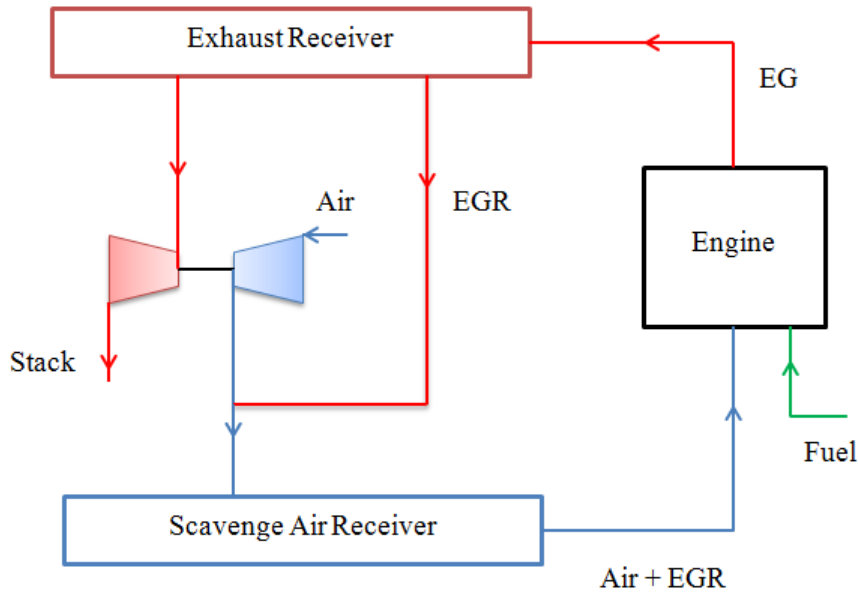


Figure 5.1: System sketch.

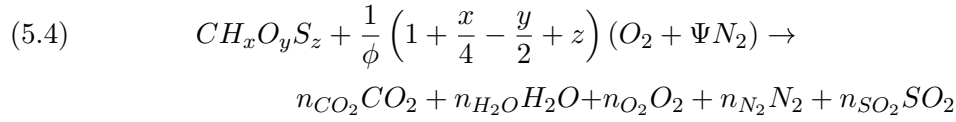
It has to be noted that in some literature, the EGR is alternatively defined as the ratio between the mass of EGR over the mass of fuel and air.

5.1.3 Exhaust gas Composition Including EGR in ECA

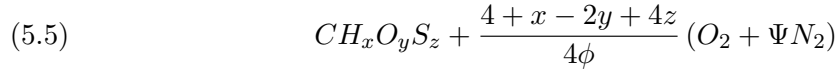
During the operation the amount of exhaust gas recirculation might change, impacting the exhaust gas content and thus its thermodynamics properties. It is then important to be able to evaluate the main characteristics of the exhaust gas for various percentages of EGR.

Burned Gas Composition

If Ψ is the molar ratio between Nitrogen and Oxygen (3.76 for air), the fuel combustion can be written as shown in Equation 5.4. Any radicals are not considered.



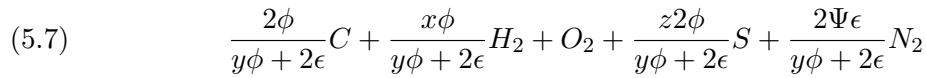
The reacting mixture can therefore be written as



By defining the coefficient ϵ as shown in Equation 5.6,

$$(5.6) \quad \epsilon = \frac{4 + x - 2y + 4z}{4}$$

the reactant mixture can be re-written as function of the number of O_2 in Equation 5.7, which facilitate the calculations for various excess air ratios.



For lean and stoichiometric mixtures ($\phi \leq 1$) the CO and H_2 amount can be neglected with regard to the thermodynamic properties of the resulting exhaust gas. Table 5.1 describes the burned gas composition under 1700 K by mole of O_2 not including dissociation. [Heywood, 1988]

Element	mole/mole O_2 reactant
CO_2	$2\phi/(y\phi + 2\epsilon)$
H_2O	$x\phi/(y\phi + 2\epsilon)$
O_2	$1 - \phi$
SO_2	$z2\phi/(y\phi + 2\epsilon)$
N_2	$(2\Psi\epsilon)/(y\phi + 2\epsilon)$
Total	n_b

Table 5.1: Burned fuel composition without EGR. No dissociation.

Unburned Mixture Diluted with EGR

Now that the burned mixture composition has been determined, it needs to be recirculated into the fresh one. The new mixture will be composed of recycled exhaust gas, fresh air, and fuel. If the composition is still written as per number of mole of O_2 , the amount of fresh fuel in the mixture will be dependent on the molecular weight. The molecular weight can be calculated as shown in Equation 5.8.

$$(5.8) \quad M_f = (12 + x + 16y + 32z)$$

x_b represents the burned gas fraction in the fresh mixture such as

$$(5.9) \quad x_b = \frac{EGR}{100}$$

Before being recycled, it is assumed that the exhaust gas is treated to reduce the sulfur content. The unburned mixture fuel, air, and burned fuel can then be written as in Equation 5.10. The new fuel and air is considered pre-mixed in the equation, which is not the case for real applications.

$$(5.10) \quad \underbrace{(1 - x_b) \left[\frac{\phi}{\epsilon M_f} (CH_x O_y S_z) + O_2 + \Psi N_2 \right]}_{\text{Air+Fuel}} + \underbrace{x_b (n_{CO_2} + n_{H_2O} + n_{O_2} + n_{N_2})}_{\text{Exhaust}}$$

The number of moles of each species in the unburned mixture before combustion can be found in Table 5.2. The fuel representing the fresh fuel and every other composition, the molar content of the exhaust gas and fresh air.

Element	mole/mole O_2 reactant
Fuel	$(1 - x_b)(\phi/\epsilon M_f)$
O_2	$1 - x_b \phi$
N_2	$(2\Psi\epsilon)/(y\phi + 2\epsilon)$
CO_2	$(x_b 2\phi)/(y\phi + 2\epsilon)$
SO_2	0
H_2O	$(x_b \phi)/(y\phi + 2\epsilon)$
Total	n_u

Table 5.2: Unburned mixture composition.

5.2 Excess Air Ratio for Tier III Conditions

MAN provides the amount of exhaust gas for the Tier III conditions. Assuming a conservation of mass as done in Section 4.6, Figure 5.2 shows the mass flow for various excess air ratio in Tier III .

A mean value for excess air ratio is less easy to identify than in Tier II applications. However it seems that a λ value of 3.75 still fits to evaluate the thermodynamics properties.

5.3 Influence of EGR on Adiabatic Flame Temperature

The amount of exhaust gas recirculated to the combustion chamber will have an influence on the adiabatic flame temperature. Indeed the fuel will be diluted which in itself will

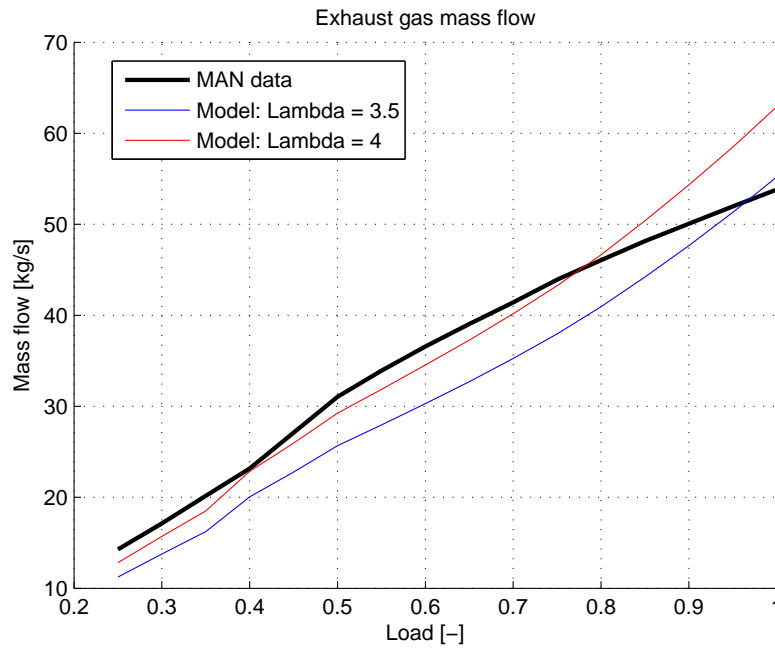


Figure 5.2: EG mass flows as function of the load for Tier III.

decrease the adiabatic flame temperature. However the other interest of EGR will be to increase the heat capacity of the gases and therefore decrease the combustion temperature. This will have an impact on the amount of dissociation and will be discussed later.

Figure 5.3 shows the impact of recirculation on the adiabatic flame temperature for various EGR percentages. The initial conditions are taken at an excess air ratio of 3.75, an initial temperature of 700 K and a constant pressure of 140 bar. A part of the exhaust calculated at equilibrium is recirculated to a new combustion.

It can be noted that the temperature is highly influenced by the dilution with exhaust gas by almost 200 K for 10% to 40%.

5.4 Influence of EGR on Dissociation

The variation in temperature due to the EGR will have an influence on the dissociation. Figure 5.4 shows the variation of mole fraction per Argon at equilibrium for the SO_x . The influence on NO_x will be studied more extensively in Chapter 6. The initial conditions for the combustion are the same than in Section 5.3.

From Figure 5.4 it can be seen that the EGR has a noticeable influence on the SO_2 formation. The fractions of SO_2 will decrease with the recirculation. However it seems that the SO_3 will increase drastically with the EGR. For Tier III applications, it is assumed that the sulfur content is taken care of by the use of a scrubber to reach the MARPOL regulation inside ECAs.

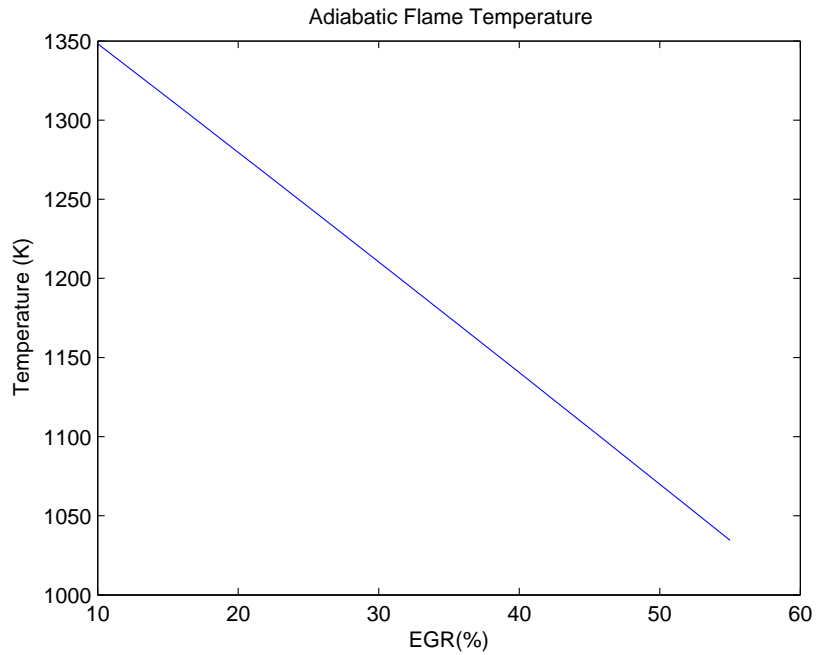


Figure 5.3: Influence of EGR on the adiabatic flame temperature.

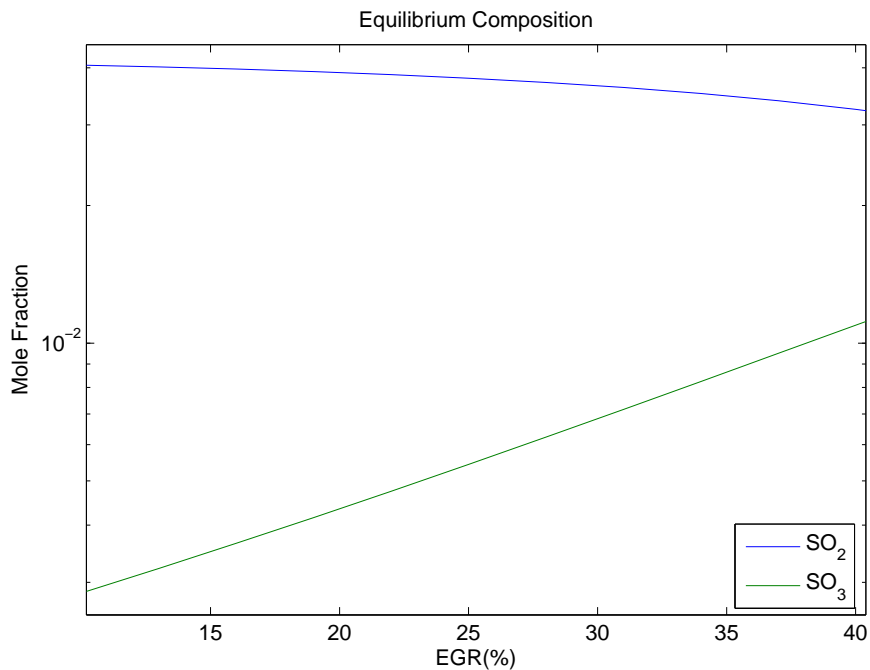


Figure 5.4: Influence of EGR on SO_x mole fractions per Argon.

5.5 Exhaust Gas Composition and Properties

Figure 5.5 shows the amount of EGR used as function of the load. The data were provided by MAN.

It can be noted that the percentage of EGR is never less than 30 % during operation. The maximum amount of recirculation is 43 % at minimum load.

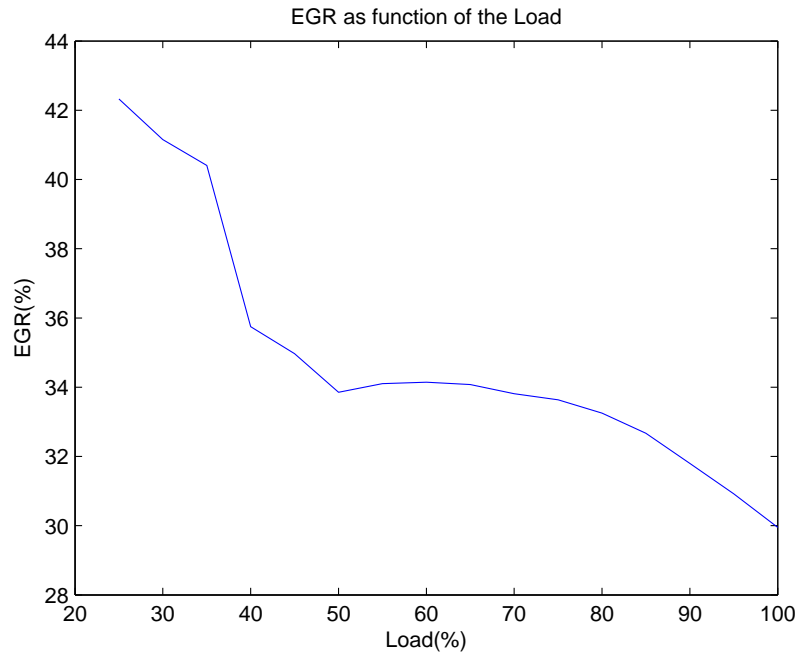


Figure 5.5: Recirculation percentage as function of the load.

After computing the combustion with EGR within 30 and 45 % it has been noticed that the composition in terms of mass fractions for the main components do not change significantly. Therefore, in order to be able to model the exhaust gas thermodynamic properties, it has been assumed that an average exhaust gas composition could be taken.

Data provided by MAN shows that the EGR is always used in a range from 30 % to 43 %. Thus the median is made at 36.5 % recirculation. As shown in Section 5.2 a equivalence ratio of 1/3.75 can also be taken. Table 5.3 shows the composition of the exhaust gas used to calculate the exhaust gas thermodynamic properties at 300 K and 1 bar with Cantera software.

Propriety	Value per kg
Enthalpy	-754273 J
Internal energy	-840087 J
Entropy	6504 J/K
Gibbs function	-2.70548e+6 J
Heat capacity c_p	1014.25 J/K
Heat capacity c_v	728.2 J/K

Table 5.3: Exhaust gas recirculation properties in Tier III per kg.

The composition neglecting the low mass fraction element ($<1e-5$) is shown in Table 5.4.

Element	Mass Fraction
Argon	0.0095
Carbon Dioxide	0.0377
Nitrogen	0.7694
Oxygen	0.1543
Water	0.0291
Total	1.0000

Table 5.4: Exhaust gas composition computed with Cantera.

5.6 Tier III Outlines

The exhaust gas recirculation will consist of taking some of the burned gas back to the combustion chamber. The mixture of exhaust gas, air and fresh fuel will then be combusted. Recycling the exhaust gas will lower the temperature of the adiabatic flame temperature and increase the heat capacity, which will influence the dissociation. The amount of CO and SO₂ decreases with the exhaust gas percentage. In order to simplify the model further, the thermodynamics properties of the recirculated gas will be taken for 36 % recirculation which fits to the median recirculation taken by MAN. For calculating the thermodynamics properties an excess air ratio of 3.75 is taken.

NO_x Emission Control 6

The following chapter will introduce the NO_x emissions. The different mechanisms of NO and NO₂ formation are described. The influence of the excess air ratio, the intake temperature and the exhaust gas recirculation rate are studied. Estimations of the NO_x emissions for Tier II and Tier III are made and discussed.

6.1 NO_x Denomination and Formation

The NO_x are gases containing Nitrogen and Oxygen. This denomination includes the Nitric Oxides (NO) and the Nitrous Oxides (NO₂). These emissions are increasing tighter and tighter controlled by the IMO in order to avoid pollution leading to health problems and environment degradations in the concerned zones. The emission level of NO_x is one of the main requirements of the Tier III regulation. While they are not directly a part of the combustion process, they are formed in the combustion environment. Generally their concentration differs from the values calculated at equilibrium, since the gas will expand and the reaction will freeze. Thus it is complex to accurately estimate the amount of NO_x molecules released through the exhaust gas in the atmosphere. [Heywood, 1988]

The Nitric Oxides are predominant during the combustion process. The principal source of Nitrogen for the formation of NO_x molecules is the Nitrogen present in the air during the combustion. The NO will form in the flame front and the post flame gases. Since the combustion occurs at maximum compression, the front flame reaction will be extremely thin, with a short residence time. Furthermore after ignition the pressure of early gases will rise during the combustion process, and the gases will be compressed at high temperature. It will be shown later that the NO formation is highly influenced by the temperature, thus the NO formation in the post flame will dominate the flame front formation.[Heywood, 1988]

6.2 NO Formation Kinetic

6.2.1 Main Mechanisms of NO Formation

The main mechanisms of NO formation have been studied extensively in the literature. It is commonly accepted that in combustion of fuel involving Nitrogen, the Zeldovich mechanism shown in Equation 6.1 and 6.2 can be used [Turns, 2000].



It has been extended by *Lavoie et al.* with a third reaction.



The forward and reverse constants are denoted k_i^+ and k_i^- respectively with i being 1, 2 and 3 for Equations 6.1, 6.2 and 6.3 respectively.

6.2.2 NO related kinetic

By considering Equations 6.1, 6.2 and 6.3, the NO formation gradient can be written as seen in Equation 6.4.

$$(6.4) \quad \frac{d[NO]}{dt} = k_1^+ [O] [N_2] + k_2^+ [N] [O_2] + k_3^+ [N] [OH] \\ - k_1^- [NO] [N] - k_2^- [NO] [O] - k_3^- [NO] [H]$$

With each forward and reverse rate constant defined as function of the equilibrium constant, $K_{c,i}$.

$$(6.5) \quad K_{c,i} = \frac{k_i^+}{k_i^-}$$

A relation similar to Equation 6.4 can be written for $d[N]/dt$ using the same coefficients k_i^+ and k_i^- . However, since the $[N]$ is extremely low, it can be neglected and considered as in steady state. By setting $d[N]/dt$ equal to 0, and by writing $K = (k_1^+/k_1^-)(k_2^+/k_2^-)$, the NO formation rate can be written as shown in Equation 6.6. [Heywood, 1988]

$$(6.6) \quad \frac{d[NO]}{dt} = 2k_1^+ [O] [N_2] \frac{1 - [NO]^2/(K[O_2][N_2])}{1 + k_1^- [NO]/(k_2^+ [O_2] + k_3^+ [OH])}$$

The NO formation is occurring mainly in the post-flame gases (see Section 6.1). Thus, the equilibrium assumption state that the concentration of H, OH, O, O_2 and N_2 can be assumed as their equilibrium values at local pressure and equilibrium temperature. Moreover, due to the strong dependency of temperature on NO formation, it can be assumed that the early $[NO]$ is much lower than $[NO]_{eq}$, and that the reverse reaction can therefore be neglected. This leads to the simplified Equation 6.7.

$$(6.7) \quad \frac{d[NO]}{dt} = k_1^+ [O]_{eq} [N_2]_{eq}$$

K_o is the equilibrium constant for the dissociation of Di-oxygen into two Oxygen, it is given by Equation 6.8[Heywood, 1988].

$$(6.8) \quad K_o = 3.6 \cdot 10^3 \exp\left(\frac{-31090}{T}\right)$$

By using Equation 6.8 to substitute the Oxygen concentration and Di-oxygen concentration at equilibrium, the initial formation rate can be re-written by combining Equations 6.7 and 6.8.

$$(6.9) \quad \frac{d[NO]}{dt} = \frac{6 \cdot 10^{16}}{T^{0.5}} \exp\left(\frac{-69090}{T}\right) [O_2]_{eq}^{0.5} [N_2]_{eq}$$

From Equation 6.9 it can be clearly identified that the rate of formation of NO is highly dependent on the temperature. The excess air amount used during the combustion will also be an influence since it will increase the concentration of Oxygen and Nitrogen at equilibrium.

6.2.3 Influence of Temperature and Excess Ratio on NO Formation

It has been shown in Section 6.2.2 that the formation of NO is highly influenced by the adiabatic flame temperature. The adiabatic flame temperature is itself influenced by the mixture intake temperature and the amount of dilution.

From Equation 6.9, Figure 6.1 shows the formation rate of NO molecules as function of the excess air ratio (representing dilution) and intake air temperature.

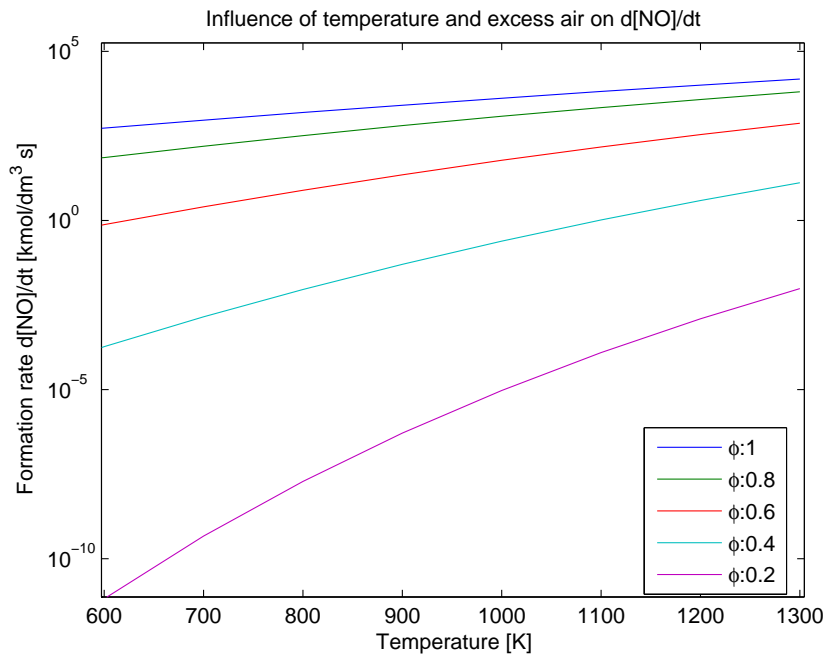


Figure 6.1: NO formation rate for various intake temperature and excess air ratio.

Figure 6.1 shows that the higher the intake temperature is, the higher the formation rate will be. This is due to a higher adiabatic flame temperature. The dilution with air will also reduce the flame temperature and therefore lower the amount of NO production via dissociation.

Figure 6.2 shows the influence of the adiabatic flame temperature on the NO formation rate calculated with the Equation 6.9.

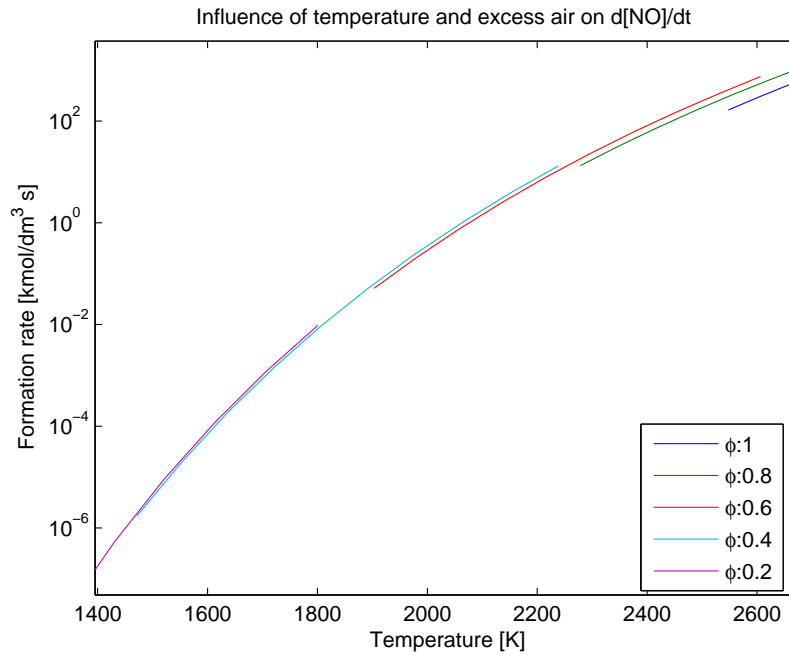


Figure 6.2: NO formation rate for various adiabatic flame temperatures and excess air ratio.

As stated earlier a higher dilution leads to a lower adiabatic flame temperature, which will reduce the NO formation rate. However, it can become problematic to compress sufficient amount of air from 1 to 3 bar to reach this dilution. An EGR system will help partially to avoid this problem.

6.2.4 Influence of EGR and Excess Ratio on NO Formation

The use of EGR has several purposes. The main aspect is to reduce the gas temperature by dilution and by increasing the specific heat capacity of the resulting mixture. This lowers the adiabatic flame temperature, thereby decreasing the amount of dissociation and therefore the formation of NO. The higher the degree of EGR, the lower the temperature and the lower the production of NO molecules. Figure 6.3 shows the NO mole fraction as function of the amount of recirculated gas. The mole fraction is normalized over the mole fraction of Argon to avoid being affected by dilution.

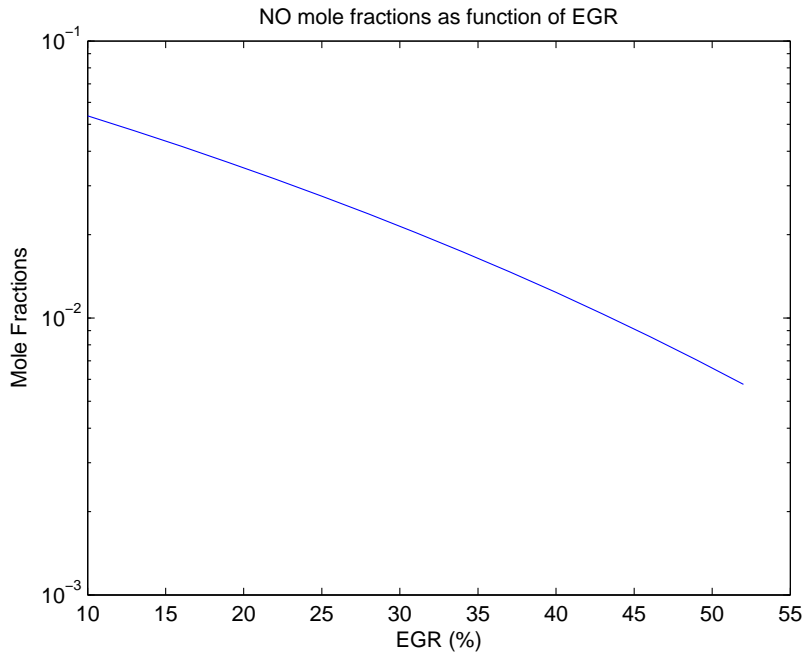


Figure 6.3: NO mole fraction as function of the EGR(%).

The NO mole fraction is lowered by a factor of 40 between 10 % and 40 % of recirculation.

6.3 NO_2 Formation

A mechanism for the NO_2 formation is shown in Equation 6.10 [Heywood, 1988].



If the NO_2 is not cooled, and sufficient Oxygen is present, NO can form by dissociation as shown in Equation 6.11.



NO_2 is part of the NO_x emissions. However the chemical equilibrium shown in Figure 6.4 shows that the ratio of NO_2/NO is extremely small for various amount of exhaust gas recirculation.

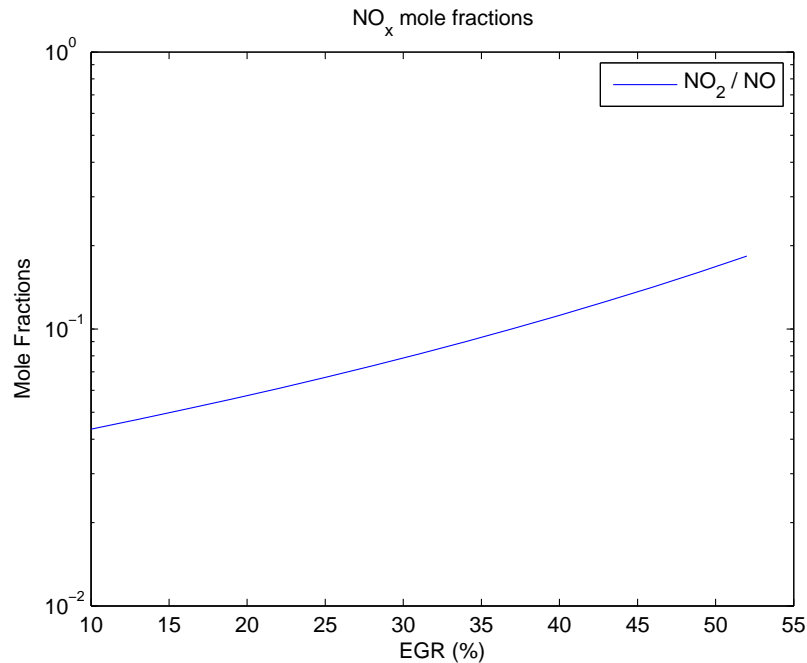


Figure 6.4: Mole fractions of NO₂ and NO at various EGR(%).

Since the NO_x emissions mainly results from NO formation, the NO₂ formation will not be studied more extensively in this report. However, it should be noted that for diesel engines, at high loads the NO₂/NO fraction can reach up to 10%.

6.4 Estimation of NO_x Emissions

The purpose of this section is to provide an estimation of the NO_x emissions for Tier II and Tier III conditions. The Tier II will be evaluated assuming TC cut-out, which has been described in Section 2.2.4 and illustrated with Figure 2.8. The results presented in this section are estimated using equilibrium under assumed conditions. Therefore, they might not accurately reflect the real emissions, but they will show the reduction trend achieved by using an EGR system.

To be as precise as possible, all emissions are modeled using MAN data regarding the amount of excess air and the amount of recirculation as function of the load. The NO_x emissions are calculated in g/kWh and shown in Equation 6.12, to be compared with the MARPOL limitations.

$$(6.12) \quad m_{NO_x} = \frac{\dot{m}_{eg} \cdot 1000 \cdot (w_{NO} + w_{NO_2})}{P_{engine}}$$

6.4.1 NO_x Emissions for Tier II

For the Tier II model, the conditions described in Chapter 4 are used. The equivalence ratio is taken as function of the load and provided by MAN. The results over the range of

loads are shown in Figure 6.5. It is recalled that in Tier II conditions, the emission limit for NO_x is 14.4 g/kWh.

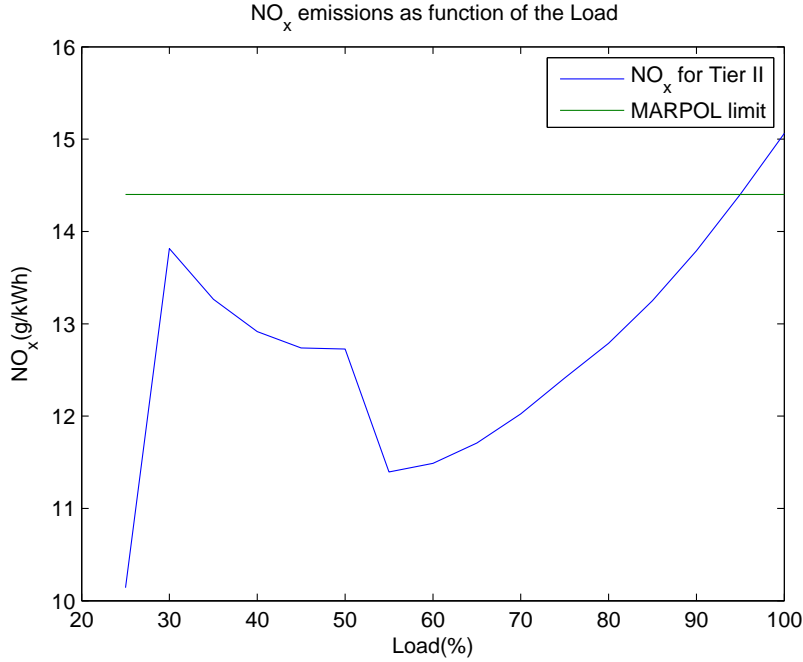


Figure 6.5: Tier II NO_x emissions.

It can be seen that the emission level is under the limitation until $\sim 95\%$ load and peak down at low load. A flatter line close to the maximum allowed value over the operation range could have been expected, and this is probably the case for an optimized system. The NO_x seems extremely low at low load, which is likely not the case in real operation. These differences are probably due to the assumptions of equilibrium. Indeed the NO_x production is closely linked to the temperature, with a higher temperature implying higher emissions. During the combustion, the temperature will reach a peak during the initial explosion. The NO concentration will follow that peak and then be reduced with the decrease of temperature, until the reaction freezes.

6.4.2 NO_x Emissions for Tier III Using EGR

Using the same method as in Section 6.4.1 and including a rate of EGR provided by MAN, it is possible to evaluate the NO_x emissions for Tier III over the load for the range of operation. It is recalled from the MARPOL convention that the amount of NO_x emissions allowed inside ECAs (i.e. in Tier III conditions) is 3.4 g/kWh. The results of the model and the MARPOL limit are shown in Figure 6.6.

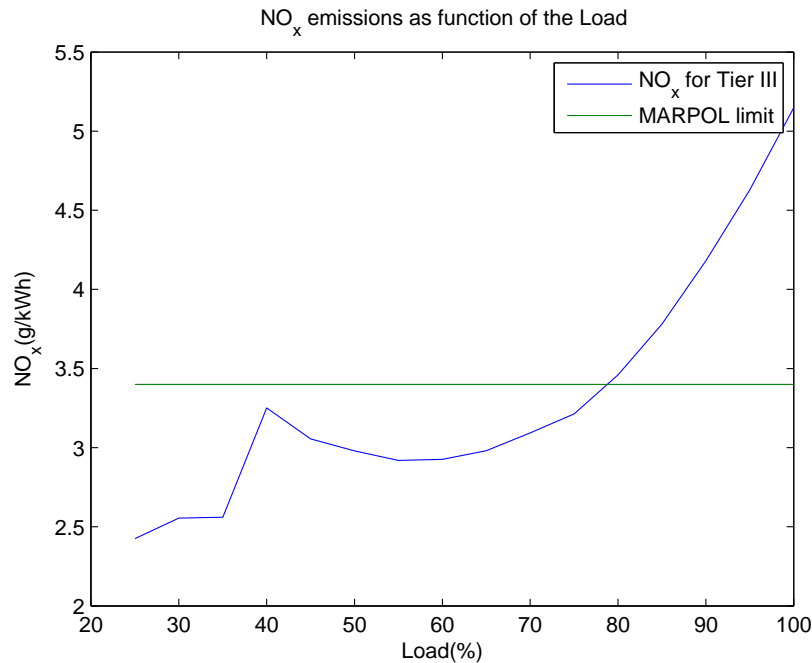


Figure 6.6: Tier III NO_x emissions.

For the Tier III model, the limit is reached at $\sim 80\%$ load. However, under that range, the NO_x emissions are much closer to the allowed limit than they were in Tier II. The peak at high load is due to the lower excess air ratio and low rate of EGR used by MAN. This will increase the temperature, which will increase the mass fraction of NO in the exhaust.

Once again a flatter line for the NO_x emissions could be expected over the range. The use of the equilibrium and maybe some engine constrains could be a reason for the difference with the presented results.

By plotting the emissions for Tier II and Tier III it can however be noted that the use of an EGR system has a significant impact on the NO_x emissions. Between Figure 6.5 and 6.6 a reduction of almost 80% in the emissions can be noted.

6.5 Discussion

This chapter has summarized the NO_x production after the combustion process. The target of this report was to demonstrate the influence of EGR on the NO_x emissions. Building an accurate model of the engine and of the resulting emissions would become an entire project in itself.

The focus has been put over the influence of various parameters on the NO_x emissions without trying to reach accurate value for the model. This decision was made due to the lack of accurate data, but also of a mechanism for large carbon chains. The influence of the equivalence ratio and of the temperature have been investigated. The influence of the EGR rate on the emissions has been illustrated to show the capacity of such a system to reduce NO_x emissions in effect. To show a trend, more than a specific value, the combustion was

estimated at equilibrium, and the initial conditions changed to calibrate in a consistent manner. Therefore results presented in this chapter might not be completely accurate, as illustrated by the inconsistency with MAN values in Figure 6.5 and 6.6, but they reflect the influence and the expected trend of various parameters by using EGR.

6.6 Conclusion

In this chapter the NO_x have been presented. The main mechanisms leading to their formation have been presented. It has been shown that the presence of Nitrogen in the air, the intake temperature, and the adiabatic flame temperature all have a large impact on the production NO_x. Using high excess air ratio will decrease the adiabatic flame temperature but will also increase the Nitrogen concentration during the combustion.

Using EGR allows the ship operator to dilute the fuel without having to use excessive amounts of air. By doing so, the adiabatic flame temperature will be decreased which will lower the emission quantities.

Given some data provided by MAN, a simulation has been made at equilibrium to evaluate the NO_x emissions and see if they were in the range of the MARPOL convention inside and outside ECA. It has been found that the values were close for the given model, even if variations are seen compared to what could be expected. An important aspect to notice, is the reduction of NO_x production due to the use of EGR. Between the Tier II and Tier III model the NO_x have been reduced by 80 %, which shows the capabilities of EGR to reach the MARPOL requirements.

Part II

Waste Heat Recovery Models

Base System 7

This chapter summarizes the working principles of a Waste Heat Recovery System, and outlines the double stage system with steam cycles used as a basis for further analysis.

7.1 Waste Heat Recovery System: General

Waste Heat Recovery extracts heat energy from the exhaust gas by heating, evaporating and superheating water in heat exchangers in the stack. Energy is converted to electricity with a turbine, where the fluid is expanded before it is condensed and process repeats. Including other heat sources available on board allows for better system performance. For example, the scavenge air for the engine requires cooling from $\sim 160^{\circ}\text{C}$ to near ambient conditions and can be used as a potential source of energy for the waste heat recovery cycles.

Before reaching the stack, the exhaust gas is first sent through a turbocharger to compress the scavenge air for the engine. Any exhaust gas, which is in excess to that needed for the compression, will be by-passed from the turbocharger and sent through a power turbine, generating electricity.

In large systems, additional cycles at different pressures can be used to increase the overall steam exergy (see Section 8.1) and thereby increase power production in the steam turbine. A system schematic of the double stage WHRS is shown in Figure 7.1. The system has already been investigated extensively in a previous project by the authors [M&M, 2013].

The output of the WHRS is the electricity produced by steam and power turbines. This will depend on the quantity of steam, the pressure/temperature at the turbine inlet, and the conditions at the turbine outlet. Some electricity is required to run the pumps in the system (mainly the feedwater pump), but the quantity power required is negligible compared to the output of the turbine.

The cycle fluid process can be described by a T-s diagram, which illustrates the states of the fluid as it progresses through the cycles. Figure 7.2 shows the T-s diagram of the double-stage WHRS using steam.

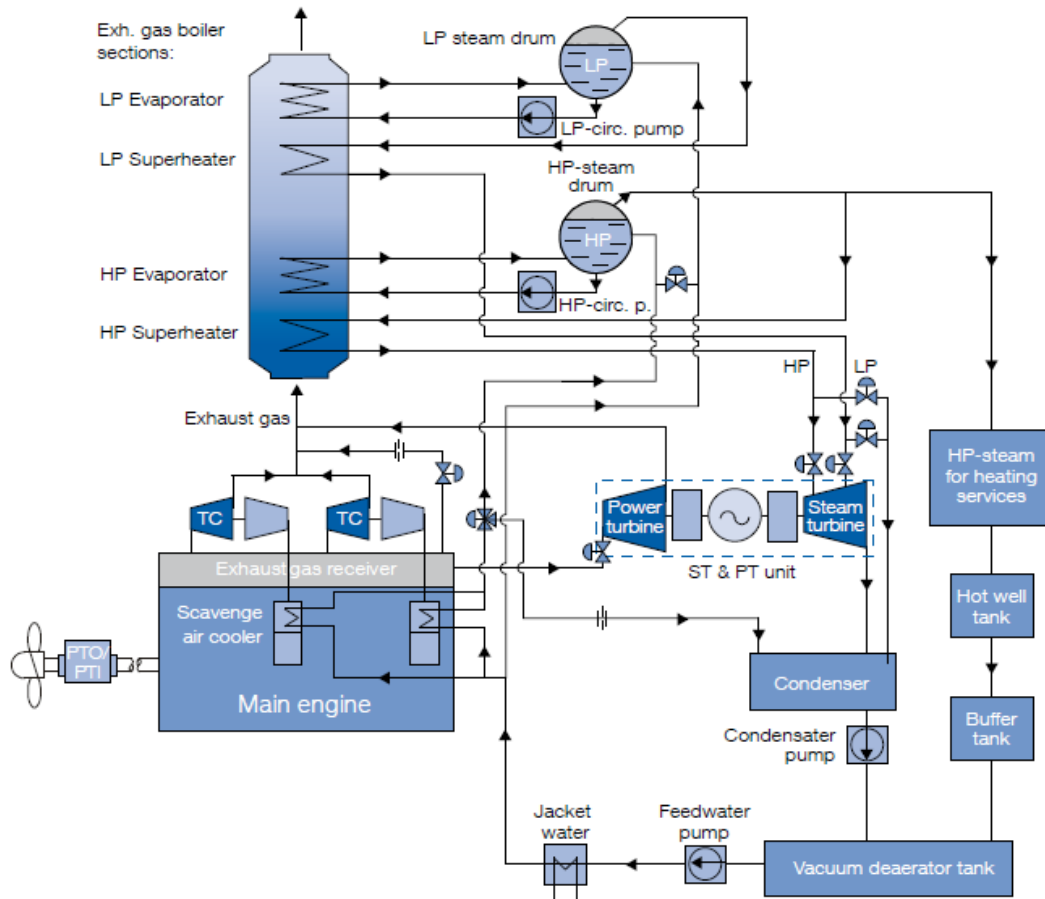


Figure 7.1: Schematic of a double stage WHRS [Diesel&Turbo, 2013a].

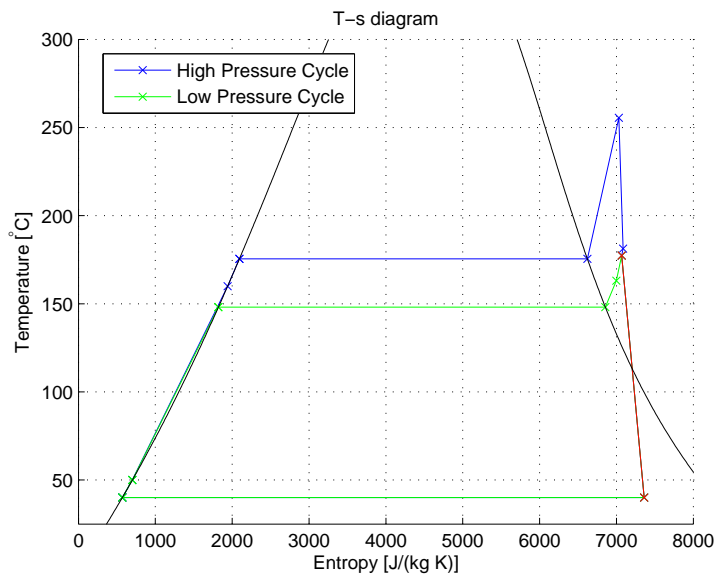


Figure 7.2: T-s diagram of a double stage WHRS [M&M, 2013].

The red line represents the mix of the high and low pressure cycles as they go through

the turbine. As seen in the T-Q diagram in Figure 7.2, the cycle fluids condenses at 40°C. Lowering this temperature would increase the turbine output, but quickly becomes problematic due to the quantity of seawater coolant required for condensation. Increasing the temperature or pressure at the turbine inlet would also increase the turbine power production. The temperature of the exhaust gas puts limitations on both pressure and temperature in the cycle fluid. This is demonstrated in the T-Q diagram in Figure 7.3

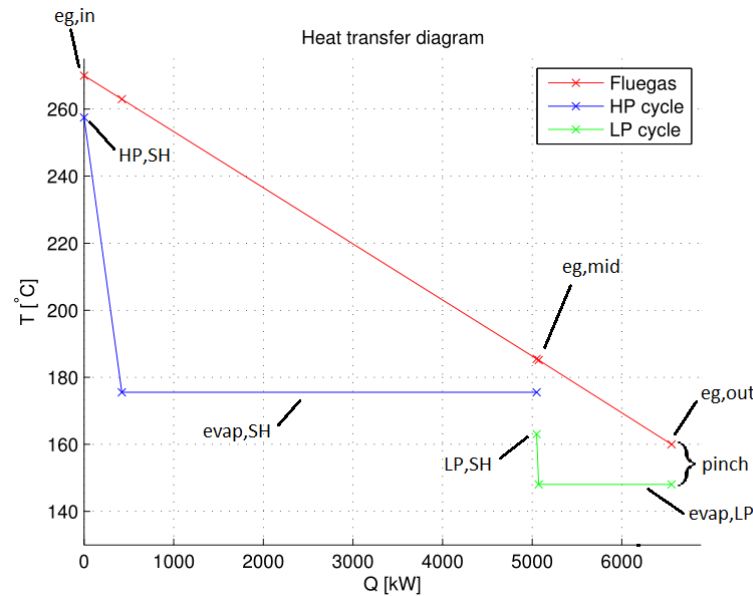


Figure 7.3: T-Q diagram example. The HP cycle was shown in Figure 7.2 [M&M, 2013].

The pressure is constrained through the evaporation temperature. A higher pressure leads to a higher evaporation temperature. Since the outlet of the stack is set at 160°C to keep all surface temperatures above sulfur condensation [Diesel&Turbo, 2012], the LP pressure cannot exceed ~ 5 bar when preheating is accomplished outside the stack. Adding another cycle means that the pressure of one cycle can be changed. Increasing the pressure in the high pressure cycle will increase the exergy in the HP cycle (See Chapter 8), but will also shift more energy to the low pressure cycle.

For any level of pressure, increasing the temperature will also increase the exergy of the steam, and increase the steam turbine power production. This superheating is limited by the inlet temperature of the exhaust gas, and a pinch of between 10 and 15 K, to avoid excessively large heat exchangers.

7.2 Stack Heat Transfer

This section will cover some of the findings of the previous project, and their implication for design/operation on the heat transfer in the stack.

For any given level of pressure, the temperature of the steam should be as high as possible [M&M, 2013]. Since the capacity flow of the cycle fluid is much smaller than that of the exhaust gas, the temperature change of the cycle fluid will be much steeper. Therefore the temperature of the outlet of the superheater will always be closer to the exhaust gas

temperature than the inlet, this can be seen in Figure 7.3. This means that given a minimum temperature difference (pinch) in the stack heat exchangers, the superheated high pressure steam can be found as Equation 7.1.

$$(7.1) \quad T_{HP,SH} = T_{eg,in} - pinch$$

A midpoint for the exhaust gas is defined, where it has passed the high pressure evaporator, this point is denoted eg, mid on Figure 7.3, and its definition is expressed in Equation 7.2.

$$(7.2) \quad T_{eg,mid} = T_{evap,HP@p_{HP}} + pinch$$

The stack process can be seen in Figure 7.3, including an assumed pressure drop in the superheater of 0.5 bar. Other heat transfers are assumed isobaric.

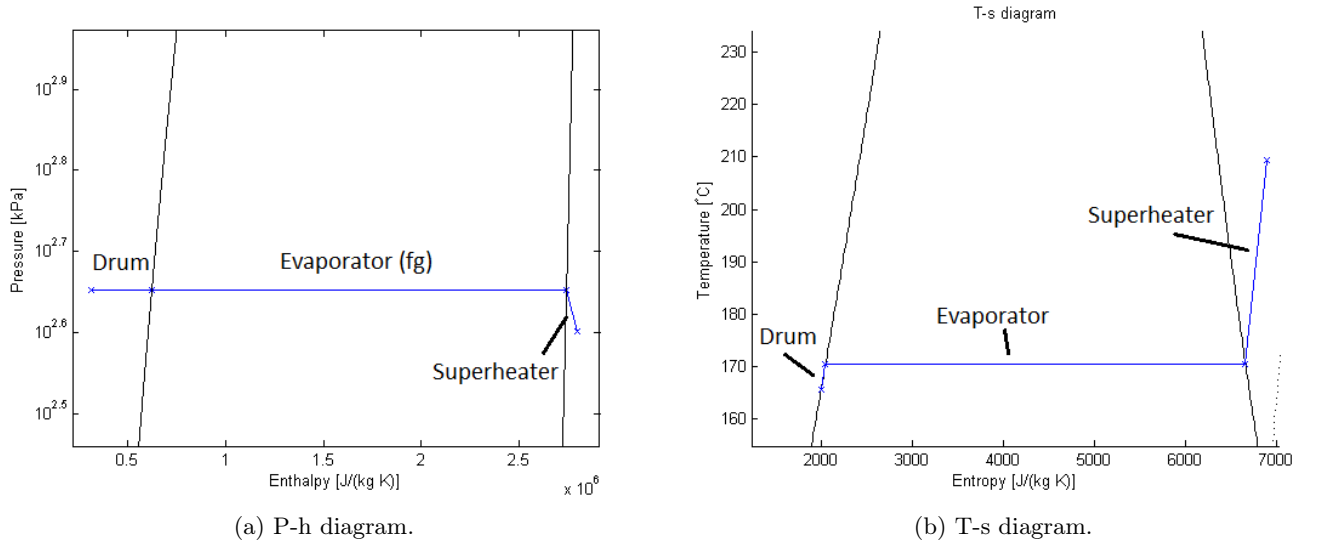


Figure 7.4: The stack heat transfer in the process diagrams.

The power transfer to the high pressure cycle can be written as an enthalpy change and a mass flow. The enthalpy change can be split into preheating, phase change and superheating. While some preheating is done outside the stack, some will also have to take place within the drum, with energy provided by the evaporation process. Hence:

$$(7.3) \quad \Delta h_{cycle,stack} = \underbrace{\Delta h_{drum}}_{f(p,\dot{m},P_{preheat})} + \underbrace{h_{fg}}_{f(p)} + \underbrace{\Delta h_{SH}}_{f(p,T_{eg,in})}$$

$$(7.4) \quad Q_{cycle,stack} = \dot{m}_{cycle} \cdot \Delta h_{cycle,stack} = \dot{m}_{eg}(h_{eg@T_{eg,in}} - h_{eg@T_{eg,mid}})$$

Since the high pressure cycle will yield more energy in the turbine per mass than the low pressure cycle, the mass flow in the high pressure cycle should be as large as possible [M&M, 2013]. As demonstrated in Figure 7.3, for a given pressure, this is the case when

$T_{eg,mid}$ approaches the evaporation temperature (which is given by a known pressure). Hence the highest possible mass flow for the high pressure cycle, for a given pressure and pinch, is found from combining Equations 7.2, 7.3 and 7.4. The full expression is shown in Equation 7.5.

$$(7.5) \quad \dot{m}_{HP} = \dot{m}_{eg} \frac{h_{eg@T_{eg,in}} - h_{eg@(T_{evap,HP}+pinch)}}{\Delta h_{HP,drum} + h_{HP,fg} + \Delta h_{HP,SH}}$$

For the mass flow in the low pressure cycle, the same derivation applies, but here the former outlet ($T_{evap,HP}+pinch$) is now the inlet. See Equation 7.6.

$$(7.6) \quad \dot{m}_{LP} = \dot{m}_{eg} \frac{h_{eg@(T_{evap,HP}+pinch)} - h_{eg@T_{eg,160}}}{\Delta h_{LP,drum} + h_{LP,fg} + \Delta h_{LP,SH}}$$

For a given energy transfer to the low pressure cycle, the pressure should be as high as possible [M&M, 2013], as long as $T_{evap,LP}$ stays below $T_{eg,out}$.

System Design 8

This chapter describes the methodology used to design the Waste Heat Recovery System. The system is designed to transfer as much energy as possible to the steam turbine. The concept of exergy is introduced, and the arrangements of the system components will be explained.

A setup with two configurations is required: inside ECAs and outside ECAs. For sailing in international waters, no exhaust gas recirculation will be required. The ship will operate on HFO, and all the exhaust gas will leave through the chimney. Inside ECAs the mass flow in the stack, while an additional source of energy is introduced.

8.1 Exergy

Exergy is a measure of potential work. It represents a combination of internal, kinetic, flow and potential energy. It quantifies the work of a substance if it was to undergo a reversible process to a dead state. The dead state is denoted by '0' and is usually defined as 25°C and 1 atm conditions. Since exergy is mainly used for comparing fluid states within a system, a different dead state can be defined as appropriate.

For a flow system, the specific exergy is defined in $\frac{kJ}{kg}$ as seen in Equation 8.1 [Cengel et al., 2008].

$$(8.1) \quad \psi = (h - h_0) - T_0(s - s_0) + \frac{V^2}{2} + gz$$

Since exergy will be used exclusively in relative terms, some simplifications can be made. With generally negligible changes in altitude, the gravitational term, gz , can be removed. Often, the change in velocity is also neglected, since the change in specific velocity is small, relative to the changes in enthalpy and entropy. Figure 8.1 shows the development of exergy for water, as it is heated from 40°C to 400°C at various pressures.

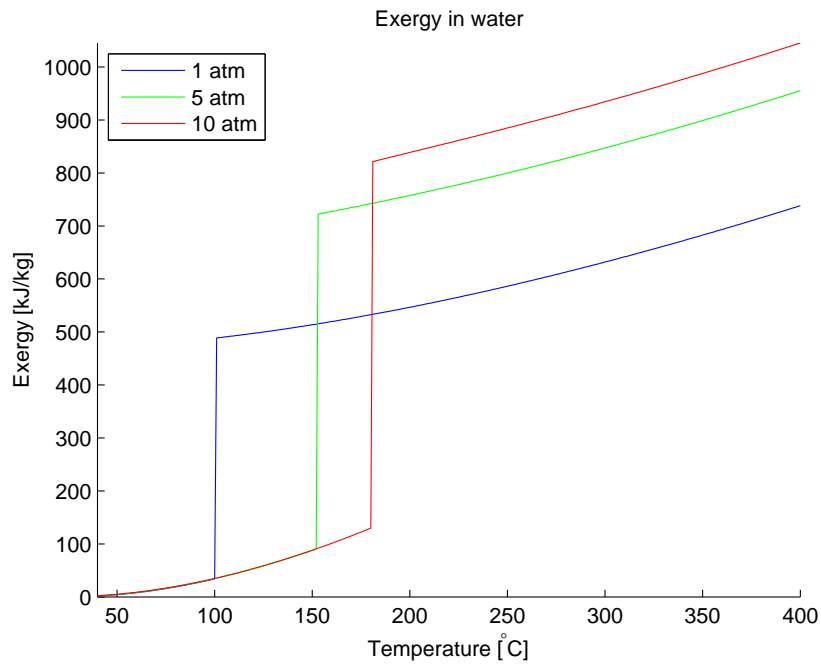


Figure 8.1: Development of specific exergy of water for varying temperature.

The vertical jump in exergy occurs when the fluid evaporates, which explains why this occurs at different temperatures for various pressures. Notably, the exergy is almost pressure-independent before evaporation, while a higher pressure means a significantly higher level of exergy when the fluid is in gas form. It can be noted that the influence of the pressure is much greater between 1 and 5 atm, than between 5 and 10 atm.

To illustrate the influence of pressure, Figure 8.2 shows the exergy of water at 200, 300 and 400°C for varying pressure.

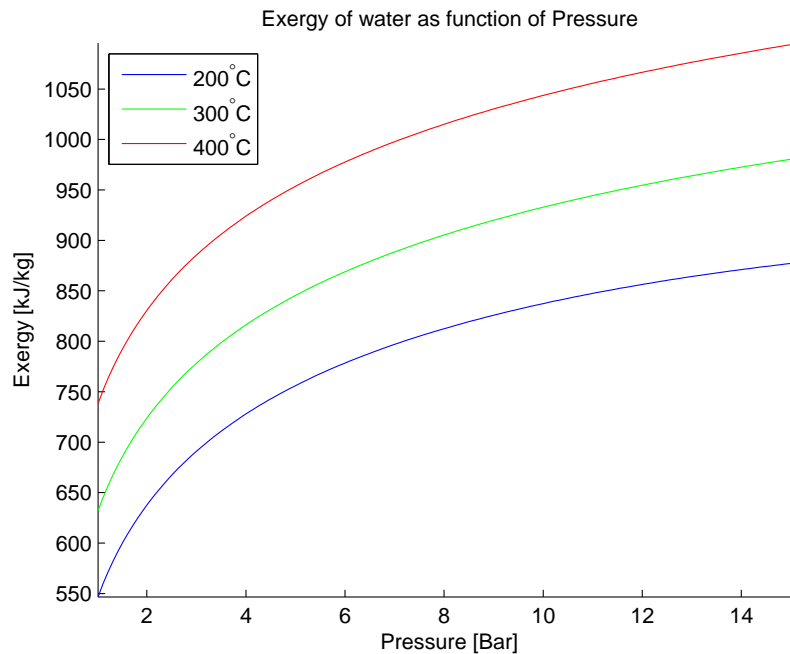


Figure 8.2: Influence of pressure on exergy for constant temperature.

Figure 8.2 shows that, while both higher pressure and higher temperature increases the exergy, the benefit of increasing the pressure diminishes as the pressure increases. The 400°C will eventually reach maximum value around 100 bar and the 300°C around 60 bar.

As previously mentioned, exergy is the potential work of a fluid in a given state. Figure 8.1 showed how higher temperatures increase the exergy of a fluid. However, to increase the temperature of a fluid, energy is also required. Considering the enthalpy change of a fluid as the quantity of energy required to heat it, and exergy as the potential work output (neglecting gravitational and kinetic terms), a theoretical maximum efficiency of a cycle can be calculated.

$$(8.2) \quad \Delta h = h_T - h_{T_0}$$

$$(8.3) \quad \psi = (h - h_0) - T_0(s - s_0)$$

$$(8.4) \quad \eta_{\psi-max} = \frac{\psi}{\Delta h}$$

η_{max} represents the ratio of total energy and useful energy in a fluid. Using 25°C as T_0 , the energy content, exergy and maximum theoretical efficiency is shown in Figure 8.3 for 10 bar pressure.

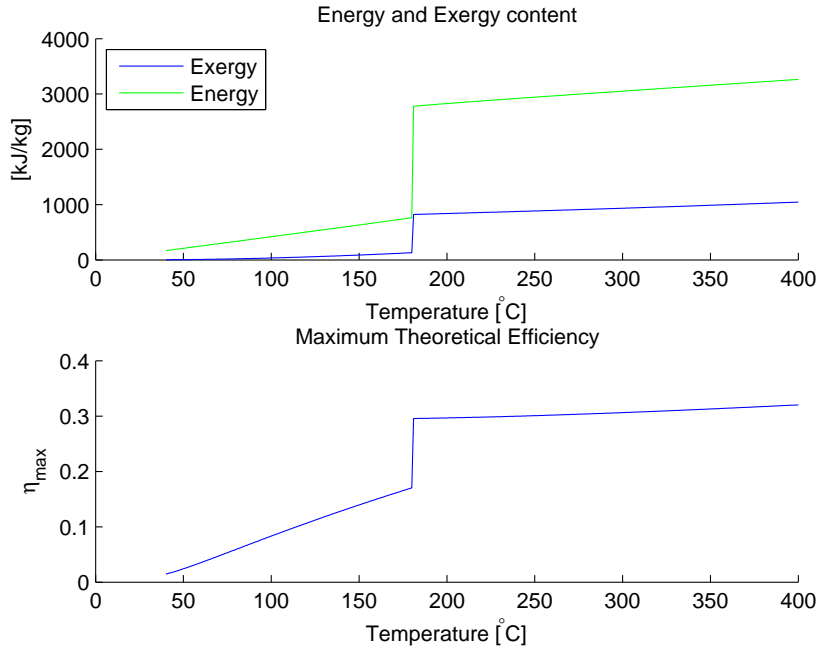


Figure 8.3: Maximum theoretical efficiency at 10 bar pressure.

Again, the vertical line on the plot represents the evaporation. From an energy-efficiency point of view, it is clear that heating generally yields better theoretical results. It is also clear that evaporating the fluid is more important than superheating it, if the energy is recovered by a liquid fluid. While η_{\max} continues to increase as the gas gets hotter, the rate of growth is much smaller.

Figure 8.4 shows the theoretical maximum efficiency in the gas state as a function of temperature for various pressures.

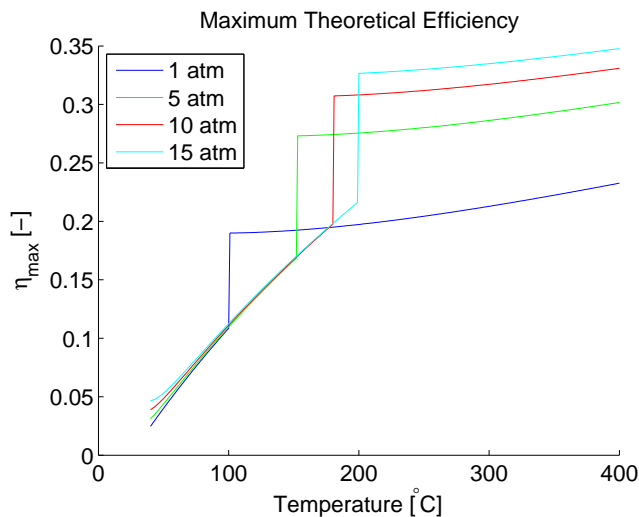


Figure 8.4: Maximum theoretical efficiency.

Even when considering the energy content, the trend from Figure 8.1 is still present; higher temperature and higher pressure both yield higher exergy. This supports the previous

project, where it was also found that a higher temperature and higher pressure would increase the system efficiency [M&M, 2013].

8.2 Utilizing Heat Sources

As shown in the previous section, to maximize potential power gain in the steam turbine, the cycle fluids should be as hot as possible, at the highest feasible pressure. Increasing the pressure will also raise the evaporation temperature, which introduces limitations in the system design [M&M, 2013].

A useful analysis in designing a heating system is the T-Q diagram. The available heat sources are defined by temperature at inlet and outlet, and by how much power they can provide between the two stages. With available inlet temperatures and possible outlet temperatures known, the power calculations are demonstrated in Equations 8.5. Heat transfers will be regarded as isobaric.

$$(8.5) \quad P = \dot{m} \cdot \Delta h_{(T_{in} \rightarrow T_{out})}$$

As mentioned in Section 7.1 the system will need to operate in two different conditions. The presence of EGR within ECAs has a significant influence on both quality and quantity of available heat. The sets of temperatures and corresponding powers are then entered into a T-Q diagram, with the hottest first. The load dependency of the heat sources is described in Section 9.3, in this chapter the properties will be taken at 80% load. The T-Q diagram for the system outside ECAs is shown in Figure 8.5a. Note that the figure portrays straight lines between inlet and outlet conditions. This does not imply that heat transfer power is linearly proportional to temperature.

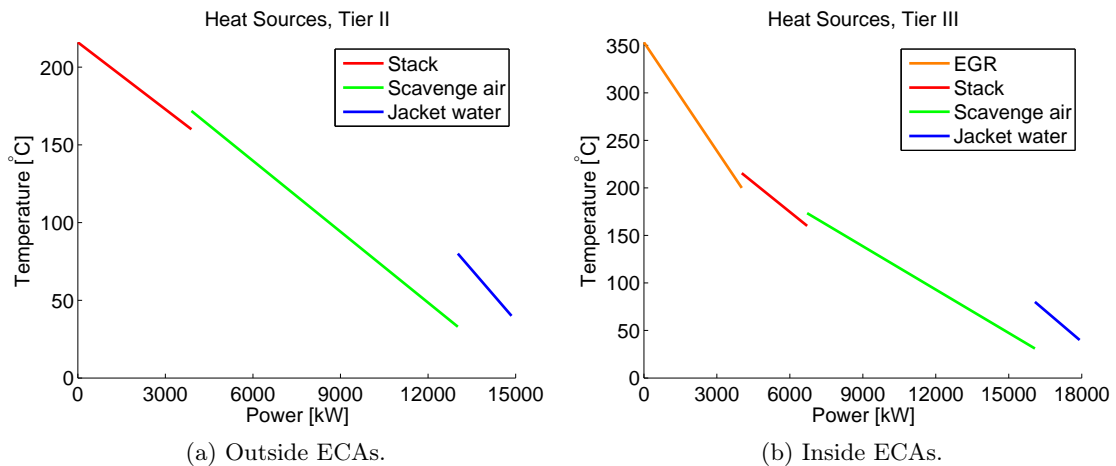


Figure 8.5: Diagram of available heat sources in Tier II and Tier III conditions.

From Figure 8.5 it can be seen that the addition of EGR provides a high temperature energy source, and that the Tier III system has an additional 3 MW of heat available. Additionally, while the high temperature EGR heat source will allow a higher level of

energy in the cycle, some energy is lost in the stack, which will see a significantly lower mass flow when operating in Tier III conditions.

8.2.1 Jacket Water

Since the cycles will condense at 40°C , the source T-Q diagram can be cut below that temperature. The jacket could also be left out of the WHRS entirely, since the capacity flow of the cycle fluid will be smaller than that of the scavenge air. Thusly, the scavenge air could heat the cycle fluid from condensation temperature to $\sim 160^{\circ}\text{C}$. However, using jacket water rather than scavenge air will yield a much higher overall heat transfer coefficient, and thereby reduce material costs.

Additionally, the temperature of the scavenge air drops below that of the jacket water at low operation loads, which means that it may be feasible to have an option to bypass the scavenge air entirely, after the jacket water.

8.2.2 Scavenge air

At high loads, the scavenge air temperature exceeds the minimum temperature in the stack. To fully use this heat, the cycles are heated to above the evaporation temperature, and will then partially flash through the expansion valve. This will reduce the required energy transfer in the evaporator, and thereby allow more steam to be produced. At low loads, when the scavenge air temperature is below the 160°C limit of the stack, the fluid will simply expand through the valve and be heated to saturation in the drum, see Figure 8.6.

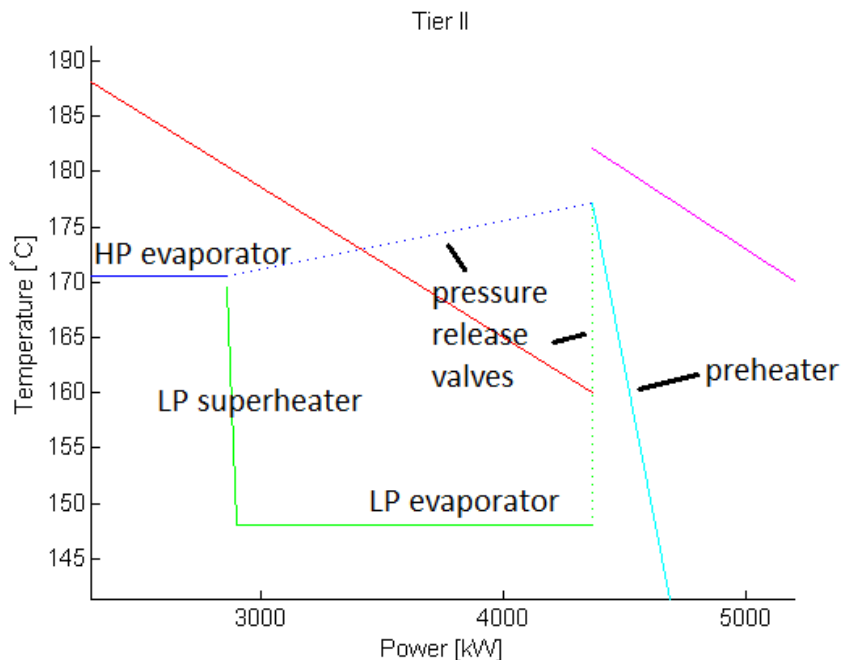


Figure 8.6: Scavenge air utility at high load.

Since the fluid temperature drop shown in Figure 8.6 is a result of a pressure drop and (partial) phase change, the same approach cannot be used between the stack and EGR

heat exchangers.

8.2.3 EGR/Stack

Since the capacity flow of the EGR will be higher than that of the cycle fluid, the slope of the T-Q diagram will again be steeper for the cycle fluid. Therefore the EGR will be able to be the only source of superheating. Since none of the available heat in the stack will be required for superheating, more energy can be used for evaporation, meaning that a higher mass flow can be supported.

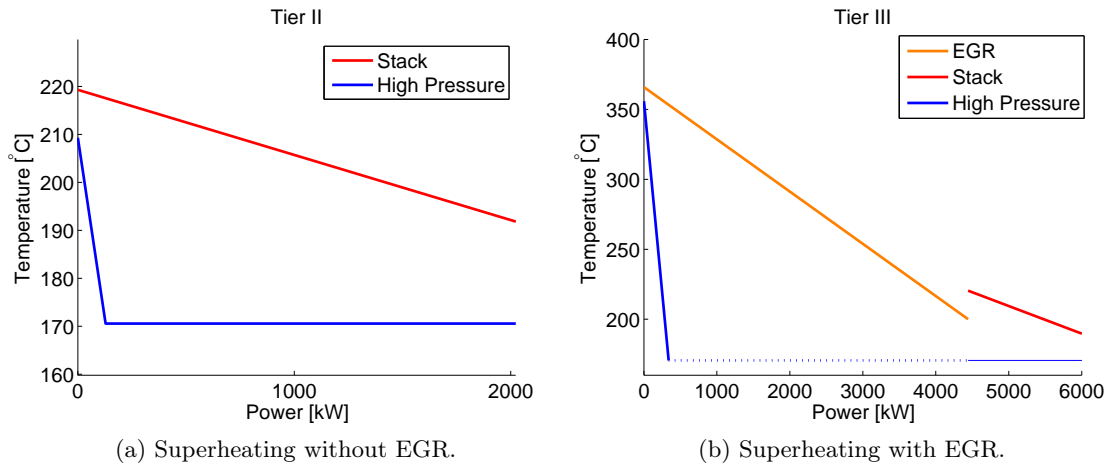


Figure 8.7: Adapting the system design to EGR availability.

The combined capacity flow of the high and low pressure cycle is expected to still be lower than that of the EGR. Hence there should be sufficient energy available to heat both cycles to within a few degrees of the EGR. This would require the heat exchangers for the high and low pressure cycles to be parallel, which introduces some problems with splitting the EGR stream in real conditions.

8.3 Proposed System

The complete system schematic for the fluid cycles can be seen in Figure 8.8. The design aims to fully utilize the addition of the high temperature heat source in the EGR, while not deviating too significantly from the standard Tier II system.

The order of the heaters is determined by the source temperatures, leaving little room for variation. Except for extreme cases, the jacket water will always be the first preheater, followed by the scavenge air. After the scavenge air, the fluids are evaporated in the stack. Depending on the operation condition, the fluids are superheated either by the EGR or also in the stack.

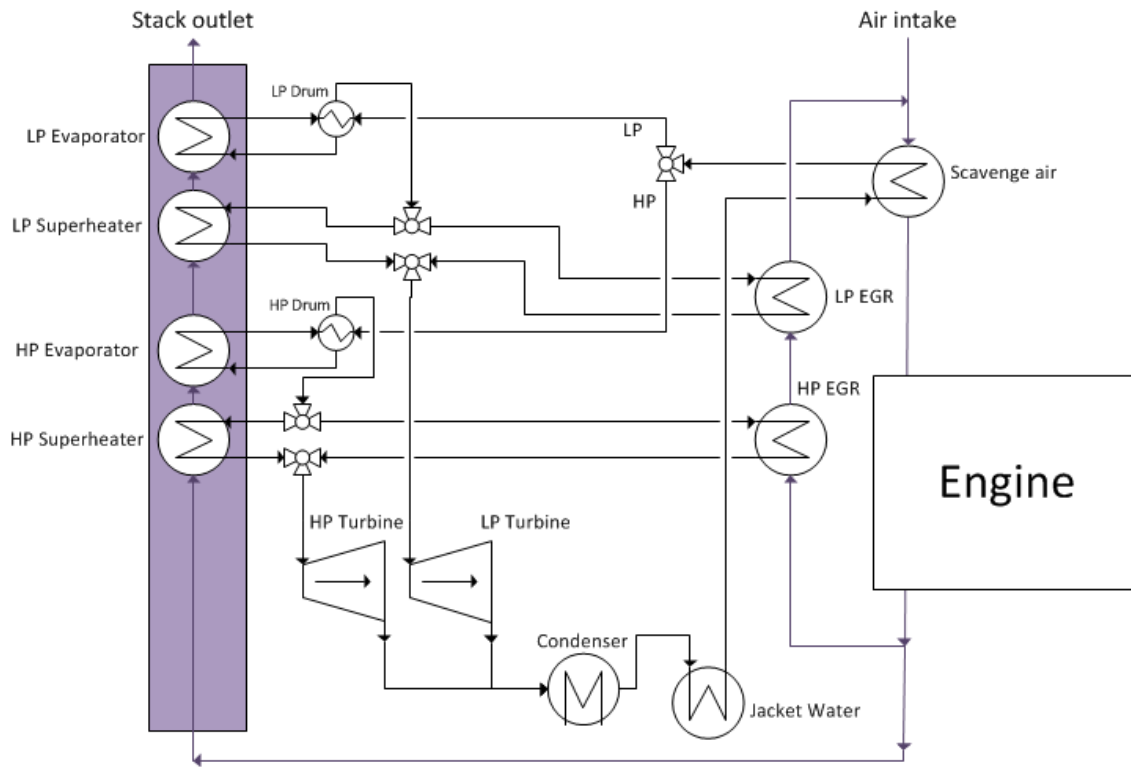


Figure 8.8: Schematic of the proposed WHRS system.

The heat exchangers in the stack will likely be a crossflow-like setup, where the heating surface is made of double gilled tubes with a spacing which minimizes soot build-up [Laval]. The condenser could be shell and tube, or a plate condenser [Laval]. The modelling of the heat exchangers is described in Chapter 9.

The system design is limited by having to accommodate both Tier II and III operation (with Tier II being the most significant).

WHRS Models 9

This chapter will describe the behavior and models of the various components in the WHRS system. The individual components will be described, and the overall model setup explained.

9.1 Turbine

The behavior of a gas turbine could be seen as that of an orifice. For given pressure at the inlet and outlet, there is a corresponding mass flow through the turbine. The mass flow depends on a flow resistance, which depends on the turbine geometry. The flow and pressure at the inlet and outlet of a steam turbine is correlated using Stodola's law, which is shown in Equation 9.1 [Nielsen, 2013].

$$(9.1) \quad C_T = \dot{m} \sqrt{\frac{p_{in} v_{in}}{p_{in}^2 - p_{out}^2}}$$

The turbine constant, C_T , can be interpreted as the resistance in the turbine, which determines the mass flow through it. It is calculated at full load, and then applied to determine the mass flow at partial load.

The expansion through the turbine is not isentropic, and an isentropic efficiency should be applied when calculating output properties. This is shown in Equation 9.3, where subscript "s" denotes isentropic.

$$(9.2) \quad h_{s,out} = f(T_{out}, s_{in})$$

$$(9.3) \quad h_{out} = h_{in} - \eta_{s,t} \cdot (h_{in} - h_{s,out})$$

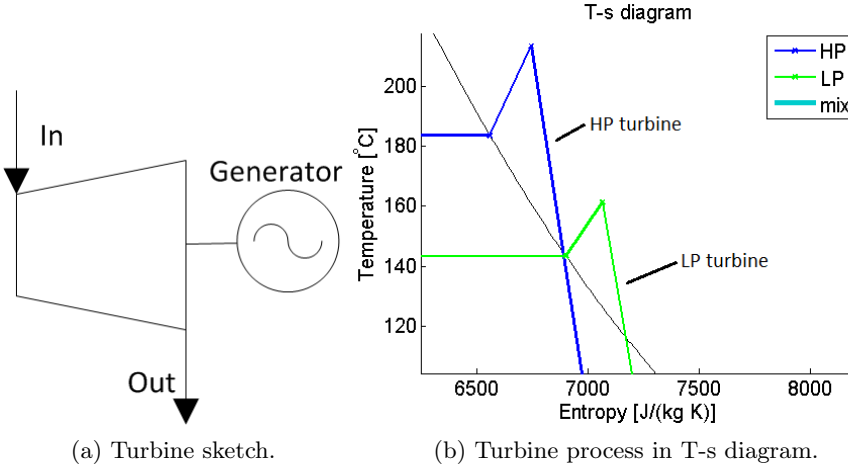


Figure 9.1: Focus on the turbine in the T-s diagram.

The turbine used in the report is a condensation turbine. This means that the temperature at the outlet is determined by the condenser cooling, and that outlet pressure will be determined by the temperature, as shown in Equations 9.4 and 9.5.

$$(9.4) \quad p_{out} = f(T_{out})$$

$$(9.5) \quad T_{out} = f(Q_{Condenser})$$

The possible mass flows in the system can be found by applying Stodola's law to the two turbines in the system, see Equation 9.6 and 9.7. Note that the prime denotes that the pressure loss in the superheater has been taken into account.

$$(9.6) \quad \dot{m}_{HP} = C_{T1} / \sqrt{\frac{p_{HP'} \cdot v_{HP'}}{p_{HP'}^2 - p_{cond}^2}}$$

$$(9.7) \quad \dot{m}_{LP} = C_{T2} / \sqrt{\frac{p_{LP'} \cdot v_{LP'}}{p_{LP'}^2 - p_{cond}^2}}$$

If insufficient heat is available to produce the quantity of steam corresponding to the inlet pressure, some pressure can be released in a valve before the turbine inlet. In addition to depending on the pressure, the mass flow depends on specific volume, and thereby temperature. Since the temperature after the superheater depends on the mass flow, the system will be solved iteratively.

9.2 Pump

The pump compression is also not an isentropic process. In the case of the pump, this means that more energy is required than if the process had been perfect. The relation between the isentropic efficiency of the pump and the enthalpy is described by Equation 9.9. [Boles and Cengel, 2011]

$$(9.8) \quad P_{pump} = \dot{m}\Delta h$$

$$(9.9) \quad \eta_{s,p} = \frac{h_{s,out} - h_{in}}{h_{out} - h_{in}}$$

Assuming no change in potential energy (no change in altitude) and no change in kinetic energy (same size pipe on both sides), the power can be rewritten as a function of pressure and specific volume, see Equation 9.10. [Nielsen, 2013]

$$(9.10) \quad \eta_{s,p} = \frac{v(p_{out} - p_{in})}{h_{out} - h_{in}}$$

$$(9.11) \quad h_{out} - h_{in} = \frac{v(p_{out} - p_{in})}{\eta_{s,p}}$$

Equation 9.11 shows why the fluid is compressed in liquid form, since the specific volume (v) is much smaller for liquid water than it is for steam, reducing the required change of enthalpy. E.g. at atmospheric pressure, the specific volume of saturated steam is 1600 times greater than that of saturated liquid water.

9.3 Heat Exchangers

The heat transferred in the heat exchangers, including the boiler and superheater, is calculated using the NTU method (See appendix E.2). The overall heat transfer coefficient U is assumed constant, even though this assumption is only valid for a small range of temperatures. The areas of the various heat exchangers have been determined using the LMTD method (See Appendix E). The parameters changing with the load will then be the mass flows and the temperatures, where outlet temperatures are to be calculated.

9.3.1 Evaporator and Drum

When the cycle fluid runs through the evaporator, it is only partially evaporated on the first run through. This means that most of the fluid mass stays in liquid form throughout the heat exchanger, greatly increasing the heat transfer coefficient. When the fluid exits the evaporator and re-enters the drum the fluid is separated from the steam. The part of it which has evaporated moves on to the superheater, and the rest is sent through the evaporator again. The evaporator and drum are sketched in Figure 9.2.

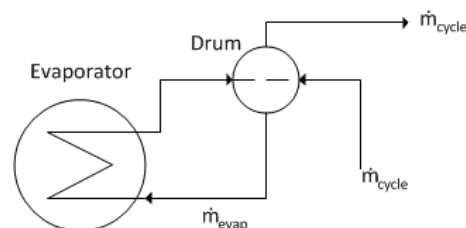


Figure 9.2: Sketch of the drum and evaporator system.

The evaporator and drum are often described by the number of times that the fluids recirculate, shown in Equation 9.12.

$$(9.12) \quad n = \frac{1}{x_{evap,out}}$$

$$(9.13) \quad \dot{m}_{evap} = n \cdot \dot{m}_{cycle}$$

The quality of steam as it leaves the evaporator and re-enters the drum can be as low as 0.20-0.25. This means that the fluid is recirculated 4-5 times in total, implying that the mass flow in the evaporator is 4-5 larger than in the other heat exchangers of the system.

9.3.2 Condenser

Like the evaporator and drum, the condenser prevents fluid from moving further in the system before it has fully condensed. Rather than alter the cycle flow, as in the evaporator, here the coolant flow is changed to match the cooling requirement. The required quantity of seawater coolant is found from Equation 9.14.

$$(9.14) \quad \dot{m}_{cond} = \frac{\dot{m}_{mix}(h_{mix@turbine\ out} - h_{mix@x=0})}{h_{seawater@(T_{cond}-pinch)} - h_{seawater@T_{ambient}}}$$

The heat transfer in the condenser is illustrated in Figure 9.3.

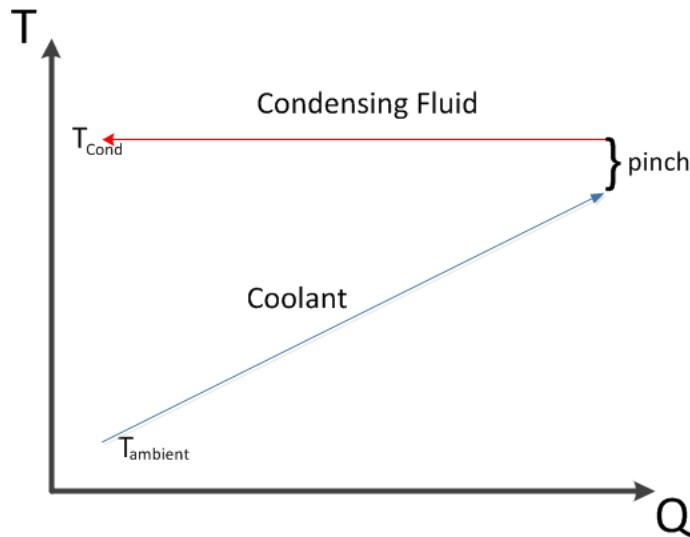


Figure 9.3: Basic condensation diagram.

9.3.3 Partial Load Inputs

The following section will describe how the temperatures and mass flows on the heat source side of the various heat exchangers in the system will change with the engine load.

Jacket Water

The jacket water is the coldest source of energy in the system. From Chapter 2 Figure 2.6 it is assumed that 6.3 % of the fuel input power consists of waste heat through the cooling jacket water.

The jacket water from various parts of the engine is mixed and enters the jacket water cooling system at $\sim 80^\circ\text{C}$ [Tveitaskog, 2013]. Assuming the jacket water is cooled using seawater, and therefore is cooled no further than to 40°C (similar to the cycle condensation temperature), heat exchange with the jacket water is given by Equation 9.15.

$$(9.15) \quad \dot{m}_{jacket} = \frac{P_{jacket}}{h_{water@80^\circ\text{C}} - h_{water@40^\circ\text{C}}}$$

The low temperature of the jacket water greatly limits its use in the WHRS. For this reason, the accuracy of Equation 9.15 is of little significance as long as it remains within a reasonable range. The temperature of the jacket water could be expected to decrease with the adiabatic flame temperature (See sections 4.5 and 5.3), though the mass flow could be adjusted accordingly. In the absence of more information, assuming $\sim 80^\circ\text{C}$ is deemed acceptable.

Scavenge air

The scavenge air is heated by the compression in the turbocharger, and is then cooled to near ambient temperatures, before being injected into the engine. The mass flow of the scavenge air will follow the engine load, the specific consumption and the air excess ratio (See Chapter 4).

$$(9.16) \quad \dot{m}_{scav} = \dot{m}_{fuel} \cdot (A/F)_{stoic} \cdot \lambda$$

$$(9.17) \quad \dot{m}_{scav} = \frac{P_{engine} \cdot SFOC}{3600 \cdot 1000} \cdot (A/F)_{stoic} \cdot \lambda$$

The temperature of the scavenge air is a function of the compression. Since the compression is a function of how much air is required in the engine, the scavenge air temperature becomes a function of both the engine load and the compressor characteristics.

$$(9.18) \quad p_{scav} = f(\lambda, \text{Engine})$$

$$(9.19) \quad T_{scav} = f(p_{scav}, h_{p=p_{scav}})$$

Where $h_{p=p_{scav}}$ is found from the isentropic efficiency of the turbocharger.

Stack Exhaust Gas

The stack mass flow accounts for all the exhaust mass flow not being recirculated, neglecting soot deposits in the system. Defining EGR as the percentage of exhaust gas

recirculation (See Chapter 5), the mass flow of exhaust gas through the stack can be written as Equation 9.20:

$$(9.20) \quad \dot{m}_{stack} = \dot{m}_{eg} - \dot{m}_{egr} = \dot{m}_{eg} - \dot{m}_{eg} \cdot EGR = \dot{m}_{eg} \cdot (1 - EGR)$$

The temperature for every heat exchanger in the stack after the high pressure superheater will depend on the heat transfer in the high pressure superheater. Hence, the only pre-determinable inlet temperature will be that of the high pressure superheater.

The exhaust gas releases energy in the turbocharger turbine before going through the chimney. Like the steam turbine, the turbocharger expansion is assumed to follow a known isentropic efficiency and an outlet property is considered known. Here the pressure, which is near atmospheric, will be used as the known outlet property.

$$(9.21) \quad h_{tc,out} = h_{tc,in} - \eta_{s,tc} \cdot (h_{s_{tc,out}} - h_{tc,in})$$

$$(9.22) \quad T_{stack,in} = T_{tc,out} = f(p_{tc,out}, h_{tc,out})$$

The system uses two turbochargers, with approximately same inlet and outlet temperatures in Tier II operation. In Tier III one of these is combined with the recirculated exhaust gas. Since one of the aims of this report is to change the way in which these streams are combined, the outlet conditions of the smaller turbocharger are considered to be as for the larger one.

EGR (Tier III)

The mass flow of the EGR is the part of the exhaust gas being recirculated. This gas does not go through a turbocharger, but is scrubbed to reduce SO_x concentrations before being mixed with the compressed scavenge air. The EGR heat exchanger is located before the scrubber, and consequently the inlet temperature. The subscripts are illustrated in Figure 9.4. A sketch of the full system can be found in Chapter 5, Figure 5.1.

$$(9.23) \quad \dot{m}_{EGR} = \dot{m}_{eg} - \dot{m}_{stack} = \dot{m}_{eg} \cdot EGR$$

$$(9.24) \quad T_{EGR} = T_{engine,out}$$

The temperature of the exhaust gas immediately after the engine are the highest temperatures available for heat recovery. It depends on a long list of parameters, such as adiabatic flame temperature, quantity of air and fuel, geometry of the cylinders/exhaust pipes, etc. As such, its value will be taken as given, and not investigated by a model.

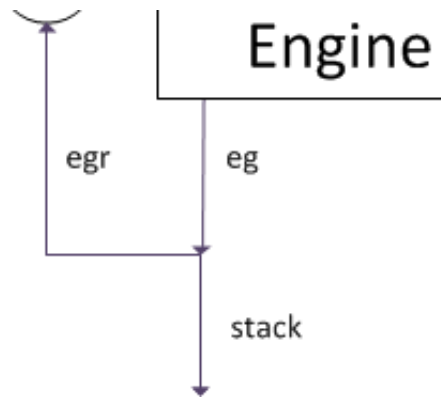


Figure 9.4: Subscript illustration.

9.3.4 Temperatures and mass flows for various loads

The mass flows and inlet temperatures of the WHRS heat sources for operation in Tier II conditions (outside ECAs) can be seen in Figure 9.5.

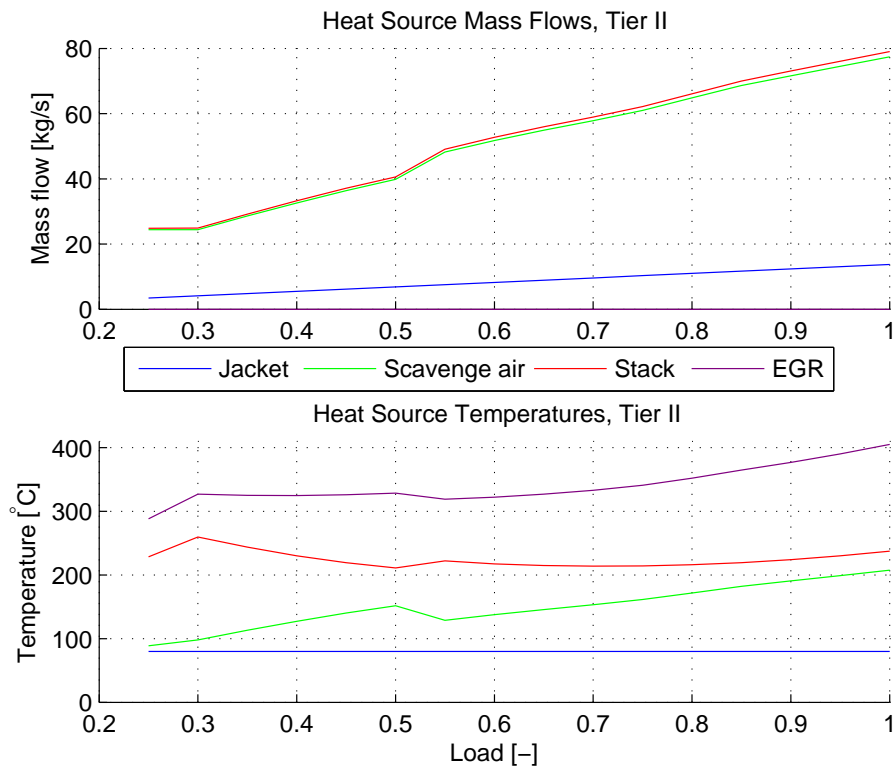


Figure 9.5: Temperatures and mass flows of the heat sources in Tier II.

Since no EGR is employed in Tier II conditions, the EGR mass flow is zero throughout the load spectrum. With all of the exhaust gas exiting through the chimney, the only difference between the scavenge air and the stack mass flow is the fuel mass flow. The jacket water mass flow increases progressively with the engine load, which makes sense given that the engine generates more heat at higher loads. It could be argued that this would also increase the temperature of the jacket water, but it is assumed to be controlled via changes in the mass flow.

Noticeably, the scavenge air temperature is generally increasing with the load. Since the temperature here is determined by the turbocharger compression, a higher temperature indicates that the air is further compressed at higher loads. Since the purpose of the compression is to increase the air density going into the combustion chamber, the increasing temperature of the scavenge air is a consequence of requiring more air at higher loads.

As a final note, the mass flow and temperature of the jacket water cooling are deceptively low compared to the other heat sources. For energy considerations it should be kept in mind that the specific heat capacity of water is almost 4 times greater than any of the other gas mixtures in the system. $\left(c_{p, \text{eg}} \sim 1.1 \frac{\text{kJ}}{\text{kg K}}, c_{p, \text{water}} \sim 4.2 \frac{\text{kJ}}{\text{kg K}}\right)$.

Figure 9.6 shows the heat source mass flows and temperatures for Tier III operation.

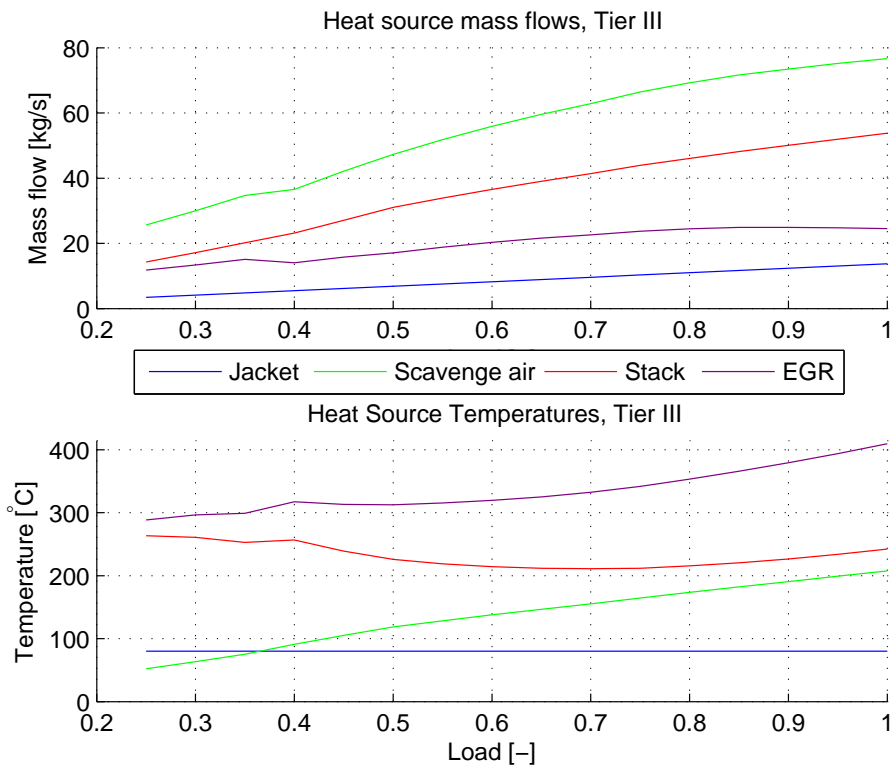


Figure 9.6: Temperatures and mass flows of the heat sources in Tier III.

With the inclusion of EGR, the stack mass flow significantly decreases. The scavenge air mass flow is almost the same as for Tier II operation, and the jacket water mass flow does not change at all.

The temperatures are also similar above 50% load. The difference below 50% load is that Tier II operation utilizes cut-out, which cannot be used while also using EGR in Tier III.

9.3.5 Heat Exchangers sizing

The sizes of the various heat exchangers used in the model have been calculated with the LMTD method detailed in Appendix E. Table 9.1 summarizes the various data and results. The attribute "phase" for the type of heat exchanger is used to identify evaporators

and condensers (i.e when a phase change occurs). The overall heat transfer coefficient U depends on material, geometry, etc. and will change with the temperature. For this report the U -values are taken as constant and approximated within a reasonable range [Condra, 2013].

Component	U-value [W/m ² K]	Area [m ²]	Type
Jacket	1500	13	Counter
Scavenge	100	299	Counter
Evaporator LP	50	1444	Phase
Superheater LP	40	49	Counter
Evaporator HP	50	2284	Phase
Superheater HP	40	134	Counter
EGR Superheater HP	40	173	Counter
EGR Superheater LP	40	70	Counter
Condenser	2000	359	Phase

Table 9.1: Heat exchangers sizing.

9.4 Power Turbine

To increase its density, the scavenge air will be compressed before entering the combustion chamber, which is done with the use of a turbocharger. The exhaust will go through a turbine, and the energy produced will be used to compress the air.

Due to its efficiency, the turbocharger will not require the total amount of exhaust gas heading to the stack after the combustion and part of it can be used to generate electricity in a power turbine. The amount of energy required in the turbocharger is determined by the quantity of the scavenge air, and the states at the inlet and outlet of the compressor, see Equation 9.25.

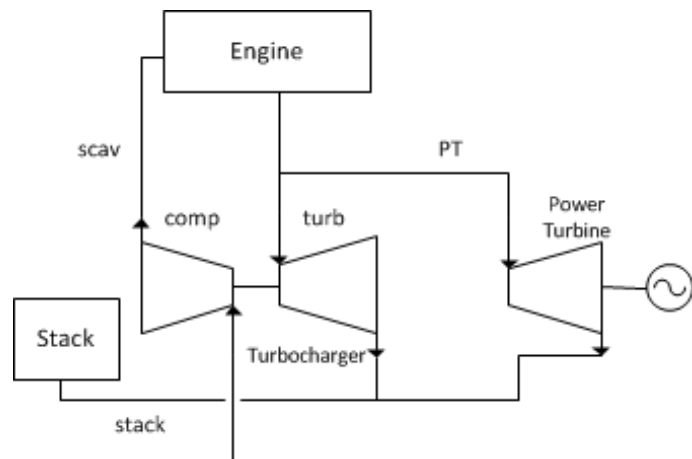


Figure 9.7: Focus on power turbine.

$$(9.25) \quad P_{comp} = \dot{m}_{scav} \cdot (h_{comp,out} - h_{comp,in})$$

The power required by the compressor will be provided by the turbocharger turbine. This will determine the mass flow of exhaust gas needed by the turbocharger turbine as shown in Equations 9.26 and 9.27, assuming no mechanical losses.

$$(9.26) \quad P_{turb} = P_{comp}$$

$$(9.27) \quad \dot{m}_{turb} = \frac{P_{turb}}{h_{turb,in} - h_{turb,out}}$$

The leftover mass flow shown in Equation 9.28 can then be bypassed through the power turbine, which will generate electricity. Assuming the same conditions for the exhaust gas at the outlet of the power turbine and the turbocharger, the electric production can be calculated with Equation 9.29. This is calculated for a 100% efficiency.

$$(9.28) \quad \dot{m}_{PT} = \dot{m}_{stack} - \dot{m}_{turb}$$

$$(9.29) \quad P_{PT} = \dot{m}_{PT} \cdot (h_{PT,in} - h_{PT,out})$$

9.5 Design Model

The purpose of the design model is to estimate constants parameters, *i.e.* heat exchanger areas and turbine constants, for use in the performance model. The areas are determined from the temperatures of the heat sources and a given minimum pressure difference; the mass flows are found from the pressures and quantity of available energy in the stack, and the turbine constants are found from the correspondence of pressure and mass flow as seen in Stodola's law (Equation 9.1).

Figure 9.8 illustrates the process of the system design model. The inputs will be a given load and a given HP and LP pressure. Other data and parameters are going to be needed for the calculation, some defined as design constants and the others as given by MAN. MAN data are mostly those that have not been modeled or that cannot be played with such as the engine outputs. Once the data are gathered, the preheating calculations are made by looking at the heat exchanged in the condenser, the jacket water and the scavenge air. The cycle is then separated into two different strings: The high and low pressure. The HP cycle calculations are made first, since the exergy will be better, and the amount of remaining energy left for the LP cycle is calculated. The mass flow of the HP and LP cycle is calculated to respect the energy balance. These mass flows are used to determinate the designed heat exchangers areas by the LMTD method. They will also be used to determine the turbine (HP and LP) constants by Stodola's law.

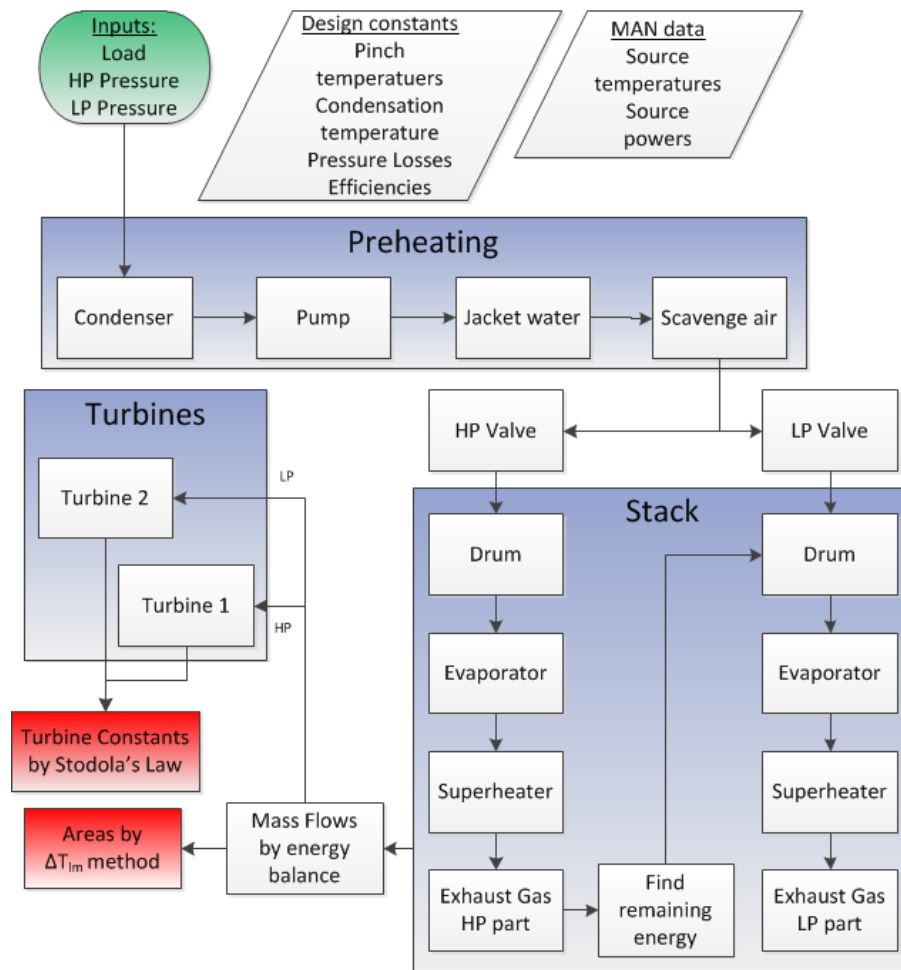


Figure 9.8: Flowchart of the Design Model.

9.6 Performance Model

The performance model evaluates the performance of the system, using given HP and LP pressures at a given load. The performance model uses load dependent temperatures and mass flows of the power sources (see Figures 9.5 and 9.6). Cycle temperatures are determined using the NTU method now that the areas have been determined with the Design Model, and the cycle mass flows are determined by Stodola's law. Since the mass flows will depend on the temperature (through the specific volume) the problem is solved iteratively.

The calculation process of the performance model is demonstrated in the flowchart in Figure 9.9. The preheating is the same as in Figure 9.8 with the exception that the NTU method is used, rather than LMTD. The Stack block is described below.

Note that the areas and turbine constants calculated in the Design Model are used as constants here.

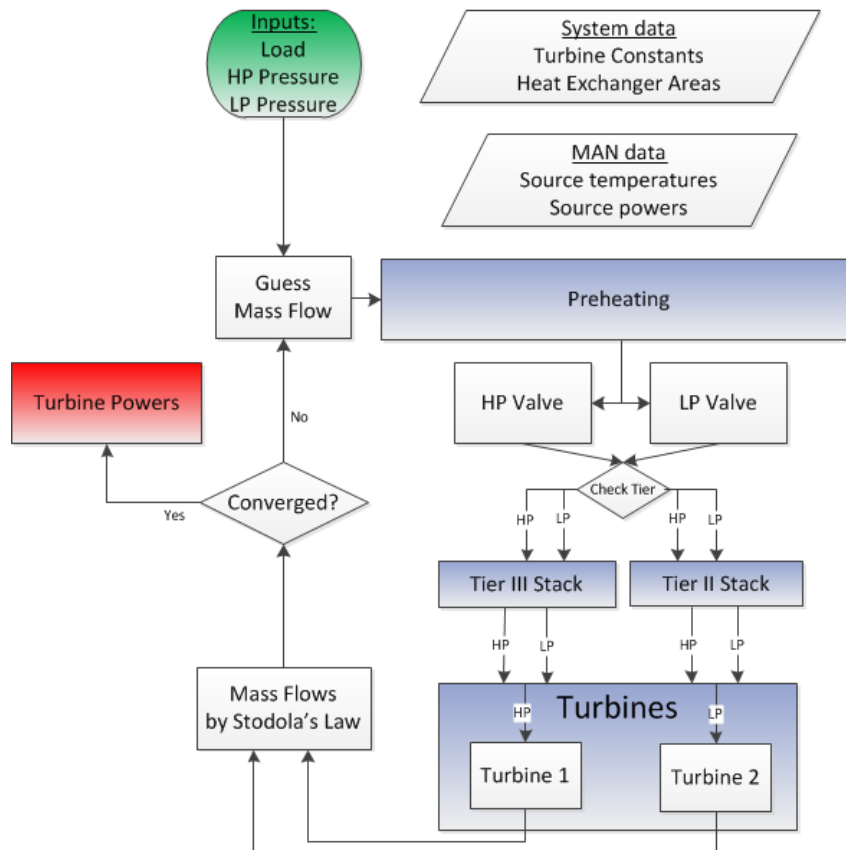


Figure 9.9: Flowchart of the Performance Model.

The stack block is shown in detail in Figure 9.10. The only change from Tier II to Tier III, is in how the fluid is heated in the stack. As shown in Figure 8.8, the superheating of both cycles is moved to the EGR string for Tier III. The figure shows the different step of calculation for the exhaust gas and the cycle by using the given mass flow and the NTU method.

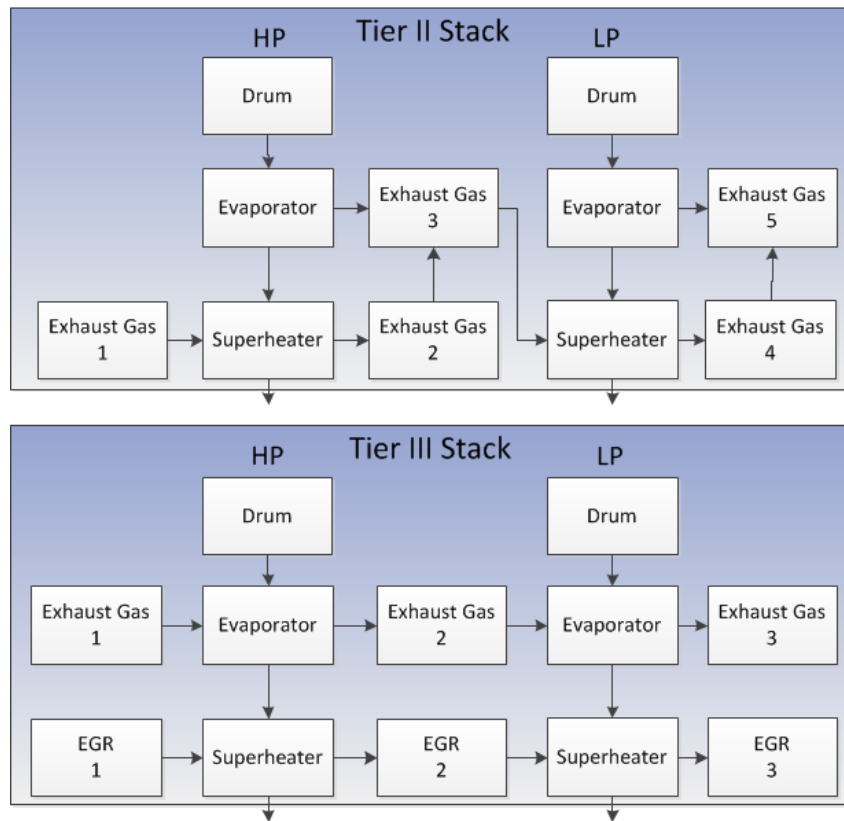


Figure 9.10: The stack block in Tier II and Tier III conditions.

9.7 Electric Production

In order to be able to evaluate the results obtained after optimization, a first model performance has been computed with a pressure for the LP cycle of 4.5 bar and 8.5 bar for the HP cycle. The interest here will be to have a first idea of the influence of EGR on the steam turbine compared to Tier II. The significance of having, or not, a power turbine is also to be evaluated.

Figure 9.11 shows the total electric production of the HP and LP turbines combined with the power turbine for Tier II and Tier III as function of the engine load. The power turbine production is also isolated in the figure for both conditions to identify the impact it has on the overall power production.

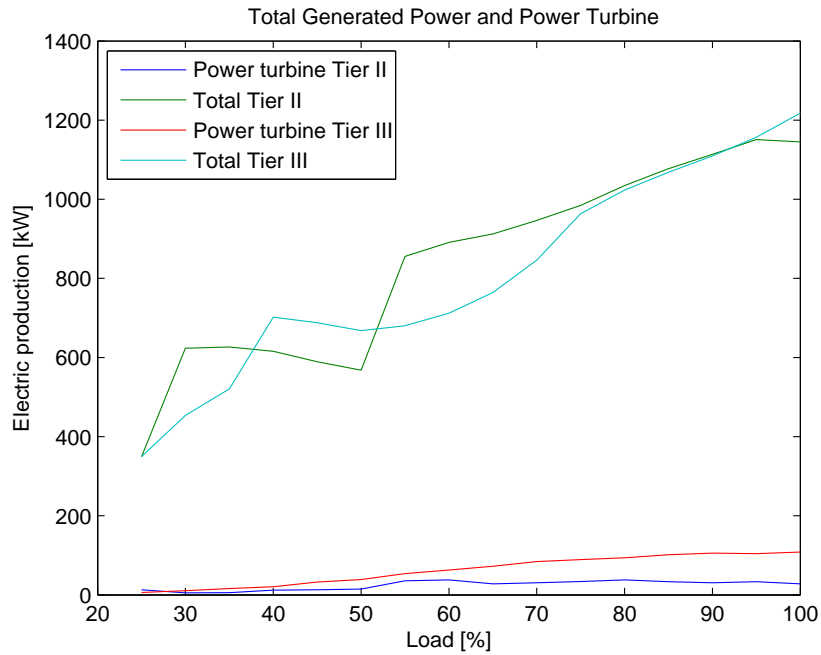


Figure 9.11: Electric production (LP: 4.5 bar, HP: 8.5 bar).

Relative to the steam turbines, the power production of the power turbine is very low in both cases. Hence, the total power production will be dominated by the steam turbines. The total electric production in Tier II and in Tier III will be similar at high load, with around 1.2 MW recovered. Larger differences will appear for lower loads. Above 55% load, the system will recover mere energy in Tier II. Below 50% load, the energy recovery decreases drastically, due to the cut-out being operated. It should be noted that the cutout is employed to reduce the SFOC, which leads to a lower quantity of energy in the exhaust gas. Since cut-out is not used for Tier III operation, the same drop does not occur for Tier III recovery. The heat recovery does not seem to be extremely affected by the Tier III operation regarding the steam turbine electric production.

Figure 9.12 shows the ratio between the power turbine electric production over the total electric production.

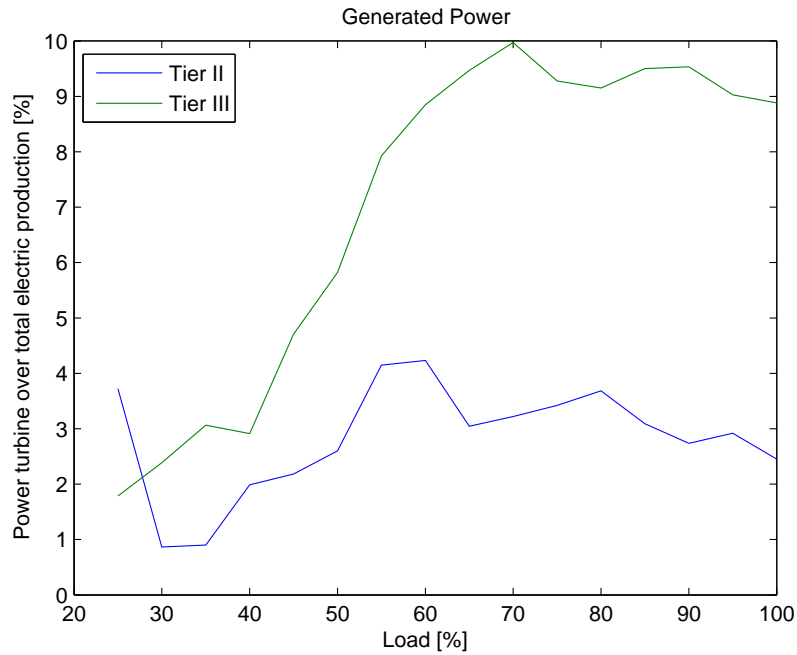


Figure 9.12: Power turbine electric production ratio.

The electric production of the power turbine in Tier II is around 2.5% of the total, whereas it goes from 2% to almost 10% in Tier III. This difference is mainly due to the lower amount of scavenge air to be compressed in Tier III compared to Tier II. While the shape of the curve in Tier II is similar to what was found in a previous report [M&M, 2013], the production is much smaller. It is recalled that in the previous study it was found that the power turbine could produce up to 1 MW, corresponding to more than 30% of the total power production. This is not the case for Tier III operation, where the electric production is limited at 100 kW. The operation for Tier III requirement will induce an extremely low exhaust gas mass flow, lowering the amount of exhaust gas to be by-passed.

Due to this relatively low amount of energy to be recovered by the power turbine, its feasibility from an economic standpoint is debatable, since it might not be worth it. This kind of discussion is beyond the field of interest of this report. Since the production of the power turbine is calculated entirely independently from the Waste Heat Recovery System, it has no influence on the optimization process, and will be left out.

Part III

Optimization, Results and Further Investigation

Optimization 10

This chapter covers the optimization of the design and operation of the WHRS. First, the overall approach to the optimization is laid out. Then, the design and operation optimizations are described in detail. Finally, the results are presented.

10.1 Design Approach

To properly evaluate the WHRS, the power production must be optimized. While the configuration (i.e. the order of heat exchangers) will not be changed, the heat exchanger sizes will have an influence on how the system operates in full and part load. However, to properly evaluate one system design, the operation of the WHRS pressure wise must be optimized for that design, for all relevant loads. Hence, two optimization problems should be solved.

1. Design Pressures and Design Load
2. Operation Pressures

The design model takes an input of HP pressure, LP pressure and load. It will output heat exchanger areas and turbine constants. The performance model uses the areas and turbine constants already determined, along with a load and operation pressures, and calculates a power production. The optimization process is illustrated in Figure 10.1

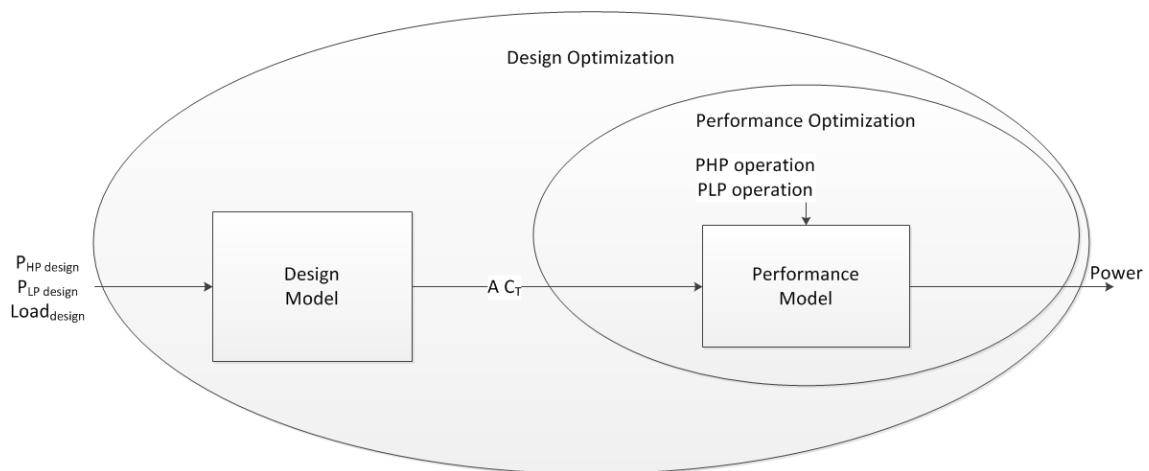


Figure 10.1: Illustration of the optimization process.

The iterative process will run as follows:

1. Design load, design HP pressure and design LP pressure are guessed.
2. Heat exchanger areas and turbine constants are calculated.
3. Power output for each load is found in the performance optimization.
 - a) Operation HP and LP pressures are guessed.
 - b) Mass flow and turbine powers are calculated.
 - c) Operation HP and LP pressures are adjusted.
 - d) Go back to b), repeat until convergence.
4. The weighed average power is calculated (function of optimal power over all loads).
5. Design Load, design HP/LP pressures are adjusted.
6. Go back to 2), repeat until convergence.

10.2 Design Parameter Optimization

Optimizing the design of the WHRS is a problematic proposition, since the design is largely limited to the physical arrangement of the components (see Chapter 8) and the dimensioning of these components. However, sizing heat exchangers would require corresponding sizes, prices and lifetimes. Without these, a larger heat exchanger area will always be better, since it would increase the heat transfer.

Since a financial analysis of heat exchanger dimensions is beyond the scope of this report, all heat exchangers will be designed using the LMTD (see Appendix E) and a system design pressure (for both HP and LP cycle) in the design model. This reduces the amount of design parameters to three: The HP pressure, the LP pressure, and a design load. These correspond to the inputs to the design model (see Section 8 for more details).

To evaluate the design, the power production for every load, in both Tier II and Tier III operation is taken into account. In the operation, the areas are considered constant, and heat transfer is calculated from the NTU method (see Appendix E).

The objective function for the design parameter optimization is seen in Equation 10.1. LR is the load repartition, as described in Section 2.3 (ex. the ship runs at 25% load 20% of the time, so the LR at 25% load would be 0.2). The coefficients 0.7 and 0.3 represent the repartition of operation between Tier II and Tier III [Diesel&Turbo, 2013b].

$$(10.1) \quad \bar{P}_{WHRs} = \sum^{load} (0.7 \cdot P_{WHRs,T_{II}} \cdot LR_{T_{II}} + 0.3 \cdot P_{WHRs,T_{III}} \cdot LR_{T_{III}})$$

P_{WHRs} for both Tiers are the optimum partial powers calculated as seen in Equation 10.5 for each load, using the optimal operation pressures. The way to find the optimal operation pressures is described in Section 10.3. The resulting \bar{P}_{WHRs} is the weighted average power.

The HP pressure cannot exceed the pressure of the pump, though the pump pressure could be increased at little expense until around 15 bar. Over 15 bar the material will reach a

performance step and the costs would increase about 20%. This is therefore taken as the highest allowable value [Condra, 2013].

The HP pressure is considered to be higher than the LP pressure. While it is possible to have a higher pressure in the second part of the stack, it would always yield poorer results (see Section 8.1 and 8.2), and would waste computation time.

To avoid negative flow in the low pressure turbine, the LP pressure has to be kept higher than the pressure in the condenser. However the limiting condition will be the condensation of sulphur in the stack (see Appendix D), which forces the LP pressure to be higher than 3.5 bar.

$$(10.2) \quad p_{HP} < 15 \text{ bar}$$

$$(10.3) \quad p_{LP} < p_{HP}$$

$$(10.4) \quad 3.5 \text{ bar} < p_{LP}$$

The design optimization objective function is extremely non-linear. Most commonly used optimization algorithms require somewhat smooth function values. For this reason, the problem is solved using a genetic algorithm solver. While time-inefficient, the genetic algorithm can work with any function, with any number of variables and any constraint. Unlike conventional solvers, the genetic algorithm is founded in stochastics, and is therefore not guaranteed to find an exact optimum. However, it will reliably find a good combination of input variables.

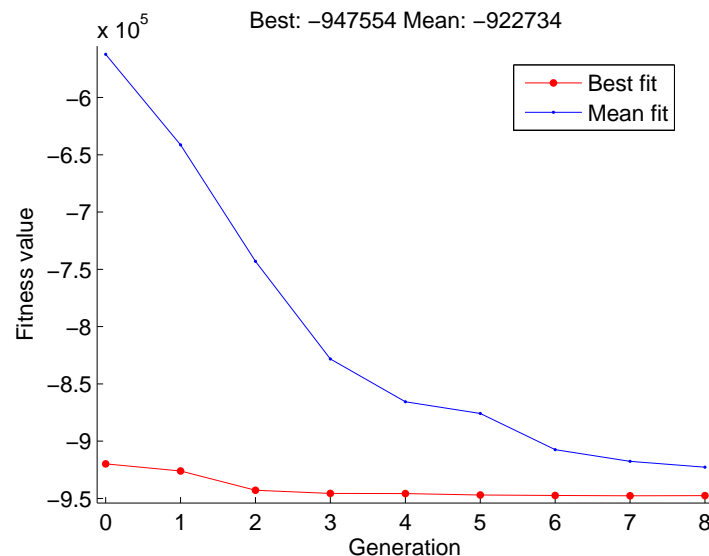


Figure 10.2: Evolution of the function value in the genetic optimization

The convergence plot in Figure 10.2 demonstrates the importance of optimization. A 'generation' consists of 20 guessed variable sets. The blue dots represent the average function value of these six guesses (i.e. The average saved power over all 6 guesses). The black dots represent the best values found. As seen already in the first generation of guesses, the best values provides a much greater power production than the average.

It can also be noted from Figure 10.2 that the best value does not improve significantly after the first round of guesses. This means that while some optimization is required, relatively few iterations are needed to find a value close to optimum.

The dependency of the optimum on the shape of the operation profile is investigated in Chapter 11.

10.3 Partload Operation Optimization

If the system is not operated optimally, the calculated power output will be skewed, and a design optimization may converge to wrong values. To ensure the legitimacy of the design parameter optimization, the operation of the system must be optimized for all attempted designs and at all loads.

Considering heat exchangers and turbines as pre-determined components, the operation will be optimized by changing the cycle pressures.

The objective function will be taken simply as the combined power production of the steam turbines, minus the power required by the pump (though this will be extremely small in comparison). The objective function to maximize is shown in Equation 10.5. The power turbine output will not be taken into account in this equation, since it will take only the leftovers of exhaust gas and will have no influence on the design performance of the system.

$$(10.5) \quad P_{WHRs} = P_{Turbine1} + P_{Turbine2} - P_{pump}$$

Since the turbine constants are found for the maximum turbine load, the turbine inlet pressure (and thereby the turbine mass flow) cannot exceed the pressure for which it was designed. Hence for both HP and LP cycle, the operation pressure must be lower than or equal to the design pressure. Additionally, the constraints of the design pressures also apply to the operation pressures. Since the HP design pressure is already lower than 15 bar, that particular constraint can be omitted. The operation pressure constraints are shown in Equations 10.6 through 10.9.

$$(10.6) \quad p_{HP} \leq p_{HP,design}$$

$$(10.7) \quad p_{LP} \leq p_{LP,design}$$

$$(10.8) \quad p_{LP} < p_{HP}$$

$$(10.9) \quad 3.5 \text{ bar} < p_{LP}$$

To summarize, for a given set of heat exchanger areas and turbine constants, the performance optimization will find the optimal HP/LP operation pressures to maximize the net power output (Equation 10.5), subject to the constraints in Equations 10.6 through 10.9. The problem is solved using *MATLAB*'s *fmincon* function. An example of the convergence of the *fmincon* function is shown in Figure 10.3

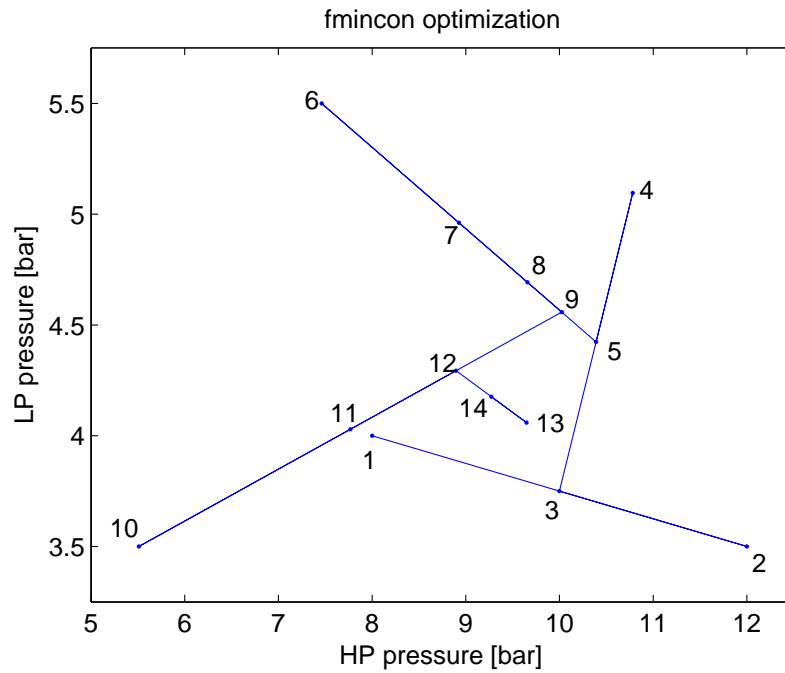


Figure 10.3: Example of *fmincon* convergence, the numbers represents the order in which the points are reached.

The *fmincon* function starts with a HP pressure of 8 bar and an LP pressure of 4 bar (point 1). A gradient in this point is calculated, and a large step is taken in the direction of the gradient (point 2). *fmincon* then find the best value between the two point (point 3), and start over by calculating a new gradient in this point. As seen in Figure 10.3 the optimum is found at around 9.25 bar and 4.25 bar (point 14). An infinite number of iterations would have shown a convergence with a snail pattern.

The optimum operation pressures were found to be 12.14 bar and 4.41 bar, with a design load of 100%. The operation pressures for this design are shown in Figure 10.4.

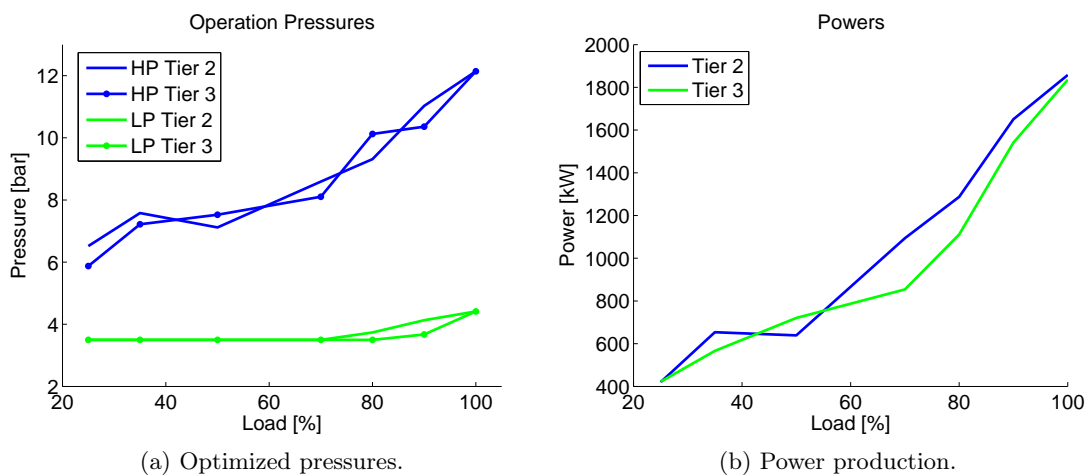


Figure 10.4: Optimised performance for design pressures of 12.14 and 4.41 bar.

Figure 10.4 shows a clear tendency for the optimum HP pressure to increase with the load. Higher loads result in a higher quantity of energy in the stack, and thereby a higher quantity of available energy for the WHRS. To increase the mass flow of the HP cycle correspondingly, the turbine inlet pressure has to increase. It is seen that the LP pressure is generally close to the minimum constraints, allowing it to absorb as much energy as possible.

Results Analysis and Discussion

11

This chapter investigates the dependency of the results on the ship operation. First, the influence the operation profile will be investigated, then the split between Tier II and Tier III.

11.1 Operation Profile Sensitivity Analysis

The influence of the operational profile on the viability of the system is investigated, since it significantly might skew the point of convergence of the optimization. The Tier III profile especially could be vastly different, since the ECA's are mainly located around coastal areas. Figure 11.1 shows four different operation profiles. Except for the MAN case, the profiles are considered the same in both Tier II and Tier III.

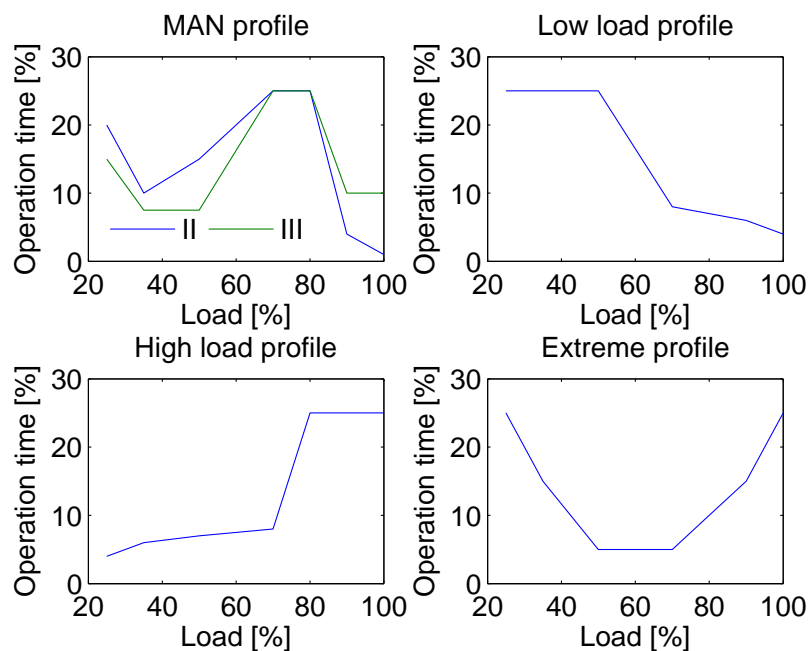


Figure 11.1: Tested operation profiles.

The first profile is given by MAN [Tveitaskog, 2013] and is the one that has been considered so far. The other profiles have been taken to test the model in extreme conditions (i.e. mostly high load, mostly low load, and only low and high load). The results of the optimization for each of the operation profiles in Figure 11.1 are shown in Table 11.1.

The HP and LP pressures are the results for optimum designed pressure. The design load represents the load at which the heat exchangers areas will be chosen and the power output represents the average heat recovery.

Profile	HP pressure [bar]	LP pressure [bar]	Design Load [%]	\bar{P}_{WHRS} [kW]
MAN profile	12.14	4.41	100	958
Low load profile	12.15	4.48	100	776
High load profile	11.54	4.73	100	1370
Extreme profile	12.14	4.41	100	1126

Table 11.1: Optimum design settings for the operation profiles shown in Figure 11.1.

From the optimized values in Table 11.1 it is clear that the design load does not appear to change with the operation profile. Generally, the quantity of heat in the system increases with the load, which leads to larger heat exchanger areas in the design model. Since the larger heat exchangers does not perform any worse at lower loads, there is no reason to design them at lower loads.

The HP and LP cycle pressures are different in that the design pressure determines the turbine constant, which has an influence on the mass flow at partial load. Hence a high design pressure can have a negative impact on the partload performance.

The higher energy content in the system at higher loads is also why the weighed average power is highest for the High load and smallest for the Low load profile.

11.2 Tier II / Tier III Operation Repartition Sensitivity Analysis

Another important parameter, which will change from ship to ship, is the ratio of Tier II to Tier III operation time repartition. MAN reports that the case study ship operates in ECA's (Tier III) 30% of the time [Diesel&Turbo, 2013b], see Section 2.3. However, this obviously depends on the route of the ship.

The optimized results for various operation distributions are shown in Table 11.2.

Tier II/Tier III distribution	HP pressure [bar]	LP pressure [bar]	Design Load [%]	\bar{P}_{WHRS} [kW]
100/0	12.14	4.41	100	944
70/30 (MAN)	12.14	4.41	100	958
50/50	12.14	4.41	100	973
30/70	12.14	4.41	100	984
0/100	12.14	4.41	100	1004

Table 11.2: Optimum design settings for ratios of Tier II to Tier III operation.

It is seen from the optimized results in Table 11.2 that the Tier II / Tier III repartition has a far smaller influence on the optimum design than the operation profile. Likely this

is because the operation profile of Tier II and Tier III looks very similar, and an optimum design for one would therefore approach an optimum design for the other.

Energy Efficiency

A way to quantify how good a WHRS is, is to measure how much of the available energy is recovered. Equation 11.1 defines the energy efficiency as the quantity of recovered energy, minus the amount of energy lost, divided by the quantity of energy available for recovery [Önder Kaska, 2014].

$$(11.1) \quad \eta_{energy} = \frac{P_{Turbines} - P_{pump}}{P_{available}}$$

$$(11.2) \quad \text{Tier II} \left\{ \begin{array}{l} P_{available} = \dot{m}_{eg} \cdot (h_{eg,stack\ inlet} - h_{eg@160^\circ C}) \end{array} \right.$$

$$(11.3) \quad \text{Tier III} \left\{ \begin{array}{l} P_{available} = \dot{m}_{eg} \cdot (h_{eg,stack\ inlet} - h_{eg@160^\circ C}) \\ + \dot{m}_{EGR} \cdot (h_{EGR,engine} - h_{EGR@200^\circ C}) \end{array} \right.$$

The definition of the available energy in Equations 11.2 and 11.3 is very close to the SPP used by MAN (Steam Power production, see Appendix D). Notably, the preheaters is not included in the available power. It should be noted that since the project focuses on the inclusion of the EGR, and thereby a significant increase in available power, the efficiency can be expected to decrease, despite the additional power production.

Exergy Efficiency

Recall from Chapter 8.1 Equation 11.4. Exergy (ψ) represents the potential work of a substance. Using a reference 'dead state', a maximum possible efficiency can be found using the quantity of thermal energy in a fluid, and the exergy level of the fluid.

$$(11.4) \quad \eta_{\psi-max} = \frac{\psi}{\Delta h} = \frac{(h - h_0) - T_0(s - s_0)}{h_T - h_{T_0}}$$

Applying exergy as a measure of maximum potential obtainable work, we define the exergy efficiency as seen in Equation 11.5 [Chen et al., 2014] [Fu et al., 2013].

$$(11.5) \quad \eta_{\psi} = \frac{\eta_{WHRs}}{\eta_{\psi-max}} = \frac{\frac{P_{Turbines} - P_{pump}}{\dot{m}_{eg} \Delta h_{available}}}{\frac{\dot{m}_{eg} \psi_{eg}}{\dot{m}_{eg} \Delta h_{available}}} = \frac{P_{Turbines} - P_{pump}}{\dot{m}_{eg} \psi_{eg}}$$

It should here by noted that Equation 11.5 only considers energy extraction from the stack. The EGR string is included by adding $\dot{m}_{EGR} \psi_{EGR}$ to the denominator.

The exergy efficiency describes how large a part of the actual available work is recovered. By defining the dead state individually for each heat source (to respect temperature constraints) the exergy efficiency illustrates how much more energy it is physically possible to extract from the system.

Figure 11.2 shows the various system efficiencies for the optimized systems.

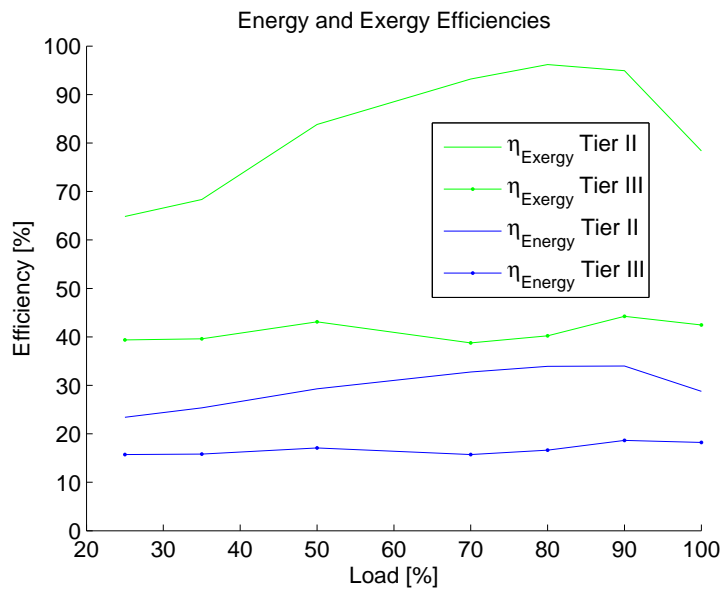


Figure 11.2: Energy and Exergy efficiencies as function of the load.

Notably, the Tier III efficiencies are much lower than the Tier II. This is not in itself alarming. The much lower capacity flow (as described in Section 8.2) means that the energy transfer in the EGR superheaters will be limited by the mass flows of the cycle, and not by the available energy in the EGR string.

To investigate whether the low mass flow is the sole purpose of the low efficiencies, the Second law efficiency is calculated in Equation 11.6. The second law efficiency is used to quantify the destruction of exergy (potential work) in a process.

$$(11.6) \quad \eta_{2nd\ law} = \frac{Exergy_{out}}{Exergy_{in}} = \frac{Exergy_{in} - Exergy_{destroyed}}{Exergy_{in}}$$

$$(11.7) \quad = \frac{m_{eg} \cdot \psi_{eg,out} + m_{HP} \cdot \psi_{HP,out} + m_{LP} \cdot \psi_{LP,out}}{m_{eg} \cdot \psi_{eg,in} + m_{HP} \cdot \psi_{HP,in} + m_{LP} \cdot \psi_{LP,in}}$$

Here, the second law efficiency of the stack and EGR heat exchangers will be calculated (Equation 11.7), to determine how much the setup or are of these negatively impact the overall efficiencies. The second law efficiencies for the stack and EGR heat transfers are shown in Figure 11.3.

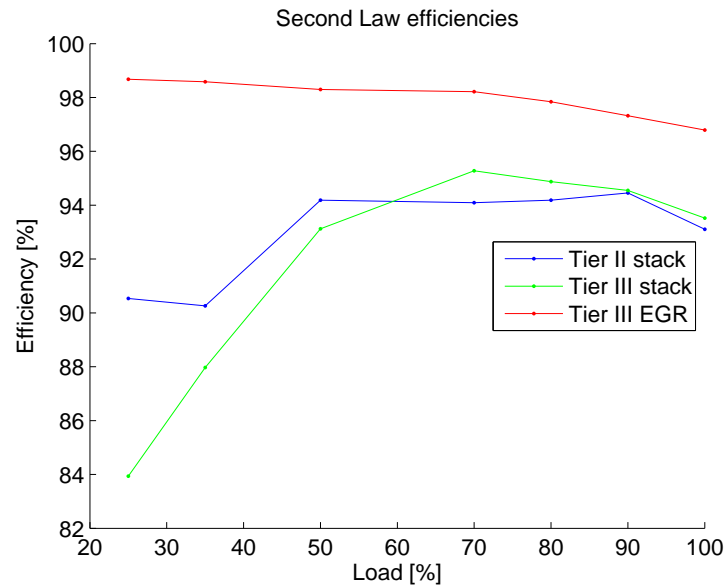


Figure 11.3: Second law efficiencies for the heat transfers in the stack and EGR. Note the scale of the y-axis.

The second law efficiencies reveal that very little potential work is destroyed. This, along with the large efficiency gap seen in Figure 11.2 means that while the system is efficient in transferring work, there is a large quantity of un-used work left in the recirculated exhaust gas.

CO₂ Reduction and EEDI 12

This chapter will present an estimate of the CO₂ savings, and describe the EEDI index. The benefits of having a WHR system on the EEDI will be outlined.

12.1 CO₂ Emission Reduction

Assuming that the Waste Heat Recovery, when put in place with the possibility to run in Tier III, recovers up to 1.2 MW, the CO₂ emissions reduction can be evaluated by doing various assumptions.

- The fuel used by the auxiliary engines is Diesel ISO 8217 [MEPC, 2012].
- The number of ton of CO₂ emitted per ton of fuel is $C_F=3.206$ [MEPC, 2012].
- The SFOC of the auxiliary is 185 g/kWh [Diesel&Turbo, 2012].
- The generator efficiency of the auxiliary engine is 93% [Diesel&Turbo, 2012].

The CO₂ savings per hour are then calculated with Equation 12.1.

$$(12.1) \quad \Delta CO_2/h = SFOC_{AE} \cdot P_{WHRs} \cdot C_F \cdot \frac{1}{93} = 765 \text{ kg/h}$$

If it is assumed that the ship will run for 6 500 hours during a year [Diesel&Turbo, 2012] and that the WHRS savings stays constant, the maximum saving is up to 5 000 tons of CO₂ per year.

12.2 EEDI

The EEDI abbreviation stands for Energy Efficiency Design Index. It quantifies the amount of CO₂ emitted by a ship, related to the amount of goods transported and the distance traveled. It is defined by the IMO under the MARPOL convention Annex VI. The attained EEDI has to be provided to the IMO by the ship owner for every new ship or which has undergone a major conversion. The ship EEDI is becoming more restrictive over time, lowering the amount of CO₂ to be emitted by ~10% every 5 years. The exact formula to calculate the EEDI can be found in the MEPC 63/23 Annex 8. It is a fairly complex equation, so for simplification purposes the BIMCO evaluation tool will be used [BIMCO, 2013].

12.3 Influence of Heat Recovery on EEDI

The WHRS converts waste heat to electricity. This electricity is used for on-board applications, that would otherwise be powered by auxiliary engines. This will lower the amount of fuel consumed and therefore the amount of CO₂ emitted. In this project the frame has been put on the engine and the WHR/EGR but not on a particular ship. An example ship will be used to show how the system studied can impact CO₂ emissions.

The MCR of the engine is 52290 kW with a SFOC of 162 g/kWh consuming HFO [Turbo, 2012]. The ship deadweight for this kind of engine is assumed to be 110 000 ton. The auxiliary engines are assumed to cover 15 % of the main engine power, so two auxiliary engines with an MCR of 3 800 kW and a consumption of 185 g/kWh using Diesel ISO 8217 will be considered in the EEDI calculation. Finally, the innovative energy efficient technology (i.e the WHRS and the power turbine) will be taken at 1200 kW.

The attained EEDI without WHRS is 14 942. The achieved EEDI with WHR in that case study is 14 429 and shown in Figure 12.1 as well as the present and future limit values.

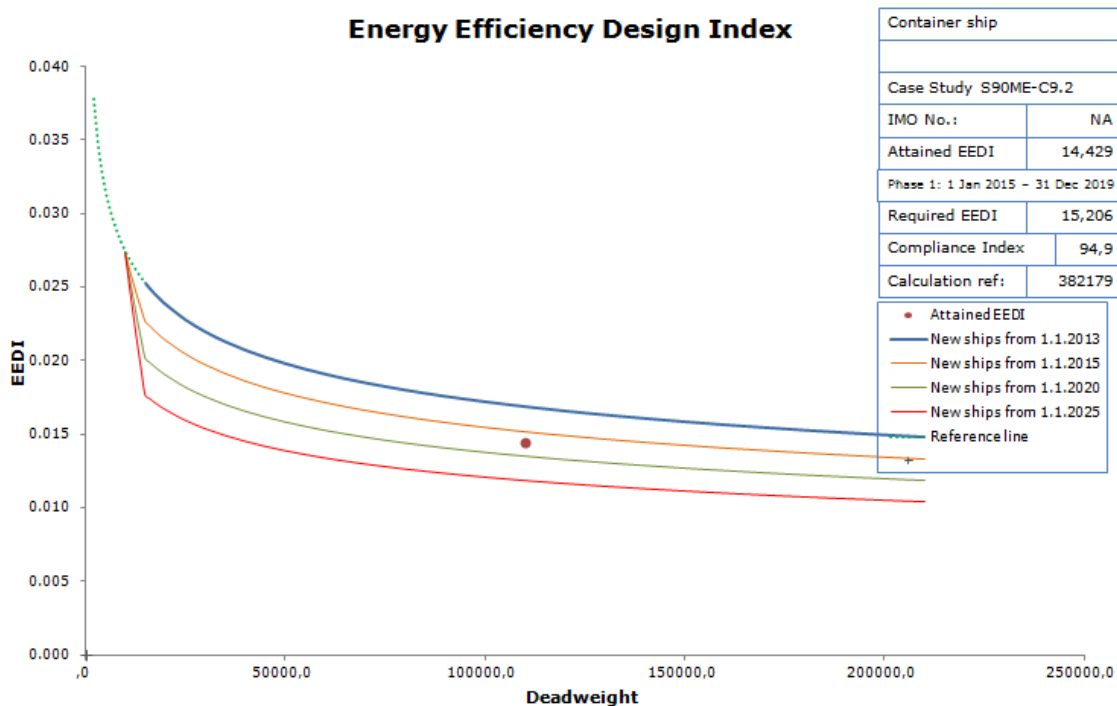


Figure 12.1: Calculated EEDI for case study.

The achieved EEDI of 14 429, corresponds to a reduction of 3.5% compared to a system without heat recovery. This represents a 500g reduction of CO₂ per deadweight and per mile. Savings are lower than a system not using EGR, due to much lower savings of the power turbine [M&M, 2013].

Tier III Exclusive Cycle 13

This chapter investigates the potential of introducing an additional Tier III exclusive cycle. The purpose of this cycle is to recover the remaining energy from the EGR, not used in the initially proposed system.

13.1 Remaining EGR Power

In an attempt to remain close to the already installed WHRS, the system shown and investigated in the report installs only two additional heat exchangers being the two superheaters in the EGR string. However, since the capacity flows of the cycle fluids are much smaller than that of the EGR, much energy is still not utilized.

To establish the full potential of Waste Heat Recovery, a third cycle is therefore installed directly onto the EGR string. This means that the cycle will not be active at all during Tier II operation.

13.2 Revised System

To ensure that the scrubbing process can still fully take place, the outlet temperature of the EGR is still limited to 200°C. Since the outlet temperature is so high, the new cycle can feasibly evaporate at a higher pressure than the HP cycle, and therefore operates at a generally higher pressure. Therefore, the superheater of the new system is placed before the HP cycle superheater, since the same exit temperature will yield greater exergy (i.e. greater system efficiency).

Since the system is generally limited to 15 bar pressure due to material constraints, the evaporation temperature will not exceed 200°C, and the new evaporator is therefore placed after the LP cycle superheater in the EGR string.

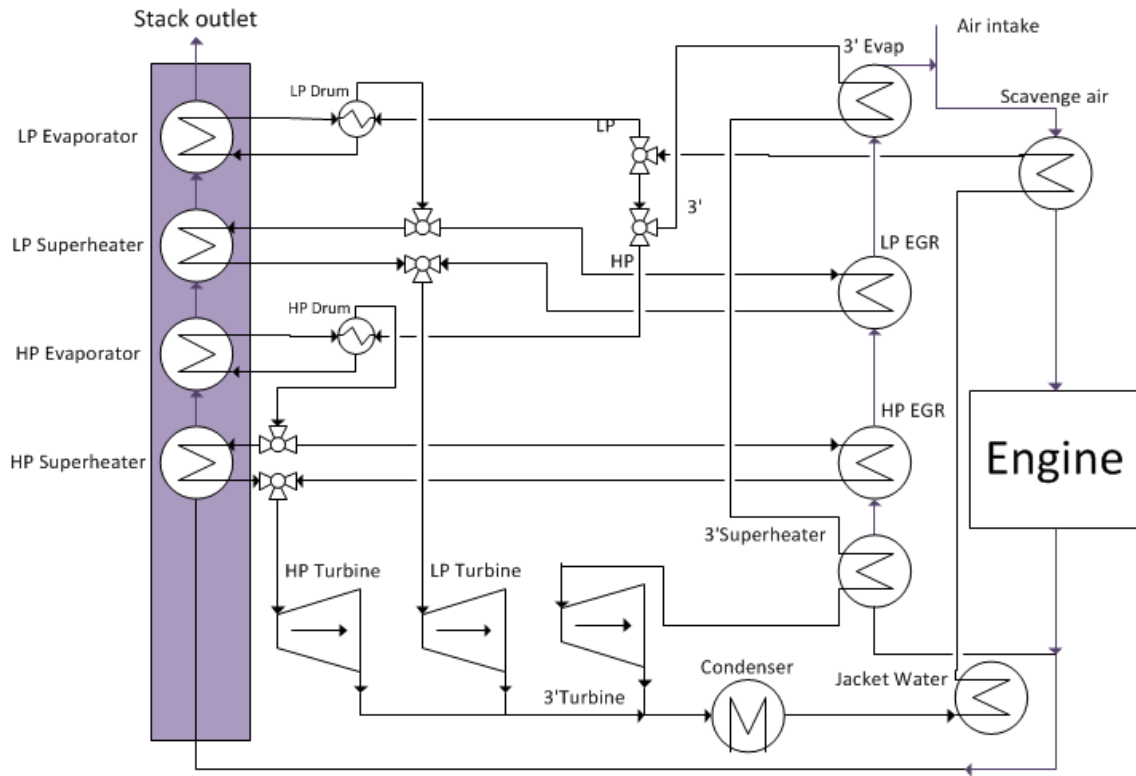


Figure 13.1: Schematic of the proposed WHRS system.

The system is investigated both as a retro-fit to the already existing system, and as a baseline plan which is optimized with the third cycle in mind.

13.3 Results

Figure 13.2 shows the operation pressures and power production of the retro-fit system. The operation is optimized as described in Section 10.3. The third cycle is kept at 15 bar at all times, and expanded in a valve before the turbine if the mass flow is insufficient. This is done to ensure the exit temperature of the EGR does not drop below 200°C , while also respecting the upper limit of 15 bar set due to the material constraints in Section 10.2. This means that to respect Stodola's law, the pressure is reduced in a valve before the turbine inlet.

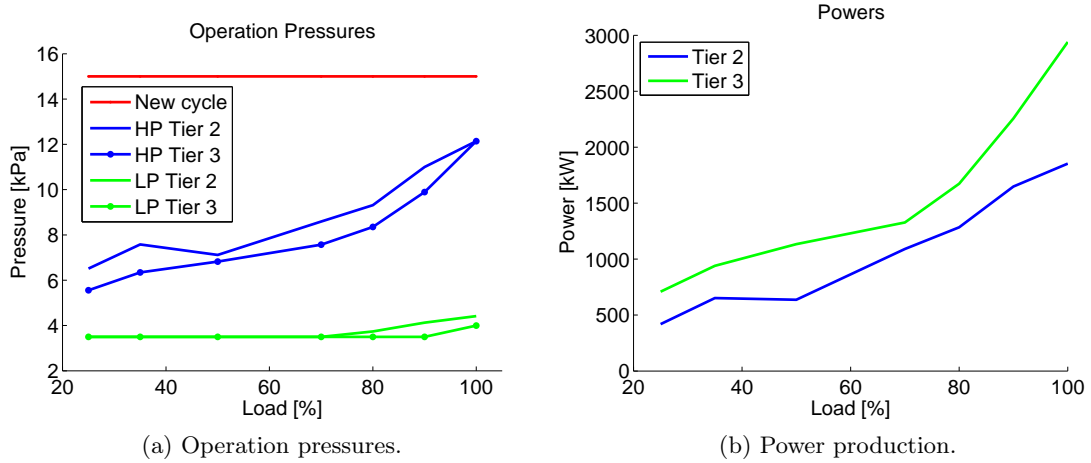


Figure 13.2: System performance of the retro-fit third cycle.

Relative to the initial proposed system presented in Section 8.3, the power production in Tier III is significantly higher. This is true for all loads, but more so at high loads. Since the system only changes in the EGR string, the Tier II production is unchanged. Table 13.1 shows the expected power production values when operating in Tier III 30% of the time (as is currently the case) and when operating in Tier II 70% of the time (if ECA's are expanded).

The system was investigated both as a retro-fit option (applying 2 additional heat exchangers to the previously optimized system) and as baseline (entire system re-optimized).

System	Ratio	HP pressure [bar]	LP pressure [bar]	3rd pressure [bar]	\bar{P}_{WHRs} [kW]
3rd Retrofit	70/30	12.14	4.41	15.00	1105
	30/70	12.14	4.41	15.00	1349
3rd Baseline	70/30	9.27	4.05	15.00	1164
	30/70	9.27	4.06	15.00	1482

Table 13.1: Performance of the system including a third cycle in the EGR string. All values use the MAN operation profile.

A benefit of approximately 150kW is found from the third cycle, relative to the originally proposed system (results of which can be seen in Table 11.1). The relatively small benefit is because the extra cycle is only active in Tier III operation, and the benefit is therefore reduced. Increased operation within ECAs significantly impacts the benefit of the third cycle.

Likewise, including the third cycle in the system optimization (i.e. designing with a third cycle as baseline) has only a small influence with current operation conditions. Here also, the difference is much larger when Tier III becomes more dominant.

While a thorough economic analysis is beyond the scope of this report, Table 13.2 shows the increase in total heat exchanger areas when implementing the third cycle, compared to

the originally proposed system. It is emphasised that the calculated areas represent gross estimates. However, the table illustrates the relative size of the additional equipment.

System	Ratio	Total Area [m ²]	+m ² [m ²]	+% [%]	+ \bar{P}_{WHRS} [kW]
No 3rd Cycle	70/30 MAN	5886	-	-	-
	30/70 MAN	5886	-	-	-
3rd Retrofit	70/30 MAN	7452	1566	27	147
	30/70 MAN	7452	1566	27	365
3rd Baseline	70/30 MAN	6963	1077	18	176
	30/70 MAN	6963	1077	18	529

Table 13.2: Changes in total estimated heat exchanger area.

As also seen in Tables 13.1 and 11.2, the optimal design pressures (and thereby the heat exchanger areas) are the same for the ratios of 70/30 and 30/70. Introduction of a third cycle represents an increase of 27% compared to the originally proposed system. An additional turbine and piping is not included in this, further increasing the cost. Notably, the system is both smaller and more efficient if the third cycle is included in the system optimization. The smaller area is a consequence of the lower design pressures, as seen in Table 13.1.

13.4 Conclusion

While the addition of a third cycle would increase the energy recovery in Tier III operation, the quantity of additional equipment required to do so is rather large. This means that the upgrade will likely not be worthwhile, if Tier III operation remains below 30%. This is especially considering the possibility that not only heat exchangers, but also a turbine would be needed.

Considering the high political focus on environmental concerns described in the introduction, it is likely that ECAs will eventually be expanded. At a such time it may prove feasible to return to the concept of a third cycle. until then, the third cycle is most likely only a good investment for ships operating mainly within ECAs.

Conclusion 14

WHRS is an efficient way to recover energy lost as heat after the combustion. International regulations have forced the ship owner to reduce emissions and to use systems such as EGR. Whether EGR and WHRS can work together has been investigated.

The HFO composition has been assumed to be a long carbon chain. The concentration of each element has been determined based on the LHV, by the use of the statistical method. The evaluated fuel is $C_1H_{1.54}O_{0.02}S_{0.01}$. To model the combustion, the Glassman mechanism was selected. A mixture of smaller fuels was used to fit with the various molar concentrations and the average LHV. The amount of excess air has been assumed as given by MAN. The resulting exhaust gas was computed with its thermodynamic properties.

The EGR re-introduces some of the exhaust gas into the combustion chamber. This recirculation will dilute the fuel, increasing the heat capacity and lowering the adiabatic flame temperature from 1350 K to 1000 K by using 10% to 55% EGR.

The NO_x production is highly dependent on the temperature of combustion. The lower the temperature is, the lower the formation will be. By lowering the combustion temperature by 200 K, the formation rate can be reduced by a factor of around 100. The NO mole fraction is decreased by a factor of 10 by going from 10% to 50% EGR. The EGR will also have an influence on the SO_x equilibrium composition. The higher the EGR, the more SO_3 will be formed, whereas the amount of SO_2 will decrease. The EGR is assumed known and optimized by MAN, with higher level for lower load. The new exhaust gas has been computed and it has been found that the thermal properties were not significantly influenced by the new composition.

A WHRS converts part of the thermal energy in the exhaust gas to electricity through one or more Rankine cycles. The WHRS model was based on a previous investigation made by the authors.

A general study of exergy showed that water could transfer more energy per mass the higher the temperature. When a WHRS was designed to include the EGR string, a superheater for each Rankine cycle was placed in the EGR string, increasing the cycle fluid temperature to near 400°C. Other sources of heat were arranged to minimize the temperature difference between the cycle fluid and the source of heat. It was found that no more than $\sim 1/3$ of the power in the stack could be transferred as work to the turbine.

Two system models were constructed. The first calculated heat exchanger areas from

the LMTD method, using design pressures and pinch values. Pinch values of 10 K were used for gas components, whilst 5 K was used for the jacket water. This method was used to obtain reasonable values for heat exchanger parameters without requiring detailed information on investment costs.

Additionally, a performance model was created, to calculate partload performance of the system. The performance model used fixed heat exchanger areas and turbine constants, and calculated system performance using the NTU method.

A power turbine in parallel with the engine turbocharger was also investigated. It was found capable of producing up to an additional $\sim 10\%$ power in addition to the WHRS.

The overall optimization consisted of two parts, an overall system design-, and a partload operation optimization. To ensure a true optimum design, the offload performance is optimized in an embedded system performance optimization, using a Hessian-based algorithm. It is found that the low pressure should generally be kept near the minimum constraint, which allows the largest amount of total energy to be transferred to the cycles. The optimum high pressure is found to be around 7 bar at the lowest load, but increases with the load to around 12 bar.

The overall system design function was found to be too unsteady for gradient-based optimization, and a genetic algorithm was used. For normal operation, the best overall expected power production was found to be 958 kW, with a design high pressure of 12.41 bar and a design low pressure of 4.14 bar. These power savings could lead to a CO₂ reduction of up to 5 000 tons per year, corresponding to an EEDI reduction of 3.5%.

An investigation of the influence of the operation repartition shows no change in design pressure optimum, though the expected power increases up to 1004 kW when more time is spent within ECAs. However, the optimum design point is found to change slightly with the operation profile.

The optimized system is found to have an energy efficiency between 25 and 35% in Tier II, and between 15 and 20% in Tier III. The exergy efficiency shows a much greater variation. In Tier II it ranges from 65 % at minimum load to 95% for the most common operation load, meaning that room for significant improvement exist only in severe partload. For Tier III, the exergy efficiency ranges from 40 to 45%, indicating that much more energy could be extracted from the EGR string.

The introduction of a third (EGR exclusive) cycle is investigated. It is found that retrofitting the third cycle would increase the expected power savings to 1105 kW corresponding to an increase of 15%. Moreover, having included the cycle in the optimization would further increase it to 1134 kW, or 18%. Furthermore, these values were found to significantly increase if the Tier III operation was to become larger.

With the introduction of the third cycle, very little potential work is left to be extracted from the post-engine exhaust gas, stack outlet temperature remaining constant. The waste heat left is mainly found in jacket water and scavenge air, which are both very low temperature sources.

Recommendations for Future Work 15

Engine Model

The exhaust gas thermodynamic properties are highly dependent of the engine characteristics. A more accurate study/model of the engine and of the combustion would give more accurate data on the consumption and results of the state of the exhaust gas at various load.

Combustion Mechanism

A relatively simple mechanism has been taken into account in this model to calculate the exhaust gas composition. Having a larger mechanism, more dedicated to large carbon chain and which includes Sulfur, could provide more accurate results.

NO_x Emissions

The NO_x emissions have been taken at equilibrium for a given pressure and temperature. Having a pseudo dynamic model, taking into account the variation of temperature and pressure with the crank angle, would be of interest to provide more realistic NO_x emission levels. Calculating and optimizing the level of EGR would then also be possible.

Sulfur Concern

Sulfur concerns have been put on the side during this project to focus on NO_x and CO₂ emissions as well as power savings. Several aspects linked to Sulfur could be investigated more extensively such as the scrubbing process in the EGR string and the water treatment unit. The Sulfur condensation also limit the outlet temperature of the stack, and therefore the energy recovery.

Concrete Component Modelling

Using concrete real component data would increase the reliability of the result. In reality, heat transfer coefficients are not constant, and heat exchangers are characterized by more parameter than an area. This is true for the turbines as well. Using data sheet for these components instead would increase the legitimacy of the model results.

Economic Optimization

The project put its focus on energy savings without considering the costs of the various components as function of their size. An economic optimization could be done and show that maximizing the power savings might not be the most profitable configuration, depending on the prices of the fuel.

Low Temperature Heat Recovery

The remaining energy to be recovered consists mostly of low temperature heat. Investigating a waste to recover this heat could further improve the global system efficiency.

References

- BIMCO, 2013. BIMCO EEDI Calculator. BIMCO. URL:
<https://www.bimco.org/Products/EEDI.aspx>.
- Boles, M.A., Cengel, Y.A., 2011. Thermodynamics, An Engineering Approach. 7th ed., McGraw-Hill. ISBN: 978-007-131111-4.
- Cengel, Y.A., Turner, R.H., Cimbala, J.M., 2008. Fundamentals of Thermal-Fluid Sciences. McGraw Hill. ISBN; 978-007-126631-4.
- Chen, K., Wang, J., Yiping Dai, Y.L., 2014. Thermodynamic analysis of a low-temperature waste heat recovery system based on the concept of solar chimney. Energy Conversion and Management 80 .
- Condra, T., 2013. Conversations with Thomas Condra, AAU.
- Diesel&Turbo, M., 2012. Waste Heat Recovery System (WHRS) for reduction of fuel consumption, emissions and EEDI.
- Diesel&Turbo, M., 2013a. AAU-2013 14000TEU CV 9S90ME-C9.2.
- Diesel&Turbo, M., 2013b. Tier III Two-Stroke Technology. MAN Group.
- EPA, 2014. Overview of Greenhous Gases. United States Environmental Protection Agency. URL:
<http://www.epa.gov/climatechange/ghgemissions/gases/co2.html>.
- Finace&Economics, C.R., 2014. US Gasoline Prices and Brent Crude Oil Prices.
- Fu, W., Zhu, J., Zhang, W., Lu, Z., 2013. Performance evaluation of kalina cycle subsystem on geothermal power generation in the oilfield. Applied Thermal Engineering 54.
- GALCIT, 1997. URL:
<http://www2.galcit.caltech.edu/EDL/mechanisms/mechs/glassman>.
- Glassman, I., 1996. Combustion, 3rd ed. (Appendix B). Academic Press. ISBN: 978-0-12-285852-9.
- Heywood, J.B., 1988. Internal Combustion Engine Fundamentals. McGRAW-HILL. ISBN: 0-07-100499-8.

- IMO, 2011. Mandatory energy efficiency measures for international shipping adopted at IMO environment meeting. International Maritime Organization. URL: <http://www.imo.org/MediaCentre/PressBriefings/Pages/42-mepc-ghg.aspx#.UviiZ4XGA6Y>.
- IMO, 2013a. Nitrogen Oxides - Regulation 13. International Maritime Organization.
- IMO, 2013b. Sulphur Oxides (SOx) - Regulation 14. International Maritime Organization.
- IMO-MEPC, 2009. Resolution MEPC 184(59), Guide for exhaust gas cleaning systems. Marine Environment Protection Committee. URL: http://www.imo.org/blast/blastDataHelper.asp?data_id=26469&filename=184%2859%29.pdf.
- J.Moldanova, e.a., 2009. Characterisation of particulate matter and gaseous emissions of a large ship diesel engine. Atmospheric Environment 43, 2632–2641.
- Önder Kaska, 2014. Energy and exergy analysis of an organic rankine for power generation from waste heat recovery in steel industry. Energy Conversion and Management 77.
- KG, A.S.G..C., . Global Maritime Trade on Course. Esplanade 23, 20354 Hamburg, Germany. URL: <http://www.auerbach-schifffahrt.de/en/knowledge/>.
- Laval, A., . Online Product Descriptions. <Http://www.alfalaval.com/solution-finder/products/Pages/default.aspx>.
- MEPC, 2012. Annex 8 Resolution MEPC.212(63), 2012 guideguide on the method of calculation of the attained energy efficiency design index (EEDI) for new ships. MEPC. MEPC 63/23 Annex 8 pages 1-20.
- M&M, 2013. Multi Stage Waste Heat Recovery Model and Analysis for Large Container Ship. Technical Report. AAU.
- Nielsen, M.P., 2013. Analysis Of Advanced Thermal Process Systems. Notes and Slides from mm1.
- Stuart, D., 2010. Acid dewpoint temperature measurement and its use in estimating sulfur trioxide concentration. International Society of Automation 3.3, 1–12.
- Turbo, M.D., 2012. MAN B&W S90ME-C9.2-TII Project Guide Electronically Controlled Two-stroke Engines.
- Turbo, M.D., 2013. Emission Project Guide MAN B&W Two-stroke Marine Engines. MAN B&W.
- Turns, S.R., 2000. An Introduction to Combustion, Concepts and Applications. McGRAW-HILL. ISBN: 0-07-230096-5.
- Tveitaskog, K.A., 2013.
- Verhoff, F., Banchemo, J., 1974. Predicting Dew Points of Gases. Chemical Engineering Progress.

Wärtsilä, 2011. Wärtsilä waste heat recovery. Wärtsilä-O-E-RT-WHR-2.

Wärtsilä, 2012. Realising the competitive potential of sulphur ECA compliance. URL:
[http://www.wartsila.com/fi/
realising-the-competitive-potential-of-sulphur-ECA-compliance.](http://www.wartsila.com/fi/realising-the-competitive-potential-of-sulphur-ECA-compliance)

CD Content A

- A.1: Digital copy of this report January-June 2014
- A.2: Digital copy of the previous report September-December 2013
- A.3: Digital copy of the scientific paper presented in December 2013
- A.4: UNESO PBL inauguration presentation poster presented in June 2013
- A.5: MATLAB script of the Model
- A.6: EEDI Calculator Data-sheet
- A.7: PDF version of used references
- A.8: Summary presented at EPF-Sceaux, France, Engineering school in April 2014
- A.9: Glassman Mechanism

IMO Emissions Regulations B

B.1 Nitrogen Oxides - Regulation 13

NO_x is a generic term that refers to nitric oxide NO_x and nitrogen dioxide NO₂. They are produced during the combustion and particularly at high temperatures. NO_x gases react and form smog and acid rain. They also react in the atmosphere in the presence of sun radiation to create tropospheric ozone. In its will to control NO_x emissions from large ships diesel engines, the IMO has given restrictions regarding emissions in function of the date of ship construction and engine's rated speed.

The NO_x limits are evaluated in a mass quantity per kWh. The full regulation can be found in the IMO Regulation 13 [IMO, 2013a] . Figure B.1 outline the different values for emissions limits.

Tier	Ship construction date on or after	Total weighted cycle emission limit (g/kWh) n = engine's rated speed (rpm)		
		n < 130	n = 130 - 1999	n ≥ 2000
I	1 January 2000	17.0	$45.n^{-0.2}$ e.g., 720 rpm – 12.1	9.8
II	1 January 2011	14.4	$44.n^{-0.23}$ e.g., 720 rpm – 9.7	7.7
III	1 January 2016*	3.4	$9.n^{-0.2}$ e.g., 720 rpm – 2.4	2.0

* subject to a technical review to be concluded 2013 this date could be delayed, regulation 13.10.

Figure B.1: NO_x Regulations [IMO, 2013a].

The Tier III controls apply only to the specified ships while operating in Emission Control

Areas (ECA) established to limit NO_x emissions. Outside such areas the Tier II controls apply [IMO, 2013a].

B.2 Sulfur Oxides - Regulation 14

SO_x is a generic term that refers to the sulfur oxides as SO, SO₂ and SO₃. They are of particular interest for the ship designer since sulfuric dioxide can oxidize in sulfuric acids and damage the equipments. Sulfur dioxide is also a major air pollutant. They are the precursor of acid rains, damaging locals fauna and flora.

IMO wish to control the SO_x and particulate matter emission to all fuel oil, combustion equipment and devices on-board. IMO has considered two case: Outside an ECA and inside an ECA. The fuel oil sulfur limits can be found in Figure B.2 and are expressed in term of % kg/kg [IMO, 2013b].

Outside an ECA established to limit SO _x and particulate matter emissions	Inside an ECA established to limit SO _x and particulate matter emissions
4.50% m/m prior to 1 January 2012	1.50% m/m prior to 1 July 2010
3.50% m/m on and after 1 January 2012	1.00% m/m on and after 1 July 2010
0.50% m/m on and after 1 January 2020*	0.10% m/m on and after 1 January 2015

Figure B.2: SO_x Regulations [IMO, 2013b].

IMO gives the following information regarding the different ECA established:

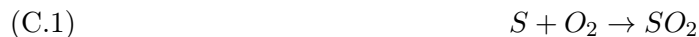
- *Baltic Sea area as defined in Annex I of MARPOL (SO_x only)*
- *North Sea area as defined in Annex V of MARPOL (SO_x only)*
- *North American area (entered into effect 1 August 2012) as defined in Appendix VII of Annex VI of MARPOL (SO_x, NO_x and PM)*
- *United States Caribbean Sea area (expected to enter into effect 1 January 2014) as defined in Appendix VII of Annex VI of MARPOL (SO_x, NO_x and PM)*

SO_x and Scrubbing C

The following chapter introduces the problem linked to the Sulfur content in the exhaust gas recirculation string. The oxidation of Sulfur is described. The purpose of using a pre-scrubber and a scrubber is explained. The water treatment system is detailed as well as the process to capture the sulfuric molecules.

C.1 Sulfur Oxidation in the Exhaust Gas

Sulfur will lead to the formation of SO_x molecules by oxidation. These formations are shown in Equation C.1 (for 95 % of the Sulfur) and Equation C.2 (for 5 % of the Sulfur). The emissions of SO_x will need to respect the IMO limitation at all times.



The presence of SO₃ combined with water can lead to the destruction of some components by the formation of Sulfuric acid when the exhaust is condensing (see more detailed explanations in Appendix D). If exhaust gas is recirculated, the exhaust will contain SO₂ molecules which can damage the combustion process and the combustion chamber by accumulating, if not treated. Therefore, the exhaust will have to be cleaned of its SO_x compounds before it is sent back to the combustion chamber.

There are two aspects in the SO_x composition of the exhaust gas. The first one regards the IMO regulation, which gives a maximum limit. The other aspect will be the accumulation of soot in the combustion chamber due to the sulfur content of the fuel and the recirculation of exhaust gas. Both problems could be resolved by the use of a high quality fuel, containing very low quantities of Sulfur. However such a fuel will be extremely expensive; which leads to the second solution: the use of a scrubber to capture most of the SO_x molecules. A third alternative will be to use a dual engine that could operate with LNG (Liquified Natural Gas) for Tier III but this solution will not be considered in this report.

By recirculating the exhaust gas, the Sulfur compounds will accumulate in the combustion chamber if not treated. Thus, before recirculating to the engine, the exhaust is cleaned by a pre-scrubber and a scrubber. Most of the information presented in the following parts have been provided by MAN and can be found more in details in the emission guide [Turbo, 2013].

C.2 System Outline

The scrubbing system presented here is developed by Alfa Laval. A pre-scrubber is placed at the beginning of the EGR string to supersaturate the exhaust with water. This will help later to capture the SO_x molecules. The exhaust will then be cooled with a heat exchanger to 200°C as recommended by MAN [Tveitaskog, 2013] to avoid condensation after the scrubbing process which will also lower the temperature of the exhaust gas. The EGR string diagram can be seen in Chapter 2, Figure 2.8. Fixing the temperature will help to avoid condensation after the scrubber when the temperature of the exhaust will be lowered.

In parallel to the scrubbing, the water treatment system will have several objectives:

- Removal of accumulated particles.
- Neutralization of the sulfuric acid.
- Delivery of water at sufficient rate and pressure.
- Capability to handle the surplus of water accumulated in the system from the combustion.
- If discharged overboard, the quality of the surplus water needs to meet the international regulations by after cleaning [IMO-MEPC, 2009].

A sketch of the scrubbing and water treatment system can be seen in Figure C.1.

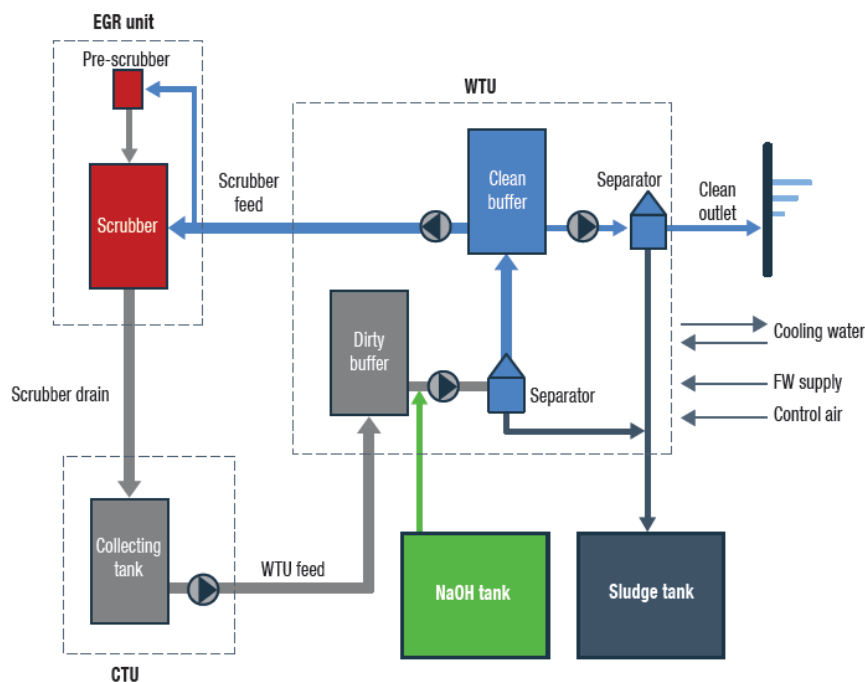


Figure C.1: Scrubbing system diagram [Turbo, 2013].

On Figure C.1, three distinct units can be identified. The EGR unit which regroups the pre-scrubber and the scrubber, the CTU (Collecting Tank Unit), the WTU (Water

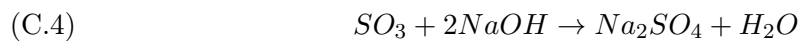
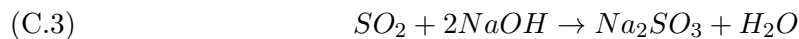
Treatment Unit) which is used to clean the scrubbing water and the Sludge and NaOH tank.

EGR Unit

The purpose of the EGR scrubber unit is to saturate the exhaust gas with water and capture the SO_x and particles by the use of a pre-scrubber and scrubber. Many different kinds of scrubbers exist, but for most of them, the exhaust will cross several layers of packed beds on which water is sprayed. This will increase the efficiency of the scrubber by increasing the reaction surface area and by improving the mixing of water and exhaust gas. Clean exhaust is released and dirty water is moved to the collecting tank unit.

WTU

The purpose of the WTU will be to clean the dirty water and, in a closed loop, pump it back to the scrubbers. Since the exhaust contains water, an accumulation will occur, and water will have to be released. A NaOH solution will be used for cleaning. The equations for the NaOH reaction with SO_x are shown in Equation C.3 and C.4.



The Sodium Sulfates will be extracted from the water by the use of separators.

NaOH and Sludge Tank

The NaOH used during the journey will have to be stored in a tank. The solution of NaOH generally used is a 50 % concentration solutions. Once the particles and sulfates have been separated from the main flow the water cannot be released in the sea and have to be stored on-board. The sludge outlet from the WTS will be aqueous. The design of the size of the tank will have to take into account the power of the engine and sailing time in ECAs as well as other parameters. [Turbo, 2013]

Power Consumption

Additional power will be required to run the cleaning system. This will have an impact on the overall efficiency of the EGR and WHR system. The additional required power to run the water treatment will come from the EGR unit and the WTS which will be the significant consumers. For the WTS, the electricity required relates to the scrubber water flow, which relates to the engine power and load. Pumps will be needed to run the water to the EGR unit. From the EGR unit the power required will be related to the fan needed to raise the pressure of the EGR. It will be function of the engine power, the load and the EGR rate. It is hard to determine exact values for the power consumption, but MAN provides a rule of thumb to obtain a quick estimation. The overall penalty for the consumption is estimated to be between 1 and 2 g/kWh, representing a consumption penalty of more or less 1% on the SFOC.

Sulfuric Acid D

The following chapter introduces the Sulfur concerns in the stack. The formation of Sulfuric acid as well as its formation condition are described. The security margin taken at the outlet of the stack is explained and its influence on the available energy to be recover is shown. An evaluation of the amount of energy lost to the security margin is made.

D.1 Sulfur Concern

When entering the stack, the exhaust gas is still at a relatively high temperature $\sim 220^{\circ}\text{C}$ for Tier II and Tier III. It contains energy that has to be recovered by a Waste Heat Recovery System. However due to the Sulfur content of the exhaust gas, this recovery will be limited. The Sulfur content in the exhaust gas will be a main concern for the ship designer.

If SO_3 and water are present in the exhaust, the SO_3 might condense in the stack under low temperatures and form H_2SO_4 as shown in Equation D.1. The concentration will increase if the fuel contains substances such as Vanadium pentoxide, which may act as a catalyst and increases SO_3 formation [Stuart, 2010].



The condensation of the sulfuric acid will occur on the surface of components when the temperature is below the dew point. Corrosion may appear and damage or even destroy some parts of the Waste Heat Recovery System. Therefore, presence of Sulfuric acid, even in low quantities in the exhaust could jeopardize the life time expectancy of the system when condensing.

D.2 Interest of Sulfur Control

The exhaust gas will contain a small quantity of Sulfur that could, under certain temperatures, lead to Sulfuric acid production on the surface of some components.

For on-shore application systems are put in place to take care of this SO_2/SO_3 . For example some processes are using Sodium carbonate and Sodium bicarbonate solutions to remove SO_3 [Stuart, 2010]. However the use of those applications can be limited on a ship due to the required volumes of such systems.

The easiest and most common solution for ship owners will be to fix the outlet temperature of the exhaust gas in order to avoid to reach the dew point. Thus, fixing the outlet temperature, will limit the exhaust gas heat recovery. This process will be easy to implement, it will not require additional components or space and if a security margin is taken, it should be efficient to avoid any sulfuric acid production. However this means a decrease in the total amount of heat to be recovered and therefore, a less efficient system. The main goal of the system designer will be to take a security margin of temperature high enough to ensure that no sulfuric acid is produced, and low enough to not harm the Waste Heat Recovery too significantly. This is summarized in Figure D.1.

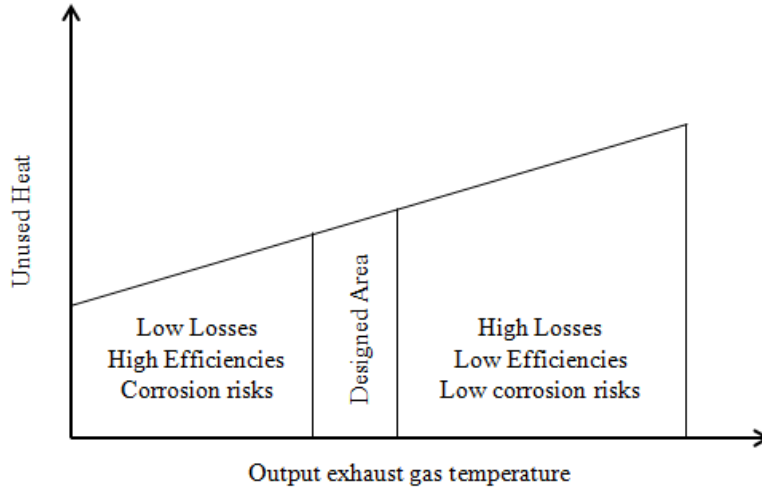


Figure D.1: Optimization of the exhaust outlet temperature.

D.3 Dew point Evaluation

The dew point represents the temperature at which the SO_3 will condense into sulfuric acid. It depends on the amount of water and SO_2/SO_3 presents in the gas. Equation D.2 gives a formula to approximate the sulfuric acid dew point as function of the H_2O and SO_3 partial pressures [Verhoff and Banchemo, 1974].

$$(D.2) \quad \frac{1000}{T_{dew_{H_2SO_4}}} = 1.7842 - 0.0269 \cdot \log_{10}(p_{H_2O}) - 0.1029 \cdot \log_{10}(p_{SO_3}) + 0.0329 \cdot \log_{10}(p_{H_2O}) \cdot \log_{10}(p_{SO_3})$$

The different pressures in Equation D.2 are the partial pressures expressed in atmospheres. The results are given with a ± 9 K accuracy [Verhoff and Banchemo, 1974]. The partial pressure can be evaluated as function of the total pressure and the molar concentration of each molecule with the Dalton Law, given by Equation D.3.

$$(D.3) \quad \frac{p_i}{p_{tot}} = \frac{n_i}{n_{tot}} = Y_i$$

For an exhaust gas outlet pressure of 1 bar, the Sulfuric acid dew point is calculated to be around 130°C. For its applications, MAN fixes the outlet temperature at 160°C, which leaves a security margin of 30 K to avoid reaching dew point for any surface temperature in the stack.

D.4 Security Margin and Energy Losses

Considering a security margin of 30 K reduces the amount of heat to be recovered in the stack. Indeed a large quantity of heat is released through the atmosphere, which has an impact on the efficiency of the system. This value is taken arbitrarily and might not reflect the lowest temperature achievable at the outlet of the stack without compromising the integrity of the system by risking Sulfuric acid condensation.

If by any means the outlet temperature could be lowered, additional energy could be recovered. This is shown with Equation D.4 [Diesel&Turbo, 2012]. The SPP will not represent the exact quantity of energy present in the exhaust gas, but will provide a quick estimation.

$$(D.4) \quad SPP = 1.06 (T_{stack} - T_{sec}) \cdot \dot{m}_{stack}$$

The SPP, or Steam Power Production, represents the energy level available that can be recovered through the stack. It is given by MAN with a usual tolerance of $\pm 7\%$. If the security margin temperature is lowered, available energy is increased. It should be noted that the security temperature is the lowest temperature of the heat exchanger surface, not the exhaust gas.

Figure D.2 shows the increases of energy available for recovery at 75 % load in Tier II and Tier III conditions by varying the outlet temperature between 160 and 130°C.

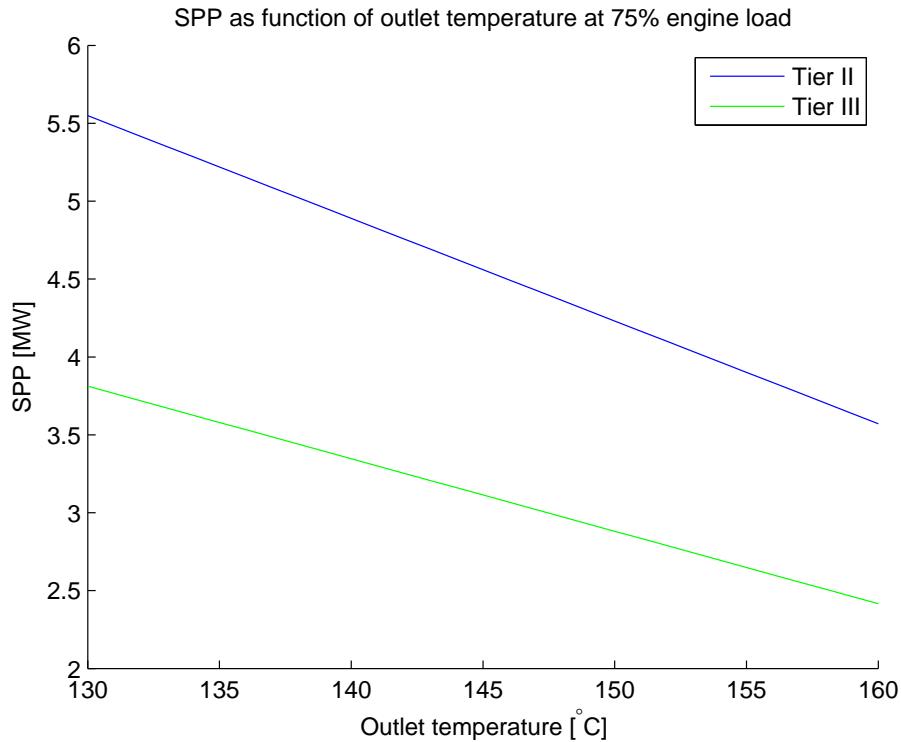


Figure D.2: Available energy in the stack in Tier II and Tier III conditions.

From Figure D.2 it can be seen that the amount of energy that is lost by taking a security margin of 30 K is around 1.5 MW for Tier II, representing an increase of 27 % of energy available, and 1.3 MW for Tier III corresponding to an increase of 35% . The outlet temperature will have therefore a major impact on the system performance.

D.5 Conclusion

The sulfur content in the exhaust gas will lead to the formation of SO_3 and H_2SO_4 by reacting with the water. If the temperature of the exhaust is not controlled, it might reach the dew point. In this case the H_2SO_4 will condense and cause damages. It is therefore essential to ensure that the temperature will never reach the dew point if the ship owner wants to avoid corrosion of the materials present in the stack. A security margin is taken at the outlet of the stack to never reach such a temperature. However, by doing so, the amount of energy that can be recovered is lowered by 1.5 MW for Tier II and 1.3 MW for Tier III applications at 75 % load. Thus, a mean to reduce this security could be extremely interesting to increase the system efficiency and the amount of energy recovered from the exhaust.

Heat transfer formulas E

E.1 Log mean temperature difference (LMTD)

For counterflow heat exchanger: [Cengel et al., 2008]

$$(E.1) \quad \Delta T_1 = T_{hot,in} - T_{cold,out}$$

$$(E.2) \quad \Delta T_2 = T_{hot,out} - T_{cold,in}$$

$$(E.3) \quad \Delta T_{lm} = \frac{\Delta T_1 - \Delta T_2}{\ln\left(\frac{\Delta T_1}{\Delta T_2}\right)}$$

$$(E.4) \quad A = \frac{P}{U \cdot \Delta T_{lm}}$$

E.2 Number of transfer units (NTU)-method

Capacity flow

$$(E.5) \quad C_{hot} = m_{hot} \cdot c_{p,hot}$$

$$(E.6) \quad C_{cold} = m_{cold} \cdot c_{p,cold}$$

No Phasechange (counterflow)

$$(E.7) \quad x_1 = \frac{U \cdot A}{C_{hot}}$$

$$(E.8) \quad x_2 = \frac{C_{hot}}{C_{cold}}$$

$$(E.9) \quad f = \frac{1 - x_2}{(1 - x_2)e^{-x_1 \cdot (1 - x_2)}}$$

$$(E.10) \quad T_{out,h} = T_{in,h} - (T_{in,h} - T_{in,c}) \cdot \frac{C_{hot}}{C_{cold}} \cdot (1 - f)$$

$$(E.11) \quad T_{out,c} = T_{in,h} - (T_{in,h} - T_{in,c}) \cdot f$$

Phasechange (evaporator)

$$(E.12) \quad NTU = \frac{U \cdot A}{C_{hot}}$$

$$(E.13) \quad T_{out,hot} = T_{sat} + (T_{hot,in} - T_{sat})e^{-NTU}$$

Thermodynamic Charts F

All included figures are valid for 90% engine load, and at optimized pressures.

Designed System

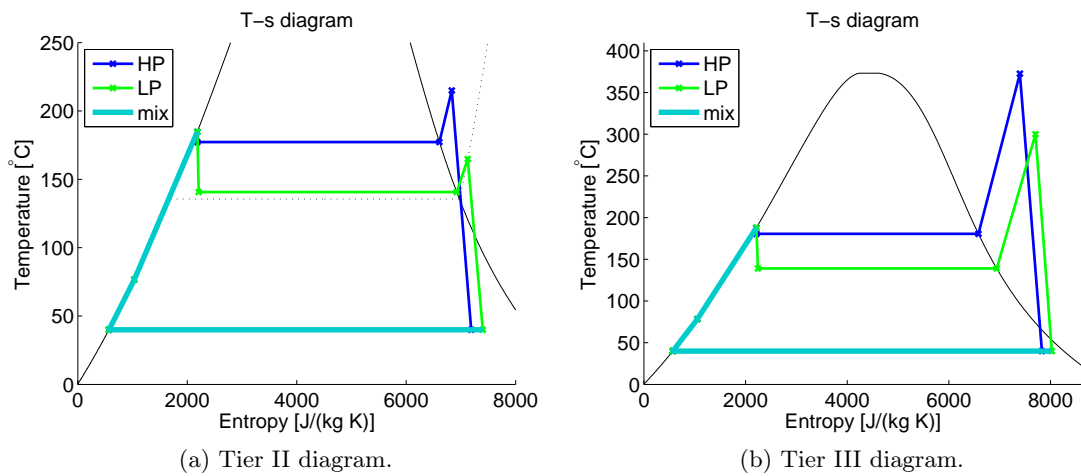


Figure F.1: T-s diagrams of the designed system.

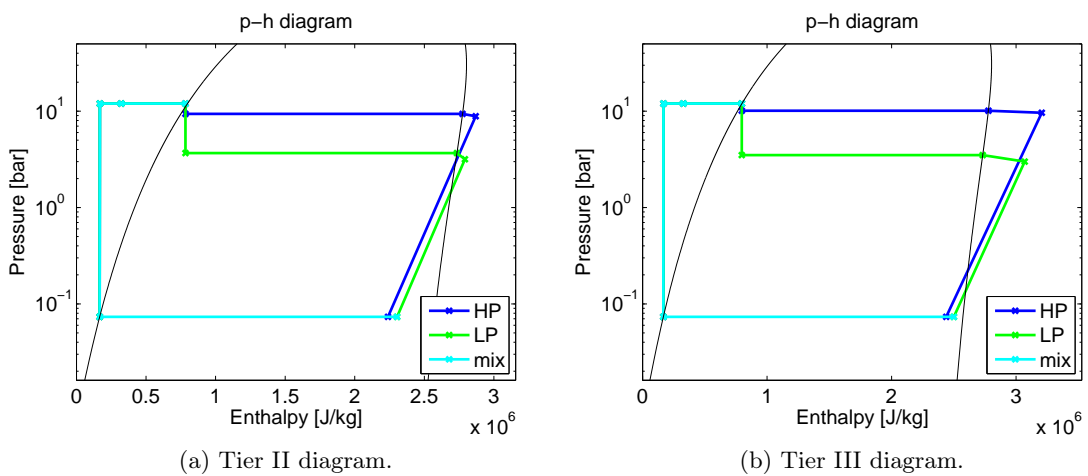
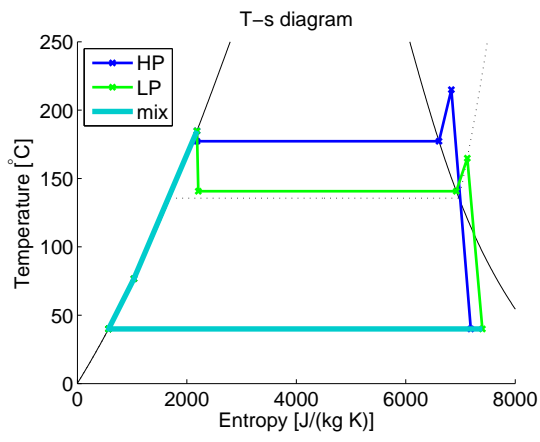
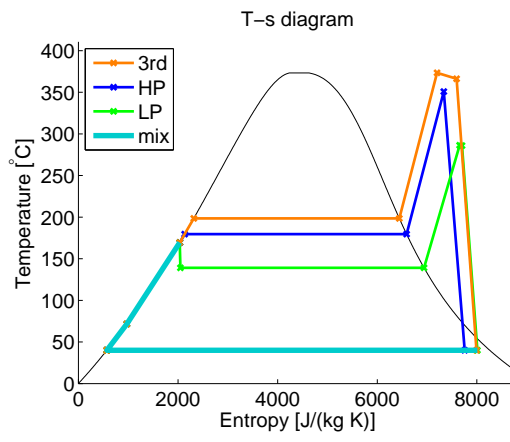


Figure F.2: p-h diagrams of the designed system.

Third Cycle System (Retrofit)

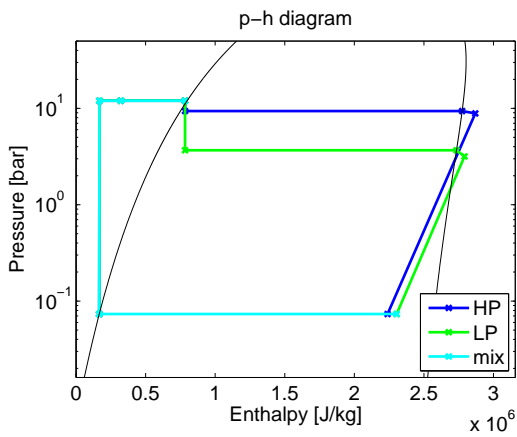


(a) Tier II diagram.

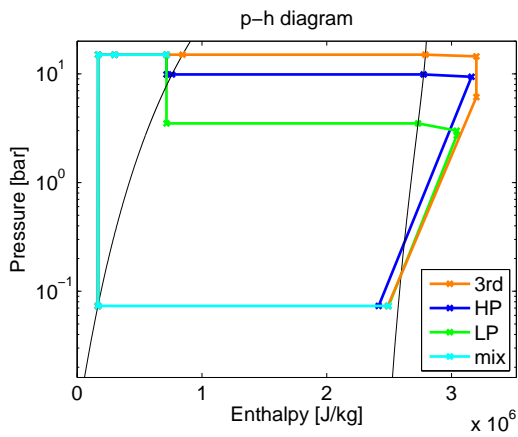


(b) Tier III diagram.

Figure F.3: T-s diagrams of the designed system.



(a) Tier II diagram.



(b) Tier III diagram.

Figure F.4: p-h diagrams of the designed system.